NAZARBAYEV UNIVERSITY

Design, Motion Planning, and Control of a Spherical Parallel Manipulator with Coaxial Input Shafts

by

Iliyas Tursynbek

Submitted in partial fulfillment of the requirements for the degree of Doctor of Philosophy in Science Engineering and Technology

Date of Completion

June, 2023

Design, Motion Planning, and Control of a Spherical Parallel Manipulator with Coaxial Input Shafts

by Iliyas Tursynbek

Submitted in partial fulfillment of the requirements for the degree of

Doctor of Philosophy in Science, Engineering, and Technology

School of Engineering and Digital Sciences

Nazarbayev University

June, 2023

Supervised by

Lead Supervisor, Associate Professor — Dr. Almas Shintemirov
Department of Robotics, Nazarbayev University

Internal Co-Supervisor, Associate Professor — Dr. Matteo Rubagotti
Department of Robotics, Nazarbayev University

External Co-Supervisor, Associate Professor — Dr. Alexandr Klimchik
School of Computer Science, University of Lincoln

Declaration

I, Iliyas Tursynbek, declare that the research contained in this thesis, unless otherwise formally indicated within the text, is the author's original work. The thesis has not been previously submitted to this or any other university for a degree and does not incorporate any material already submitted for a degree.

Signed: Iliyas Tursynbek

Dated: 01.06.2023

BLANK

Abstract

A special class of parallel manipulators, known as spherical parallel manipulators (SPMs), can offer a three degrees-of-freedom (3-DOF) pure rotational motion. Among the various 3-DOF SPMs that have been developed, the most commonly used one is the 3-RRR type SPM. Many applications, such as machining, target tracking, and object stabilization require full-circle or infinite roll rotation from an SPM. Hence, this thesis aims to design a coaxial SPM with an infinite roll rotation feature, which could be used in such applications.

The thesis starts with a kinematic analysis of the proposed coaxial SPM model, providing methods and algorithms for obtaining unique solutions to the forward and inverse kinematic problems. Then, it is followed by a numerical estimation of its Cartesian workspace and configuration space ensuring no singular configurations or configurations with link collisions. To perform link collision checks, a simulation model of the coaxial SPM was created in the CoppeliSim robot simulator for the first time. It was found that for the given SPM geometry its maximum tilt is equal to 39°.

Then, a convex approximation of the obtained configuration space was obtained. Subsequently, it was used in a constrained control for external target tracking with joystick, and object stabilization based on the IMU orientation sensor measurements.

Results presented in this work are supplemented with examples, and the final prototype of the functional motion control system based on a coaxial SPM structure is presented.

BLANK

Acknowledgments

First and foremost, I would like to express my sincere gratitude to my Lead Supervisor, Associate Professor, Dr. Almas Shintemirov for his invaluable patience and feedback. I want to give my deepest appreciation to my Internal Co-Supervisor, Associate Professor, Dr. Matteo Rubagotti, and my External Co-Supervisor Dr. Alexandr Klimchik, Associate Professor from the School of Computer Science, University of Lincoln, UK. Having such an experienced and knowledgeable supervisory team gave me confidence in the research I did.

I am also thankful to the Department of Robotics at Nazarbayev University for providing good laboratory facilities, financial support, and guidance. In addition, I would like to mention and thank the Directors of the Ph.D. program in Science, Engineering and Technology, Dr. Luis Rojas, and Dr. Konstantinos Kostas, and Ph.D. student managers from the School of Engineering and Digital Sciences for their work and time put in improving and coordinating this program.

I am also grateful to my colleagues and friends, for their moral support. Thanks should also go to the research assistants from the Alaris Lab, and study participants from the university, who impacted, helped, and inspired me.

I would be remiss in not mentioning my family: my parents, grandparents, brother, and other relatives. Their belief in me has kept my spirits and motivation high during this process.

Lastly, I would also like to thank my defense committee members, without whom I could not have undertaken this journey. The time they spent on the review process, providing feedback, and examining the oral defense is invaluable.

BLANK

Abbreviations

- RRR - a chain of three consecutive revolute joints
- C-space - configuration space
- DOF - degree of freedom
- H - helical joint
- IMU - inertial measurement unit
- P - prismatic joint
- PM - parallel manipulator
- QP - quadratic program
- R - revolute joint
- S - spherical joint
- SM - serial manipulator
- SPM - spherical parallel manipulator
- U - universal joint

List of publications co-authored by the candidate in relation to the thesis work:

1. I. Tursynbek, A. Niyetkaliyev and A. Shintemirov, "Computation of Unique Kinematic Solutions of a Spherical Parallel Manipulator with Coaxial Input Shafts," *2019 IEEE 15th International Conference on Automation Science and Engineering (CASE)*, Vancouver, BC, Canada, 2019, pp. 1524-1531. (associated with Sections 2.2, 2.3, 2.4)

2. I. Tursynbek and A. Shintemirov, "Infinite Torsional Motion Generation of a Spherical Parallel Manipulator with Coaxial Input Axes," *2020 IEEE/ASME International Conference on Advanced Intelligent Mechatronics (AIM)*, Boston, MA, USA, 2020, pp. 1780-1785. (associated with Sections 2.5, 4.2, 4.3, and 4.5)

3. I. Tursynbek and A. Shintemirov, "Modeling and Simulation of Spherical Parallel Manipulators in CoppeliaSim (V-REP) Robot Simulator Software," *2020 International Conference Nonlinearity, Information and Robotics (NIR)*, Innopolis, Russia, 2020, pp. 1-6. (associated with Chapter 3)

4. I. Tursynbek and A. Shintemirov, "Infinite Rotational Motion Generation and Analysis of a Spherical Parallel Manipulator with Coaxial Input Axes," in *Mechatronics*, vol. 78, 102625, Oct. 2021. (associated with Sections 4.2, 4.3, 4.4, and 4.5)

Contents

List of Figures

BLANK

List of Tables

Chapter 1

Introduction

1.1 Background

A parallel manipulator (PM) [1] is a mechanism with several independent legs connecting its end-effector to the fixed base. An alternative to such a mechanism is a serial manipulator (SM) with only one leg linking the end-effector and the base, as shown in Fig. 1-1. In PMs, the desired position and/or orientation of the end-effector, also referred to as a mobile platform, is achieved by the simultaneous and coordinated movement of all its actuators, whereas in SMs, the motion of their actuators can be sequential and non-simultaneous in some cases. They can be controlled sequentially to reach a specific configuration of the end-effector. In general, SMs have broader use in industrial settings and are more widely spread on the robotic manipulators market than PMs, due to the more simplistic nature of their architecture and control. On the contrary, due to their parallel kinematic

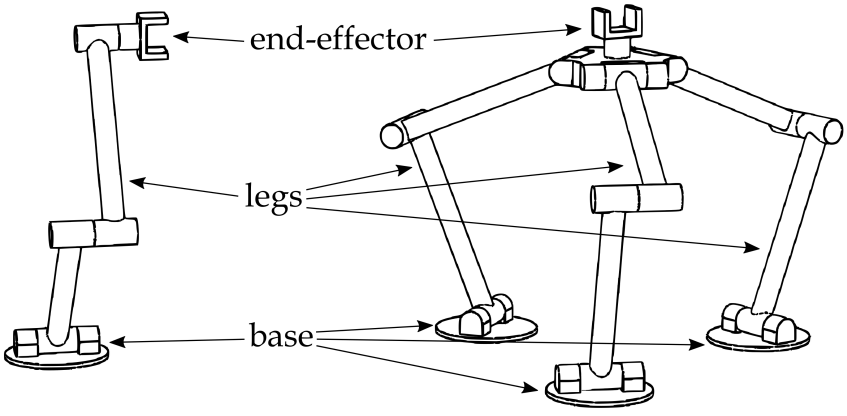

Figure 1-1: Serial and parallel manipulators

structure, PMs can still possess several advantages over traditional SMs. These advantages can be exploited to improve the performance of specific tasks and applications.

Most PMs have a better load-to-weight ratio compared to SMs since the weight of an object mounted on the mobile platform is distributed across several parallel legs. This makes use of more powerful and thus heavier actuators at the base and the first joints, which are important to withstand the weight of the handled object and the manipulator itself, less necessary. Consequently, it can lead to a cheaper manipulator design. Due to a more advantageous load-carrying capacity, PMs are finding their application in robotic exoskeleton designs [2, 3], and heavy-object handling systems [4–6]. Additionally, parallel kinematic architecture also results in mechanically more rigid and stiffer manipulators since the end-effector's position and force are induced simultaneously by several legs. This leads to fewer vibrations during the manipulator's motion, which helps PMs to be used in machining-related applications [7–14]. Furthermore, the possibility of having more light-weight structures in PMs can decrease the inertia of a manipulator, thus allowing PMs to be suitable for dynamic applications in manufacturing where high speed of operation is of importance, such as in pick-and-place tasks [15–17] or object stabilization [18–20]. Another advantage of PMs is their high accuracy in positioning and orienting objects. Compared to SMs, where actuators' positioning errors add up, in PMs, such errors are not accumulated but rather reduced/averaged due to balancing forces exerted by other parallel legs. Such precision is usually required in medical applications, where PMs can be used as mechanisms for medical tool handling [21–25], or as haptic medical devices [26–30]. Most of the application examples mentioned above benefit from several advantages of PMs.

Despite the advantages listed above, PMs have several drawbacks as well, such as their comparatively small workspace and complicated kinematic analysis as a consequence of their complex architecture. PMs require a lot of studies and experiments to be conducted before they find any real application in the industry sector.

In general, PMs can be classified into three main categories depending on the

motion characteristics of their mobile platforms: planar, spatial, and spherical. It is a common practice to use a robot that matches the required workspace and mobility specifications as it affects its cost. The mobile platform of a planar PM [32–36] has two translational degrees-of-freedom (DOFs) and moves in one plane, mainly x-axis and y-axis, and it also can have a rotational DOF to orient an object around z-axis. A typical example of a planar PM is a 3-RRR (R denotes a revolute joint) manipulator shown in Fig. 1-2a. Spatial PMs can have up to six DOFs, i.e., three translational DOFs, and three rotational ones. A famous example of a spatial manipulator is the Stewart-Gough platform [4–6, 37] (also known as the Gough-Stewart or simply the Stewart platform) shown on Fig. 1-2b. Another well-known example of a spatial PM is the Delta robot [15, 38, 39], which has only three translational DOFs, and can not change the orientation of its end-effector, though such modifications are introduced when

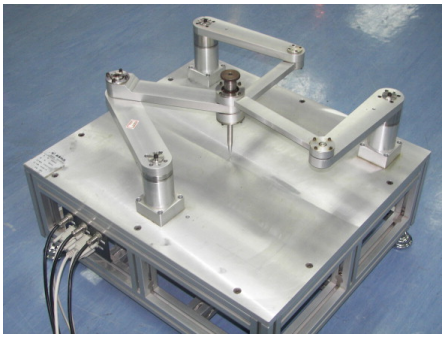

(a) Planar PM [31]

(b) Spatial PM: Stewart Platform (courtesy of Physik Instrumente (PI))

(c) Spatial PM: Delta Robot (courtesy of B&R Industrial Automation GmbH)

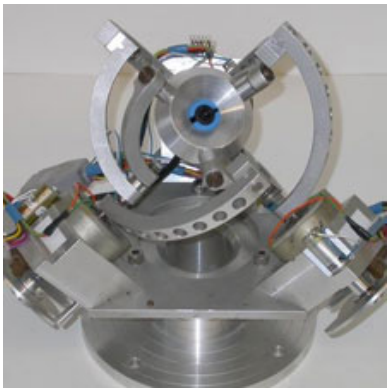

(d) Spherical PM: Agile Eye (source https://robot.gmc.ulaval.ca/)

Figure 1-2: Examples of parallel manipulators

needed. The Delta robot is illustrated in Fig. 1-2c. The Stewart-Gough platform and the Delta robot are successful examples of PMs that were studied in detail and found their commercial application in tasks as flight simulators and pick-and-place assembly, respectively. The last group of PMs is spherical parallel manipulators (SPMs) that can offer three rotational DOFs and orient an object around a fixed point. They can be treated as an alternative to the standard robot orientation wrists with serial kinematic architecture [40] and can be used as spherical motion generators [41], i.e., as active ball joints. Robot wrists are an important part of a manipulator design and development contributing to its dexterity [42]. The need for manipulators providing spherical motion is important for orientation mechanisms [18], machining [43], medical and rehabilitation devices [27,30,44–48], prosthetics [49], exoskeletons [3] and humanoids [50, 51].

1.2 Review of Spherical Parallel Manipulators

1.2.1 3-RRR Spherical Parallel Manipulators

A robot wrist is usually the last structural part in the kinematic chain of most industrial robotic manipulators, which contributes to an overall improvement of their dexterity. In particular, its movement is confined by rotational DOFs, hence it is intended for orienting the end-effector without changing its position. Conventional serial wrists are commonly designed as the roll-pitch-roll (spherical) or the pitch-yaw-roll (non-spherical) configurations. Contrary to this, parallel wrists [42, 52–57] are often based on the model of SPMs capable of generating a spherical motion [41] and having two or three rotational DOFs with intersecting axes. A detailed review and comparison study of serial and parallel state-of-the-art wrists is conducted in the survey paper by Bajaj *et al.* in [40].

One of the earliest research works that considered a parallel wrist is [58] by Asada and Granito. In this work, serial and parallel wrists were analyzed and compared based on their kinematic and static characteristics, demonstrating an optimization method for wrist performance improvement and finding an optimal mechanical design. Later, several works [59–62] related to the development of a three DOF (3-DOF) parallel shoulder module employing dyads with R joints

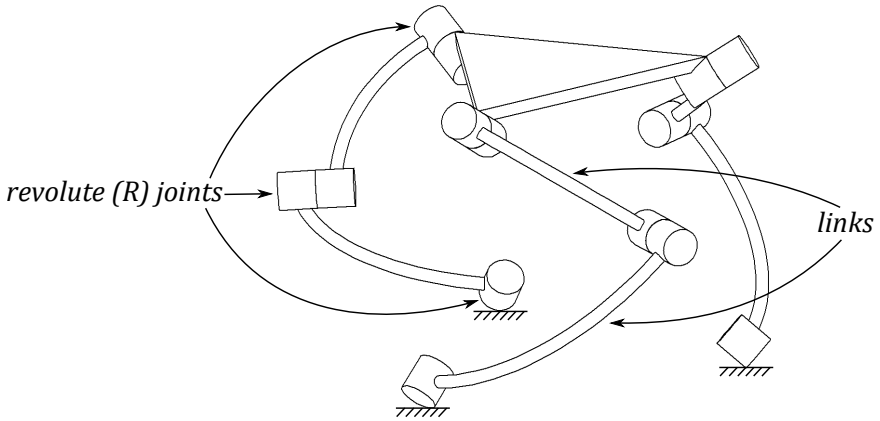

Figure 1-3: General 3-RRR SPM

were published. These modules can also be used as wrists since they generate pure spherical motion. The shoulder module design presented in these works is of the 3-RRR kinematic type, meaning that it has only three R joints at its three parallel legs.

This kinematic design was later extensively studied by Gosselin *et al.* For instance, following their earlier research work on a planar 3-RRR PM [63], Gosselin and Angeles used a similar analysis approach as a foundation for the kinematic analysis and optimum design of the 3-RRR type SPMs as shown on Fig. 1-3 (hereafter will be referred to as general SPM) in [64]. This article introduced the standards of notation and terminology for the field of research related to SPMs. The equations for solving the inverse kinematic problem were derived, with the forward kinematic problem not being addressed. As a matter of fact, solving the inverse kinematics of PMs is generally an easier problem compared to solving forward kinematics. Additionally, symmetry-related issues together with conditions leading to singular configurations were also discussed in the referenced work. It was reported that given a symmetrical general SPM, the actuators should be equally spaced, and links of each chain should all have the same dimensions and ideally be equal to 90° for maximization of the workspace and isotropy of the manipulator. A special case of the general SPM with the axes of the end-effector joints and the axes of the base joints being independently coplanar and symmetrically arranged was later analyzed, and a polynomial solution to its forward kinematic problem was presented in [65]. This particular geometry allowed to

introduce some simplifications to the forward kinematics analysis. A minimal polynomial of degree 8 was derived meaning that a manipulator of this type admits a maximum of 8 real solutions, which were also found and illustrated in that reference for some of the manipulator's configurations. Another special case of the general SPM with a collinear positioning of its input joints (and coplanar end-effector joints) similar to the one in [58] was also examined following the same approach, and it was found that this manipulator has at most 8 real solutions to its forward kinematic problem as well. Finally, a methodology for solving forward kinematics of a 3-RRR SPM of any architecture was completed in [66]. Likewise, as in [65], a polynomial of degree 8 was obtained and proven to be minimal by demonstrating examples with 8 real solutions. Following different approaches, 8th-order polynomials for solving forward kinematics of general SPM were also derived in [67] by Innocenti and Parenti-Castelli, and in [68] by Huang and Yao.

Afterward, multiple works on singularity, workspace analysis, and optimal design of general SPMs were published. SPM design optimization based on the unified method involving conditioning and stiffness indices was carried out in [69]. A global dexterous performance index was formulated and used in the design optimization of general SPM in [70]. Analysis of 3-RRR SPMs singularity based on Tilt-and-Torsion angles was considered in [71]. It was extended to obtain an analytical determination of the workspace in [72]. More recent works on general SPMs include analysis of the effect of a manipulator's self-rotation angle on the dexterity and singularity in [73], workspace characterization based on graphical methods in [74], and dynamic analysis in [75].

Previously mentioned special cases of the general SPM (coplanar and collinear) were further studied in [77] to achieve the optimal kinematic designs. Subsequently, a family of isotropic architectures was obtained by a proper adjustment of particular geometric parameters. The conducted kinematic optimizations and identified isotropic designs from this paper resulted in the development of the Agile Eye manipulator [18–20] (Fig. 1-4a), a 3-RRR SPM with orthogonal axes of adjacent joints causing an isotropic configuration with high-performance dynamics. An application of this manipulator as a camera-orienting device was demonstrated with the real prototype. It was reported that it can orient a mounted

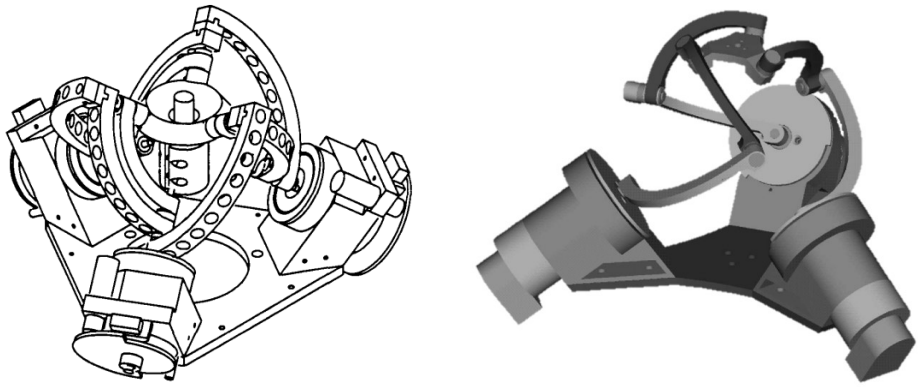

(a) Agile Eye [18] (b) Agile Wrist [76]

Figure 1-4: SPMs with special design structure

camera within a cone of 140° opening with ±30° in torsion. Forward kinematics of the Agile Eye was addressed in [78]. The authors derived a closed-form solution specific to this manipulator, which is useful for real-time control. Analysis of the Agile Eye was complemented in [79] by examining its three types of singularity in the joint and Cartesian spaces with the explanation and illustration of their physical interpretation. Furthermore, the Agile Eye's singularity analysis was extended in [71], and its working and assembly modes were explored in [72] by Bonev *et al.* It was also validated that at most 8 solutions exist to the forward kinematic problem; the same applies to the inverse kinematic problem. Finally, in [80, 81], Kong and Gosselin developed an alternative formulation for the Agile Eye's kinematics and proposed a formula for obtaining a unique solution to the forward kinematic problem corresponding to its current working and assembly modes. Having a unique solution is very important for the manipulator's control purposes. Several research works utilized the Agile Eye and tailored its design for application as a biomedical device [44, 46, 82]. A more generalized view of the optimal design with respect to kinetostatic performance characteristics was provided in [83].

A mechanically modified version of the aforementioned manipulator with enhanced load-carrying capacity, named as the Agile Wrist and shown on Fig. 1-4b, was proposed by Angeles *et al.* in [76]. The methods for the kinematic analysis of the general SPM hold true for this manipulator as well. A follow-up work, [84], focused on the structural optimization of the proposed SPM. Dynamics of the

Agile Wrist was studied in [85–87], with its motion control techniques suggested in [88]. Later, Shintemirov *et al.* worked on an approach for finding a unique solution to both forward and inverse kinematic problems of this SPM in [89] with the application of this methodology to numerical optimal control and constrained orientation control in [90] and [91], respectively.

Somewhat similar to the Agile Eye and the Agile Wrist is the SHaDe (an acronym standing for Spherical Haptic Device) mechanism (Fig. 1-5a) from [92], but with different dimensions for the angles of the axes of the base and the end-effector. A real-time force control scheme with haptic feedback was developed for the teleoperation of the Agile Eye using the SHaDe as the master device. One more master haptic device based on the 3-RRR SPM (Fig. 1-5b) was developed in [28–30] by Saafi *et al.* However, in their case, an extra actuator was integrated into one of the mobile platform joints making it redundantly actuated. This modification was introduced to eliminate some of the manipulator's singularities. Another modification of the Agile Wrist can be observed in [93]. It was proposed to use cylindrical (denoted as C) joints to replace unactuated R joints as a means to overcome an overconstrained nature of general 3-RRR SPMs. The drawback of overconstrained manipulators is that they require very high-precision manufacturing technologies and assembly processes in order to properly function which is not always an option due to the increased production costs or lack of machining facilities. It is noted that the resulting mechanism (3-RCCC) is not a spherical one anymore, but rather spatial, capable of producing almost spherical displacements. Following the same motivation, the authors in [94] aimed to design a non-overconstrained variant of the Agile Eye.

1.2.2 Non-3-RRR Spherical Parallel Manipulators

In general, among the large number of structural types of 3-DOF SPMs that were synthesized and systematized in [95,96] by Karouia and Hervé, in [97,98] by Kong and Gosselin, and by others in [56, 99–102], the 3-RRR type SPMs are the most detailly investigated ones as it can be seen from the examples presented so far. However, there are other SPMs with different architectures being designed as well. For example, Vischer and Clavel presented their parallel wrist, named Argos, in

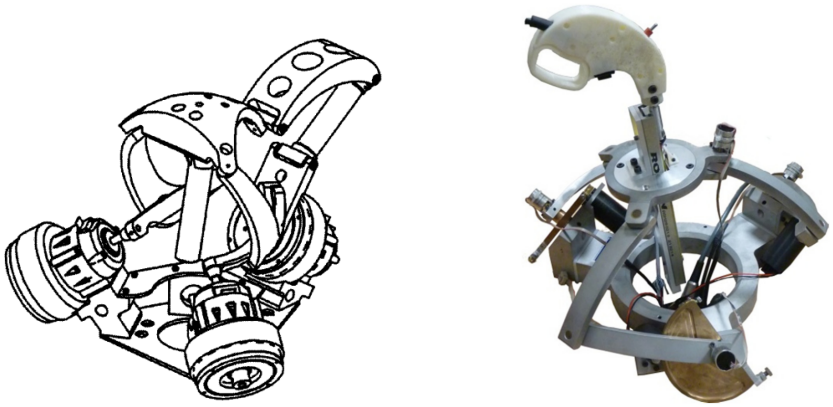

(a) SHaDe [92] (b) [30]

Figure 1-5: Haptic devices based on SPMs

[103, 104]. It is a 3-DOF SPM with a 3-R(2R/2S)S (S stands for spherical joint) architecture able to achieve $\pm 60^\circ$ in roll angle. The referenced works described its forward and inverse kinematics as well as demonstrated a real prototype and its calibration. Its singularity analysis was done in [79]. It should be noted that in the notation used for PM architecture (e.g., 3-RRR, 3-R(2R/2S)S, etc.), the first digit represents a number of parallel kinematic chains of the type specified afterward, where an order of letters correspond to their sequence in the chain starting from the base towards the end-effector.

SPMs with Cylindrical, Universal, and Spherical Joints

Similarly to the proposed replacement of the R joints with the C ones for the Agile Wrist in [93], [105] introduced SPMs of type 3-RCC, 3-CCR, and 3-CRC. The C joints can be viewed as a combination of the R and P (prismatic) joints, i.e., as RP or PR pair sequences. Only after satisfying some necessary geometrical conditions listed in the article these mechanisms can be considered as true SPMs. Otherwise, orientational motion can not be attained, and the manipulators would rather be considered spatial ones. The 3-RCC SPM was also considered in [106].

Instead of using the C joints as a substitution for the R joints for achieving non-overconstrained designs, another common practice is to use universal (U) and spherical (S) joints or a combination of them. Generally, RRRRR type chains provide 5-DOFs and if used as the limbs of an SPM can make them not over-constrained. A more practical case is to use the U joint instead of a pair of R ones

(RR). For example, a 3-RUU type SPM was synthesized in [107] by Di Gregorio. A similar type SPM with no idle pairs was designed in [108] by Karouia and Hervé. 3-RUU SPM was also considered in [106]. Later, a 3-URC type SPM was presented in [109] by Di Gregorio. An inverted architecture, 3-CRU, was outlined in [100] and used in [110, 111] to design a manipulator prototype. 3-URU type was used in a pure rotational mode in [112].

In a similar way as for the U joint, three consecutive R joints, i.e., RRR, can be substituted by the S joint. Karouia and Hervé worked on a 3-RRS type SPM in [113], where they also discussed its variations with a different assembly order, namely 3-RSR type, and 3-SRR inverted type. The 3-RRS type SPM was independently synthesized at about the same time in [97] by Kong and Gosselin, and in [114] by Di Gregorio. One of the interesting features of this type of SPM is that it possesses no translation singularities. 3-RRS architecture was also considered in [106]. The 3-RSR type SPMs were treated in [115].

In all of these SPM architectures, the R joints are the ones being actuated, and the actuators are aimed to be located as close to the base as possible if not on the base itself. As was mentioned before, such location decreases the weight of the links, hence decreasing inertia and facilitating faster speeds of manipulators. Some manipulators consider links with more than 3 joints in a chain such as in [116].

SPMs with Prismatic Joints

Another popular option is to use prismatic actuators that result in the P joints in the kinematic structure of the SPM. In [77], the 3-UPS type SPM was presented and its kinematics was analyzed. Its forward kinematics was formulated and numerically solved in [117] for real-time control applications. A workspace optimization for the 3-UPS structure-based parallel orientational platform was conducted in [118]. In [119], a 3-UPU architecture for a 3-DOF tripod with spherical rotations was synthesized by Karouia and Hervé. A detailed study of the kinematics of such architecture was followed up by Di Gregorio in [120], and in [121] with respect to its singularities. Workspace optimization was done in [118]. Reference [122] extended these analyses. An alternative method of

kinematic analysis was considered in [123]. Application of such parallel wrist as sun tracking systems and its path planning was discussed in [124]. Singularity-free path planning for 3-UPS and 3-UPU wrists was also considered in [125].

As a modification of a 3-UPU and following the work [119], Callegari *et al.* presented an SPM in [126] with a combination of the P and C joints where one of the U joints is substituted by the C joint, i.e., 3-CPU. This topology was later exploited in [127] to design a parallel wrist. Its position control was considered in [128]. The 3-CPU wrist can be reconfigured and this aspect was studied in [129]. While reconfiguration this mechanism falls into a translational mode of operation and thus can be considered as a spatial mechanism, not a pure orientational one. To stay in one mode of operation, lockable S joints were investigated in [130,131]. SPM with the R joints as the terminal point of the limbs with the P joints 3-RPR was studied in [132] and [133]. An architecture where a passive P joint is located at the edge of the limb's kinematic chain 3-RRP was investigated in [134–138]. The authors called this mechanism a Spherical Star Triangle (SST) manipulator. Another SPM with a passive R joint and inverted case of the previous topology, i.e., 3-PRR, was designed in [139, 140]. A reconfigurable SPM with more than 3 joints, 3-RPRP, was presented in [141].

SPMs with Extra Limbs

Most of the manipulators even though being non-overconstrained as one of their advantages, still require meeting specific assembly conditions to avoid translational motion, of which some of them are capable. To overcome this drawback and impose rotational motion about a center of rotation, and to increase stiffness and load-carrying capacity it is a general practice to add extra limbs to parallel manipulators. For example, one of the first works that considered kinematics of 3-SPS-S type SPM, in particular its forward kinematics, was [67]. A special structure of such SPM with identical pyramids and its forward kinematics was analyzed in [142]. Its structural optimization was done in [143]. An approach for finding a unique current solution to the forward kinematic problem was derived in [81]. Another method for its kinematic analysis was presented in [123]. More insights into its singularities were given in [144]. A mechanism with the same

actuated limbs, but with a different passive limb was reported in [145]. It has a passive limb with three chains with the P joints connected to a single point on the end-effector with the S joint. The authors named this manipulator as Stewart Spherical Platform. The 3-UPS type SPM previously mentioned, has a modified version where a passive limb with the S joint is added in the center of the manipulator to comprise a new 3-UPS-S type SPM. Again, similar to the 3-SPS-S type SPM, its kinematics was studied in [67]. Its singularity loci were analyzed in [71, 146, 147], and their effects on the overall workspace were considered in [148]. Forward kinematic problem and working modes were studied in [149, 150]. Structural optimization was conducted in [151]. Its application for laparoscopic surgeries was investigated in [152]. Other works with passive spherical limbs include [153] with 3-SPU-S type SPM, [154] with 3-PSU-S type SPM, [155] with 3-PUS-S type SPM, [156, 157] with 3-PSS-S type SPM, and [158] with 3-RSS-S type SPM. In [159–164], several underactuated 3-DOF SPMs were derived from modifications of 3-SPU-S architecture. SPMs with more than three joints per each actuated limb were considered as well in [165] for 3-RRRS-S topology, and in [166–168] for 3-RPSP-S topology. An SPM with a passive limb and a helical (H) joint and double mobile platforms was developed in [169–176] for simulation of hip joint motion. SPMs with active middle limbs also exist, for example, 3-RRR-RUR in [177, 178].

Asymmetrical SPMs

The non-3-RRR SPMs discussed so far are symmetrical. Symmetrical PMs can be considered more general since they are not designed with a specific application in mind. Oppositely, asymmetrical PMs are tailored for specific applications known *a priori*. For example, a 3-DOF parallel mechanism for the design of the mechanical spine was built in [179]. A spherical parallel wrist with the application to the vertebrae of an eel robot was designed in [180]. Mechanisms for ankle rehabilitation were designed using the 3-RUS/RRR and 3-UPS/RRR architectures in [181] and [182], respectively. A particular design feature of this mechanism is that it has an active RRR limb that constrains the motion of its mobile platform, however, it is not located in the middle as in the case of previously discussed SPMs,

but outside, making it asymmetrical, preferring one dimension over the other, to better suit its application as an ankle rehabilitation device. The RSC-RRU-RRS and 2RSC-RRR SPMs were considered in [106]. The work on the systematic synthesis of asymmetrical SPMs was done by Karouia and Herve in [183]. Others are with more "exotic" architectures such as the one in [184] which uses parallelogram linkage as one of its limbs.

1.2.3 2-DOF Spherical Parallel Manipulators

In addition to 3-DOF SPMs, SPMs with 2-DOF are also available. For example, an RR-RRR-RRR (1-RR-2-RRR) SPM proposed by Kong in [185], which can be obtained as a modification of the Agile Eye by eliminating one of the actuated joints and changing the working mode of one of the limbs. Later, its motion characteristics were compared with that of the 2-DOF serial gimbal structures and the 2-DOF equal-diameter spherical pure rolling (ESPR) rotational parallel manipulator (RPM) in [186–188]. ESPR RPM is a special RPM with a non-fixed center of rotation whose axes intersect instantaneously, and the centers of rotation lie on a sphere under any configuration as defined in [189]. Hence, ESPR RPMs are not considered as a subclass of SPMs, even though they also have pure rotational DOFs. One of the well-known examples of ESPR RPMs is a patented Omni-Wrist III actuated by two linear actuators and developed by Rosheim *et al.* [190–193]. It is a 2-DOF manipulator of 4-RRRR type with 180° singularity-free semi-spherical movement. Variations of this manipulator exist, namely Omni-Wrist V (3-RSR-SS) and Omni-Wrist VI (4-RSR-SS). Kinematic analysis and study of mobility and singularity of the Omni-Wrist III, its variations, and two other mechanisms derived on its basis (T-type and Δ-type) were performed in [194, 195]. Other notable ESPR RPMs include [196]. Type synthesis of 2-DOF ESPR RPMs was presented in [197]. Type synthesis of 2-DOF RPMs with a fixed center of rotation was implemented in [198].

2-DOF SPM similar to the Agile Wrist, but with coincident end-effector joints, was presented and analyzed in [199–201]. In general, most of 2-DOF SPMs are designed on the basis of a patented five-bar structure of 5R type [202], and having 2 limbs such as the one in [203,204], which looks like the previously mentioned one

but with one of the legs removed. Forward kinematics of such mechanisms was studied in [205, 206]. Workspace and optimal design of this structure were presented in [207] and [208], respectively. Other works on the 2-DOF 5R SPMs with a modification of one of the links to a platform include [209–212]. A structurally enhanced version of this modification is available at [213–216]. SPM where one of the links is replaced with a slotted arc is presented in [217]. In [218], a modification with a reverse motion transmission was developed. 2-DOF SPM based on a six-bar linkage was proposed in [219]. A wrist that is based on spherical eight-bar linkage was analyzed in [220]. Fully decoupled 2-DOF parallel wrist was introduced in [221]. Several 2-DOF SPMs with passive limbs were also suggested in [222–224] with 2-RRR-U, 2-PUS-U, and 2-PUS-U, respectively. [225] deals with the synthesis of 2-DOF SPMs with legs of the US type. Overconstrained 2-DOF parallel wrists are presented in [53]. Non-overconstrained SPMs with 2 legs are given in [226]. Several 2-DOF SPMs driven by cables are available as well [227–229].

1.2.4 Spherical Parallel Manipulators with Infinite Rolling

Some applications require an extended, complete full-circle, or infinite rolling of SPM's mobile platform around its normal vector, that is in addition to its limited pitch and yaw rotations. Examples of these applications may include machining tasks such as drilling [13] and milling, or it can be required for orientation purposes such as for the case of active ball joint [230]. The Agile Eye 3-RRR SPM previously mentioned [18] (Fig. 1-4a) is capable of only $\pm 30^\circ$ of the end-effector's twist. A special case of the general SPM with a collinear (coaxial) arrangement of its input axes (hereafter - coaxial SPM) does not have this limitation, making it a potential candidate for such applications.

Coaxial SPM's kinematic structure shown in Fig. 1-6 was proposed as parallel orientation wrist in [58]. One of the advantages of this SPM is that it has no singularities inside its spherical workspace, only on the boundaries, compared to the serial counterparts. This SPM architecture was further studied in [65] by Gosselin *et al.*, where it was shown that coaxial SPMs' forward kinematic analysis also leads to a polynomial of degree 8 similar to the general SPM. This study

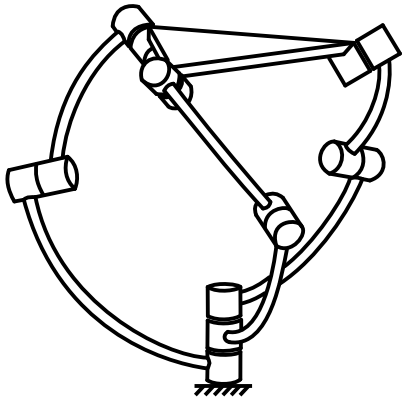

Figure 1-6: Coaxial SPM

was extended by Bai *et al.* in [231] where they proposed a method for workspace analysis and formulated the global singularity surface for coaxial SPM. References [232, 233] proposed a new approach for solving forward kinematics based on I/O equations of spherical four-bar linkages. A numerical example with eight solutions to the forward kinematic problem (assembly modes) with their visual representation was also presented. In [234], Bai *et al.* focused on workspace modeling with Euler parameters. Based on this, the authors explored SPM's dexterity and singularity. The optimum design for a prescribed workspace was considered in [235] for a 3-RRS coaxial SPM. Kinematic analysis based on screw theory was done in [236, 237]. In [234, 235], a model of coaxial SPM with circular guide was proposed (Fig. 1-7). Research on this SPM was continued by Wu *et al.* In [238], he was dealing with the kinematic synthesis of this manipulator based on the evaluation of the multi-objective performance criteria. This work aimed to find structural and geometric parameters to maximize dynamic and kinematic dexterities. Reference [239] extended design optimization of this SPM and worked on minimization of the mechanism mass. Modeling and optimization with respect to stiffness parameters were implemented in [240]. Effects of limb flexibility and the resulting center shift of the mobile platform were investigated in [241]. A reconfigurable version of the coaxial SPM with a circular guide and actuated with four-bar linkages was proposed in [242, 243]. In [244–246], electromagnetic actuation of this SPM with its control was developed.

Apart from the aforementioned version of SPM, a circular guide was considered for providing decoupled motion of the mobile platform around the z-axis of

the manipulator in [247]. An exoskeleton wrist based on coaxial SPM with a circular guide was developed in [248, 249]. A reconfigurable version was designed in [250–252]. In [253], a 3-RUS-S modification is introduced. The authors decided to label a circular prismatic guide as the P joint and identified their mechanism as the 3-PUS-S architecture, however, staying in line with similar works using the same circular guide it is labeled as 3-RUS-S here. A review of PMs with circular guides is presented in [254]. One of the drawbacks of the SPM with a circular guide is its sliding actuators, which lead to increased inertia and can result in a decreased speed of operation.

Coaxial SPMs with fixed actuators are mainly based on the architecture proposed by [58]. For example, it was used in the design of marine propulsors [255, 256], for rehabilitation device [257], and in robotic link mechanism in [258–260]. In the latter works, the authors added an extension joint for adding an extra rotational DOF for remote actuation of the next joint in the arm they design. A model of a mechanism with the R joints and only two attachments to the end-effector capable of unlimited rotation around any axis inside the workspace was analyzed in [261]. In [262], the 3-RSS-S architecture was utilized. The main difference, apart from the addition of the S joints, is that it uses belts for the actuation of the system; it also has a fixed limb in the middle of the structure. A driveable limb was used in [263] to provide an unlimited rolling capability to the designed SPM. The limb direction was controlled by two orthogonal semi-circular tracks, similar to the one used in [264] for the design of a positioning system for brain biopsy. Several SPMs with unlimited rolling and based on asymmetrical architecture were proposed, among others. Architectures proposed include 2-RRR-RUR-RRU or 2-RRR-RUR-RPU [265], 2-PUU-RUR-RPS [13, 43, 266, 267], 2-UPU-RUR-RPS [43, 266–268], 2-RRR-RUR-RPS [43, 266, 269–271], PSS-PRU-RUR [267]. In general, all of these SPMs have a mobile platform composed of outer and inner rings connected to each other through the rolling bearing. The inner ring's decoupled rotation is provided by the RUR link. The outer ring is controlled by two active links and constrained by one passive link (except the PSS-PRU-RUR case where there is no passive link). One more example of the asymmetrical SPM is [272], where it was synthesized and optimized to have

$-55° - +15°$ of rolling as having more is not required by the application as a prosthetic wrist. Analysis of such mechanisms is more complex than that of symmetrical SPMs, which demands further efforts for their physical realization. A hybrid (serial-parallel) architecture where a third rotational DOF responsible for unlimited rolling is added to the base or the end-effector in a serial chain is also available [273].

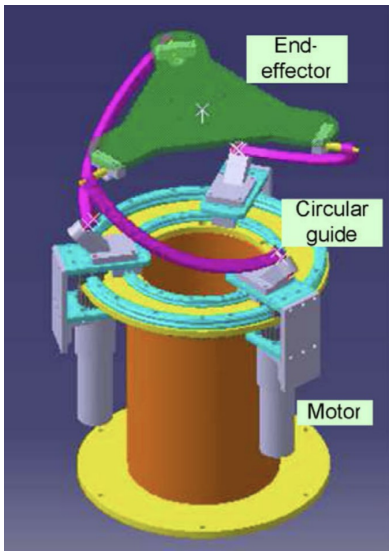

Figure 1-7: SPM by Bai *et al.* [240]

1.3 Motion Planning and Control of Spherical Parallel Manipulators

PMs require coordinated and simultaneous actuation of their input joints to achieve specific motions and follow desired trajectories. During these actions, it is also crucial to avoid any singular configurations and link collisions. Thus, studying the workspace and joint space in advance is essential to identify unfeasible regions and detect unwanted inputs. However, this analysis is complicated by the fact that most PMs have multiple solutions to their inverse and forward kinematic problems, and coaxial 3-RRR SPMs are not an exception.

The Cartesian workspace of an SPM, excluding singular configurations, can be obtained both analytically and numerically. However, configurations leading to link collisions depend on the specific manipulator design, such as the shape

of its links. Numerical analysis of the discretized version of the workspace can be used to identify these configurations, and it is desired to have a unique solution corresponding to a particular working mode of an SPM. To generate optimal trajectories and smooth motions of a manipulator, it is necessary to study its joint space. This is done using solutions of the forward kinematic analysis. As it was previously mentioned, forward kinematic analysis of the coaxial SPM results in a polynomial that has a maximum of eight real solutions [66, 67]. Usually, such high-order polynomial solutions can not be expressed in closed form and are very complex. One of the options is to use a numerical approach to solve such expressions. Numerical methods can also be used to compute unique solutions to the forward kinematic problem as proposed in [89, 90] for a general SPM case. Later, a constrained orientation control for Agile Wrist was developed based on the convex approximation of the feasible configuration space that utilized such unique solutions while its pre-computation stage [91]. This approach allowed to implement a real-time inertial stabilization of the SPM, in which optimal trajectories are generated, and singular configurations and configurations leading to link collisions are avoided.

Accurate application of PM-based devices requires designing a feedback orientation control system that utilizes kinematic and/or dynamical models of manipulators [274, 275]. Various sensors, such as IMUs, can provide feedback on the orientation of an SPM's mobile platform [149].

Despite the progress made in SPM research, several open issues still exist. For instance, developing efficient control algorithms that can handle the complex kinematics and dynamics of these manipulators remains a challenge. Moreover, integrating sensing and actuation systems to improve the accuracy and reliability of SPMs is another area that requires further research. Therefore, future research should focus on addressing these open issues and expanding the applications of SPMs in various fields.

1.4 Hypothesis, Objectives, and Scope of the Work

After reviewing the literature on SPMs, it becomes evident that much of the research focuses on the design optimization, kinematic and dynamic analyses of the SPM models discussed earlier. However, only a few of these models, such as those developed in [58, 256], are capable of the extended or infinite rotational motion within their feasible workspace, which has applications in fields such as machining, medical robotics, stabilization, and orientational platforms. Therefore, there is a need to investigate the infinite rotational capability of a coaxial SPM and develop motion control platforms exploiting this capability. In this thesis, it is hypothesized that motion control platforms can be developed based on the coaxial SPM with capabilities to infinitely rotate its mobile platform and achieve target tracking and object stabilization.

Following this, the objective of this thesis is to study the kinematics of the developed coaxial SPM, the effects of the infinite rotational motion by obtaining the Cartesian workspace and configuration space of the manipulator, and apply obtained result for the target tracking and object stabilization on a manufactured prototype by demonstrations through experimental examples.

The scope of work of this thesis arises from the objective to achieve target tracking and object stabilization, thus making kinematic analysis and implementing specific motion planning approaches as required to achieve these goals. For motion planning, it is required to have computed workspace and configuration space of the coaxial SPM. The obtained configurations space has to exclude singular configurations and link collisions. An example of the SPM's motion has to be provided.

1.5 Thesis Outline

The remainder of the thesis is structured as follows:

Chapter 2 provides a detailed kinematic analysis of the coaxial SPM under study. It begins with a description of the general terminology and notation,

followed by the presentation of computation approaches for obtaining unique solutions to the forward and inverse kinematic problems of the SPM. The chapter also includes a discussion of the infinite rotation motion of the coaxial SPM.

Chapter 3 describes the 3D-printed mechanical prototype developed for conducting experimental tests. It also demonstrates the simulation model designed in the CopelliaSim robotic simulator to verify link collision detection and control strategies used later in the thesis.

Chapter 4 presents the numerical methodology used to generate the Cartesian workspace and configuration space for the coaxial SPM, including singularity analysis and link collision detection approaches. Three case studies with the simulation model and the real prototype are presented to demonstrate the application of the developed configuration space in motion trajectory generation.

Chapter 5 demonstrates the orientation control developed for the coaxial SPM prototype with external reference tracking and object stabilization capabilities. Two cases are presented to demonstrate the application of the developed orientation control.

Chapter 6 concludes the thesis by highlighting its main achievements and contributions, as well as informing on the limitations of the conducted research and providing recommendations for future studies and experiments.

Chapter 2

Kinematic Analysis

2.1 Overview

The design process of any robotic mechanism should start with its kinematic modeling and analysis, which is followed by the detailed characterization of its Cartesian workspace and its joint space. The operation and control of robot manipulators are based on the results of their kinematic analysis. Due to the complex architecture of PMs, their kinematic analysis is usually a lot more complicated if compared to SMs. For example, forward and inverse kinematic problems of general 3-DOF 3-RRR SPM, and coaxial SPM in particular, result in at most 8 solutions each [65]. As is the case for most PMs, inverse kinematics of 3-RRR SPMs is easier to solve and can be solved analytically as derived in [61, 64], though the problem of obtaining several solutions still exists. Unfortunately, forward kinematics of 3-RRR SPMs has no closed-form solutions and is usually solved using numerical methods, that are often computationally demanding.

An approach to solve SPM's forward kinematics based on the derivation of the polynomial characteristic equation was described in [66]. It was demonstrated that this polynomial is of 8-th order and is minimal; solving it results in at most 8 real solutions to the SPM forward kinematic problem. In this approach, the orientation of the mobile platform is described by means of Euler angles. Another approach for describing the mobile platform's orientation is based on using the input-output equations of spherical four-bar linkages as reported in [232]. Solving obtained trigonometric equations using a semi-graphical approach

was outlined in [233]. Other methods based on solving polynomial expressions of forward kinematics of 3-RRR SPMs include [68, 276]. A method that involves training neural networks was attempted in [277]. It is also a common practice, to design special kinematic architectures that result in simplified forward kinematics as in [65, 78]. In such designs, geometric parameters are selected in a way that allows for simplifying trigonometric equations. For example, the special geometry of Agile Eye as in [78] allows obtaining a closed-form solution for the forward kinematics and succeeded by its application in the real-time control. Redundant additional sensors such as external video cameras and rotary position sensors can also be used to simplify the forward kinematic analysis and estimate the actual orientation of the mobile platform [149, 278–284]. This allows for determining a single solution corresponding to the manipulator's assembly mode uniquely, which is desirable for fast and correct control algorithms. However, it requires the addition of extra sensors, which in some occasions is not desired as it can increase the cost of the system. In this regard, a numerical approach for obtaining unique solutions, corresponding to a working or assembly mode of an SPM's prototype, with no extra sensors use, was proposed in [89].

The kinematic analysis of the coaxial SPM studied in this thesis follows a similar numerical approach as in [89]. Being a specific case of the general SPM, coaxial SPM's kinematics is based on the same fundamentals adapted from [66, 77, 232, 233]. This Chapter briefly introduces these fundamentals (Section 2.2), as well as an approach for obtaining unique forward and inverse kinematic solutions of the coaxial SPM (Sections 2.3 and 2.4, respectively). Methodology and algorithms presented in these Sections were published in a conference paper titled *"Computation of Unique Kinematic Solutions of a Spherical Parallel Manipulator with Coaxial Input Shafts"* [285], and presented at the 2019 IEEE 15th International Conference on Automation Science and Engineering. This paper was later extended with an approach and algorithm for generating infinite rotational motion of the coaxial SPM (Section 2.5). This work was published in a conference paper titled *"Infinite Torsional Motion Generation of a Spherical Parallel Manipulator with Coaxial Input Axes"* [286], and presented at the 2020 IEEE/ASME International Conference on Advanced Intelligent Mechatronics.

2.2 Kinematic Model

The kinematic structure of a general 3-RRR SPM shown in Fig. 2-1 is composed of a *mobile platform*, whose geometry is defined by angle β, and a fixed *base* platform, whose geometry is defined by angle γ. These triangular pyramid-shaped platforms (outlined in Fig. 2-1 with dotted lines) are connected to each other by three equally-distributed *legs*, which are numbered as $i = 1, 2, 3$ in the counter clockwise direction. Each leg is a chain of two *links*, a *proximal/lower link* and a *distal/upper link*, with all their joints being of a revolute (R) type. Dimensions of these links are defined by angles α_1 and α_2, respectively. All joint axes intersect at a common point, known as a *center of rotation*, around which the mobile platform has its 3-DOF spherical motion.

The axes of the joints are defined by unit vectors $\mathbf{u}_i$, $\mathbf{w}_i$, and $\mathbf{v}_i$, for $i = 1, 2, 3$, and correspond to input joints, intermediate joints, and mobile platform's joint, respectively. In the special case of the coaxial SPM, the base platform is degenerated to a single line due to the coaxial placement of the input joints, as demonstrated in Fig. 2-2. In this arrangement of the input joints, angle $\gamma = 0°$. It is due to this geometric feature an infinite rotational motion of the SPM's mobile platform is possible.

Orientation of the coaxial SPM, i.e., of its mobile platform, is described by unit vectors $\mathbf{v}_i$, $i = 1, 2, 3$. To describe orientation, the fixed reference frame (coordinate system) is used with an origin at the center of rotation. The z-axis is

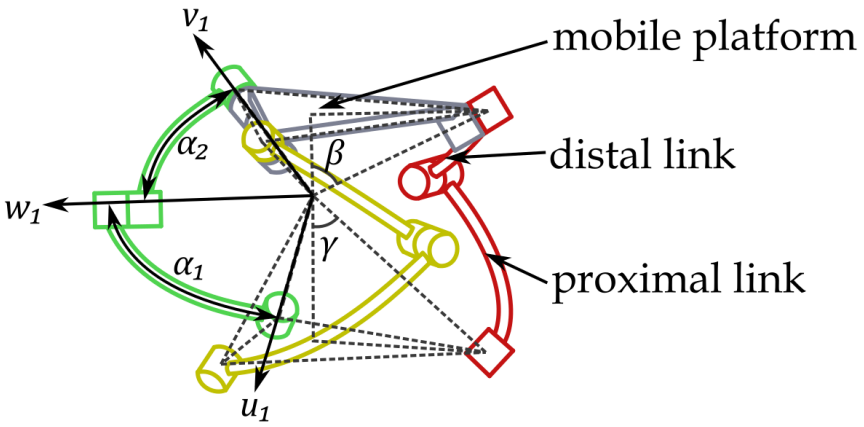

Figure 2-1: General SPM model

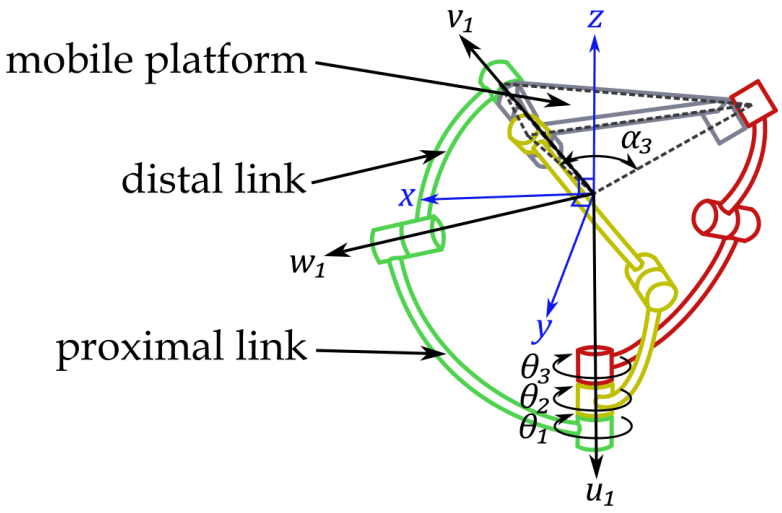

Figure 2-2: Coaxial SPM model

collinear with input joint axes and is directed upwards. At the *home configuration*, the x-axis is located in the plane formed by the z-axis and the unit vector $\mathbf{w}_1$. Moreover, the normal vector of the mobile platform coincides with the z-axis. The y-axis is determined by the right-hand rule. The axes of the input joints of the coaxial SPM are defined in the reference frame as:

$$\mathbf{u}_i = \begin{bmatrix} 0 \\ 0 \\ -1 \end{bmatrix}, \quad i = 1, 2, 3. \tag{2.1}$$

Actuation of the manipulator happens through the input joints, and their positions are defined in the vector form as $\boldsymbol{\theta} \triangleq \begin{bmatrix} \theta_1, \theta_2, \theta_3 \end{bmatrix}^T$. Input commands also can be treated as a movement of proximal links. In this case, input joint positions are treated as the angular distance between central planes of the proximal links at the home configurations and at any other configuration of coaxial SPM. So, at the home configuration, input joint positions are set to $\boldsymbol{\theta} = \begin{bmatrix} 0, 0, 0 \end{bmatrix}^T$. As depicted in Fig. 2-3, the clockwise direction of rotation is chosen as the positive direction.

The axes of the intermediate joints of the coaxial SPM are expressed in the

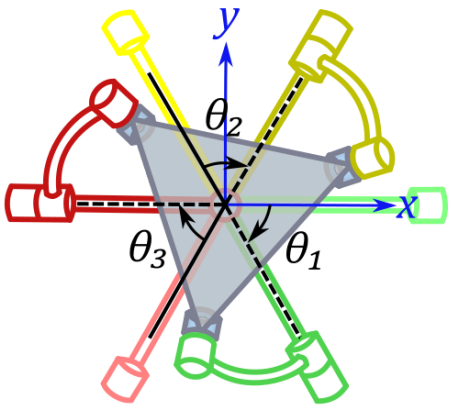

Figure 2-3: Coaxial SPM's input joint positions

reference frame as:

$$\mathbf{w}_i = \begin{bmatrix} \cos(\eta_i - \theta_i)\sin\alpha_1 \\ \sin(\eta_i - \theta_i)\sin\alpha_1 \\ -\cos\alpha_1 \end{bmatrix}, \quad i = 1, 2, 3, \tag{2.2}$$

where angle $\eta_i = 2(i-1)\pi/3$, $i = 1, 2, 3$ is the angular offset distance between each leg and stays as a constant value for each i-th leg.

To rotate the mobile platform by some angle σ preserving the direction of its normal vector $\mathbf{n}$, as pictured in Fig. 2-4, the new instances of unit vectors $\mathbf{v}_{i,rot}$, $i = 1, 2, 3$, are computed using the Rodrigues' rotation formula [287]:

$$\mathbf{v}_{i,rot} = \mathbf{v}_i \cos\sigma + (\mathbf{v}_i \times \mathbf{n})\sin\sigma + \mathbf{n}(\mathbf{n} \cdot \mathbf{v}_i)(1 - \cos\sigma), \quad i = 1, 2, 3 \tag{2.3}$$

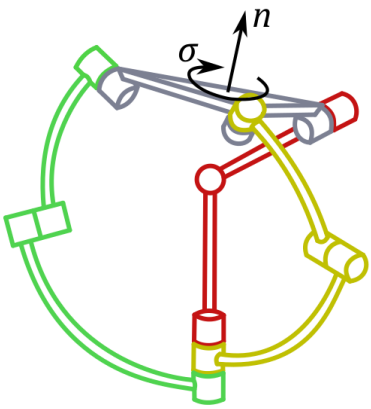

Figure 2-4: Positive direction of the roll-rotation

2.3 Forward Kinematics

Solving the forward kinematic problem of a coaxial SPM is defined as finding each possible orientation (pose) of the mobile platform, i.e., the unit vectors $\mathbf{v}_i$, $i = 1, 2, 3$, for the given input joint variables, $\boldsymbol{\theta}$.

There exists multiple solutions to the forward kinematic problem of a coaxial SPM for any given input configuration [66]. For example, as for the cases of the coaxial SPM with $\alpha_1 = 45°$, $\alpha_2 = 90°$, and $\beta = 60°$ as shown in Fig. 2-5, and coaxial SPM with $\alpha_1 = 45°$, $\alpha_2 = 90°$, and $\beta = 90°$ as shown in Fig. A-1 at their home configurations, i.e., when angular displacements of all input joints are equal to zero, $\boldsymbol{\theta} = \begin{bmatrix} 0°, 0°, 0° \end{bmatrix}^T$. The eight solutions are given in Table 2.1 and Table A.1, respectively, and were found using SolidWorks CAD software. These solutions represent different assembly modes of the mentioned SPMs [72], with only poses (a) and (b) in both figures being of any meaningful use due to the absence of orientations with almost folded legs, which would require distal links to pass through each other which physically is not possible. Solutions (a) represent assembly modes with the left-sided arrangement of their distal links, i.e., these links are located to the left of the central symmetry plane of the respective proximal links at their home configuration. In this thesis, such a pose is called the *l-l-l* assembly mode. Following the same explanation, solutions (b) represent the *r-r-r* assembly mode. To predict the motion of a manipulator correctly while it is controlled via the input joints, it is required to obtain unique solutions from the forward kinematic analysis corresponding to its current assembly mode.

To define the forward kinematic problem, a system of nine independent equations with nine unknowns can be derived from geometric constraints of a coaxial SPM [233]:

$$\begin{cases} \mathbf{w}_i \cdot \mathbf{v}_i = \cos\alpha_2, & i = 1, 2, 3, \\ \mathbf{v}_i \cdot \mathbf{v}_j = \cos\alpha_3, & i, j = 1, 2, 3, \quad i \neq j, \\ \|\mathbf{v}_i\| = 1, \end{cases} \tag{2.4}$$

where $\alpha_3 = 2\sin^{-1}\left(\sin\beta\cos\frac{\pi}{6}\right)$ is the angle between axes of the i-th and j-th mobile platform joints (Fig. 2-2), and $\|\cdot\|$ is the Euclidean norm.

The system of equations (2.4) is nonlinear, leads to multiple solutions (not limited to 8 solutions), and can not be solved in a closed form. Therefore, a numerical method-based approach can be used to compute unit vectors $\mathbf{v}_i$, $i = 1, 2, 3$. For example, trust-region numerical optimization method was used in this thesis for this case [288]. This method is implemented in `fsolve` function in MATLAB, requiring an initial guess vector $\boldsymbol{x}_0$. The values of this vector are the guesses of x, y, and z components of the unit vectors $\mathbf{v}_i$, $i = 1, 2, 3$, represented as follows:

$$\boldsymbol{x}_0 = \Big[v_{1x}, v_{1y}, v_{1z}, v_{2x}, v_{2y}, v_{2z}, v_{3x}, v_{3y}, v_{3z}\Big]^T. \tag{2.5}$$

This method can provide multiple solutions depending on the selection of the guess vector. Selecting an appropriate vector can ensure that an SPM stays in its current assembly mode. For example, for the *l-l-l* assembly mode, it is expected that the unit vectors $\mathbf{v}_i$, $i = 1, 2, 3$, are always positioned further in the positive direction of link rotations (clockwise). Thus, the guess vector can be chosen as the positive-shifted instance of the unit vectors $\mathbf{w}_i$, $i = 1, 2, 3$, and pointing in the same z direction as at the home configuration. An example of such shift of the unit vectors $\mathbf{w}_i$, $i = 1, 2, 3$, could be a 10° rotation around the z-axis, expressed using the Rodrigues' rotation formula [287] as follows:

$$\mathbf{w}_{i,rot} = \mathbf{w}_i \cos 10^\circ + \left(\mathbf{w}_i \times \begin{bmatrix}0\\0\\1\end{bmatrix}\right) \sin 10^\circ + \begin{bmatrix}0\\0\\1\end{bmatrix} \left(\begin{bmatrix}0\\0\\1\end{bmatrix} \cdot \mathbf{w}_i\right)\big(1 - \cos 10^\circ\big), i = 1, 2, 3. \tag{2.6}$$

The resultant guess vector is then formulated as follows:

$$\boldsymbol{x}_0 = [w_{1x,rot}, w_{1y,rot}, -w_{1z,rot}, w_{2x,rot}, w_{2y,rot}, -w_{2z,rot}, w_{3x,rot}, w_{3y,rot}, -w_{3z,rot}]^T. \tag{2.7}$$

The z components of the guess vector, i.e. $w_{1z,rot}$, $w_{2z,rot}$, and $w_{3z,rot}$, are negated as the unit vectors $\mathbf{w}_i$, $i = 1, 2, 3$, have these components in the negative z direction (for cases when $\alpha_1 < 90^\circ$), but typically the unit vectors $\mathbf{v}_i$ $i = 1, 2, 3$, have z components pointing in the positive z direction. Selecting this guess vector allows obtaining a unique solution of the forward kinematic problem correspond-

ing to the *l-l-l* assembly mode. Note that for the *r-r-r* assembly mode, Equation (2.6) will have -10° shift (negative direction of rotation).

The process of computing a unique forward kinematics solution is summarized in Algorithm 1.

Algorithm 1: Obtaining a unique solution of the forward kinematic problem of a coaxial SPM

Input: $\boldsymbol{\theta}$, α_1, α_2, β, $\boldsymbol{x}_0$, η_i, $i = 1, 2, 3$
Output: Unique unit vectors $\mathbf{v}_i$, $i = 1, 2, 3$

Calculate $\alpha_3 = 2\sin^{-1}\big(\sin\beta\cos\frac{\pi}{6}\big)$;
for $i \leftarrow 1$ **to** 3 **do**
    Calculate $\mathbf{w}_i$ using (2.2) given $\boldsymbol{\theta}$;
    Calculate $\mathbf{w}_{i,rot}$ using (2.6);
Calculate initial guess vector $\boldsymbol{x}_0$ using (2.7);
Calculate $\mathbf{v}_i$, $i = 1, 2, 3$, by solving system of equations (2.4) numerically, given $\mathbf{w}_i$, $i = 1, 2, 3$, with initial guess vector $\boldsymbol{x}_0$;

A numerical example is included here to demonstrate the application of Algorithm 1 in determining the unique orientation of the coaxial SPMs with different mobile platform geometry presented in Fig. 2-5. Three additional examples are included in Appendix A. Figs. 2-5 and A-1 depict SPMs at their home configuration, while Figs. A-2 and A-3 represent non-zero input examples with $\boldsymbol{\theta} = \Big[60^\circ, 90^\circ, 120^\circ\Big]^T$ and their orientations described as recorded in Tables A.2 and A.3, respectively. Note the geometry of coaxial SPMs in the figures. For Figs. 2-5 and A-2, $\alpha_1 = 45^\circ$, $\alpha_2 = 90^\circ$, $\beta = 60^\circ$, whereas, for Figs. A-1 and A-3, $\alpha_1 = 45^\circ$, $\alpha_2 = 90^\circ$, $\beta = 90^\circ$. Following Algorithm 1, solutions corresponding to *l-l-l* and *r-r-r* assembly modes were obtained and verified by comparing with the results retrieved from SolidWorks CAD software and recorded in Tables 2.2 and A.4. All calculations were conducted using MATLAB.

Orientations obtained for the poses from Figs. 2-5a and 2-5b, can be compared to the ones from [232]'s Table II, solutions No. (8) and (2), respectively. They do match if the difference in the base reference frames is accounted for. In [232], the y-axis is formed between the y-axis and the unit vector $\mathbf{w}_1$, whereas here it is the x-axis formed in this way. So, it is similar to positive 90° rotation of the unit vectors $\mathbf{v}_i$, $i = 1, 2, 3$ obtained here around the z-axis, in which the x-component becomes y-component, and y-component becomes negative x-

component.

Table 2.1: Solutions to the forward kinematics using CAD (Example 1).

Solution	$\mathbf{v}_1^T$	$\mathbf{v}_2^T$	$\mathbf{v}_3^T$
Fig. 2-5a	$[0.500, -0.707, 0.500]$	$[0.362, 0.787, 0.500]$	$[-0.862, -0.079, 0.500]$
Fig. 2-5b	$[0.500, 0.707, 0.500]$	$[-0.862, 0.079, 0.500]$	$[0.362, -0.787, 0.500]$
Fig. 2-5c	$[-0.538, -0.649, -0.538]$	$[-0.733, 0.289, 0.616]$	$[-0.061, 0.769, -0.636]$
Fig. 2-5d	$[-0.616, -0.490, -0.616]$	$[-0.697, 0.332, 0.636]$	$[0.294, -0.790, 0.538]$
Fig. 2-5e	$[0.616, 0.490, 0.616]$	$[0.697, -0.332, -0.636]$	$[-0.294, 0.790, -0.538]$
Fig. 2-5f	$[0.538, 0.649, 0.538]$	$[0.733, -0.289, -0.616]$	$[0.061, -0.769, 0.636]$
Fig. 2-5g	$[0.636, 0.438, 0.636]$	$[-0.831, 0.141, 0.538]$	$[-0.116, 0.779, -0.616]$
Fig. 2-5h	$[-0.636, -0.438, -0.636]$	$[0.831, -0.141, -0.538]$	$[0.116, -0.779, 0.616]$

Table 2.2: Comparison of the forward kinematics solutions (Example 1).

Orientation	$\mathbf{v}_1^T$	$\mathbf{v}_2^T$	$\mathbf{v}_3^T$
Fig. 2-5a CAD	$[0.500, -0.707, 0.500]$	$[0.362, 0.787, 0.500]$	$[-0.862, -0.079, 0.500]$
Fig. 2-5a calculated	$[0.5000, -0.7071, 0.5000]$	$[0.3624, 0.7866, 0.5000]$	$[-0.8624, -0.0795, 0.5000]$
Fig. 2-5b CAD	$[0.500, 0.707, 0.500]$	$[-0.862, 0.079, 0.500]$	$[0.362, -0.787, 0.500]$
Fig. 2-5b calculated	$[0.5000, 0.7071, 0.5000]$	$[-0.8624, 0.0795, 0.5000]$	$[0.3624, -0.7866, 0.5000]$

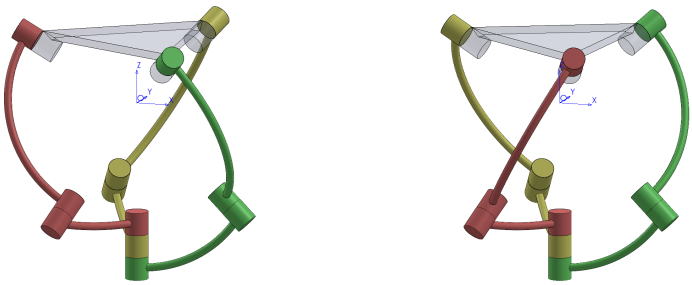

(a)

(b)

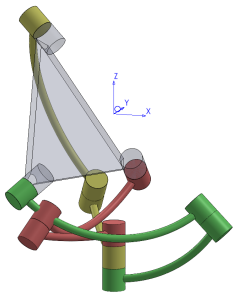

(c)

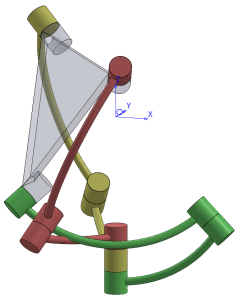

(d)

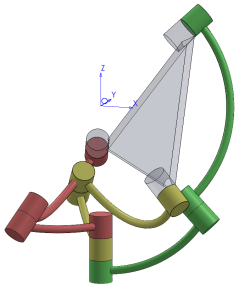

(e)

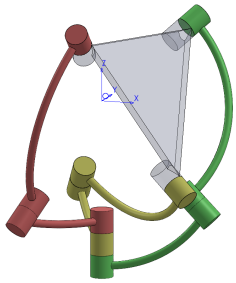

(f)

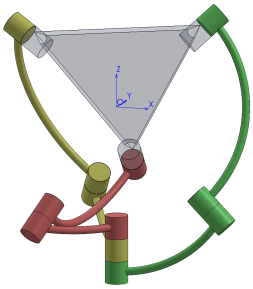

(g)

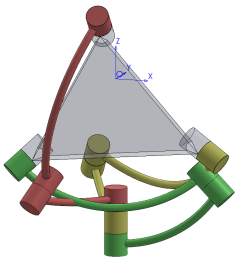

(h)

Figure 2-5: Solutions to the forward kinematics for zero input (Example 1)

2.4 Inverse Kinematics

Solving the inverse kinematic problem of the coaxial SPM is defined as finding each possible input joint variables, $\boldsymbol{\theta}$, given the orientation (pose) of the mobile platform, i.e., the unit vectors $\mathbf{v}_i$, $i = 1, 2, 3$.

The inverse kinematic problem of the coaxial SPM is easier than the forward one since it can be solved analytically. Although the problem of obtaining multiple solutions persists. Obtaining unique solutions to the inverse kinematic problem of a manipulator corresponding to the current configuration is necessary to generate smooth trajectories for its motion.

Three uncoupled equations used to compute each of input joint variable θ_i, $i = 1, 2, 3$, are formulated as [77]:

$$A_i T_i^2 + 2\, B_i T_i + C_i = 0, \quad i = 1, 2, 3, \tag{2.8}$$

with

$$T_i = \tan\left(\frac{\theta_i}{2}\right). \tag{2.9}$$

These equations are derived from the first equation from the system of equations (2.4), and have coefficients A_i, B_i, and C_i defined as:

$$\begin{aligned} A_i &= -\cos\eta_i \sin\alpha_1 v_{ix} - \sin\eta_i \sin\alpha_1 v_{iy} - \cos\alpha_1 v_{iz} - \cos\alpha_2; \\ B_i &= \sin\eta_i \sin\alpha_1 v_{ix} - \cos\eta_i \sin\alpha_1 v_{iy}; \\ C_i &= \cos\eta_i \sin\alpha_1 v_{ix} + \sin\eta_i \sin\alpha_1 v_{iy} - \cos\alpha_1 v_{iz} - \cos\alpha_2, \end{aligned} \tag{2.10}$$

where v_{ix}, v_{iy}, and v_{iz} are components of the unit vectors $\mathbf{v}_i$, $i = 1, 2, 3$.

Equations (2.8) are decoupled quadratic equations for each input joint variable θ_i, $i = 1, 2, 3$ with two roots for each T_i. This results in eight combinations of possible solutions for the input joint variables, representing eight *working modes*. Four examples representing coaxial SPM with different geometry of the mobile platform, and at different orientations are shown in Figs. 2-6 and B-1-B-3. It can be observed from these figures that the orientation of the mobile platform is the same in each case, and eight possible solutions are formed by changing the bending (left-bended or right-bended) of one of the legs while the other two are

fixed. Obtaining solutions by having two legs fixed, and changing the bending of the other is also supported by the uncoupled nature of Equation (2.8). Similarly to the forward kinematic analysis, the location of the distal links can be defined as left-sided or right-sided relative to the proximal links. Therefore, in this thesis, this parameter is used to label obtained working modes. Due to the symmetry, the *l*-*l*-*l* and the *r*-*r*-*r* working modes are preferred.

To compute a unique solution to the inverse kinematic problem that corresponds to the *l*-*l*-*l* working mode, it is necessary to select the solution derived from the roots with the added square root of the discriminant (the definition of the positive direction of rotation) while solving Equation (2.8). On the other hand, the combination corresponding to the roots with the subtracted square root of the discriminant presents the solution for the *r*-*r*-*r* working mode.

Similarly to the forward kinematics, Algorithm 2 for obtaining unique solutions to the inverse kinematic problem can be outlined and is given below.

Solutions, i.e., input joint variables, $\boldsymbol{\theta}$, corresponding to the *l*-*l*-*l* and *r*-*r*-*r* working modes are given in Tables 2.3 and B.1. These solutions were retrieved using SolidWorks CAD software and compared with the ones obtained with Algorithm 2 using MATLAB. The results match, with the only difference in some signs, which are the same locations on the unit circle but measured from the opposite direction. The sign difference comes from Equation (2.9) and the used arc-tangent function, `atan` function in MATLAB, that returns the results on the closed interval from $-180°$ ($-\pi$) to $+180°$ ($+\pi$).

Table 2.3: Comparison of the inverse kinematics solutions (Example 1).

Orientation	$\mathbf{v}$	$\boldsymbol{\theta}_{CAD}$	$\boldsymbol{\theta}_{calculated}$
Fig. 2-6a	$\begin{bmatrix} 0.500 & 0.362 & -0.862 \\ -0.707 & 0.787 & -0.079 \\ 0.500 & 0.500 & 0.500 \end{bmatrix}$	$\begin{bmatrix} 0.00° \\ 0.00° \\ 0.00° \end{bmatrix}$	$\begin{bmatrix} 0.0000° \\ -0.0455° \\ 0.0473° \end{bmatrix}$
Fig. 2-6b	$\begin{bmatrix} 0.500 & 0.362 & -0.862 \\ -0.707 & 0.787 & -0.079 \\ 0.500 & 0.500 & 0.500 \end{bmatrix}$	$\begin{bmatrix} 109.47° \\ 109.47° \\ 109.47° \end{bmatrix}$	$\begin{bmatrix} 109.4631° \\ 109.4480° \\ 109.4799° \end{bmatrix}$

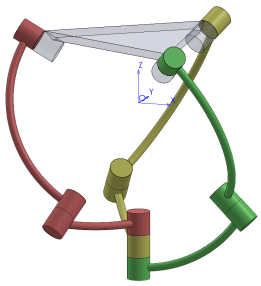

(a) *l-l-l* working mode

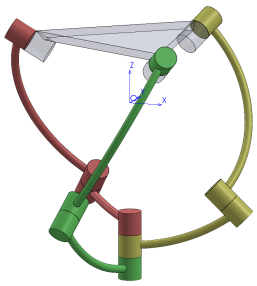

(b) *r-r-r* working mode

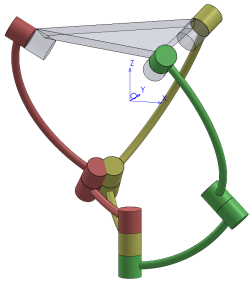

(c) *l-l-r* working mode

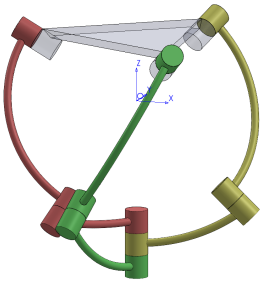

(d) *r-r-l* working mode

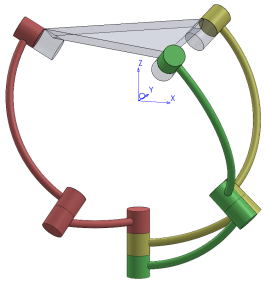

(e) *l-r-l* working mode

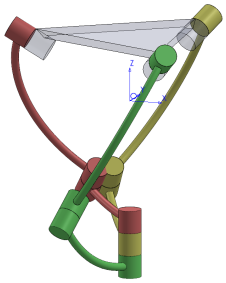

(f) *r-l-r* working mode

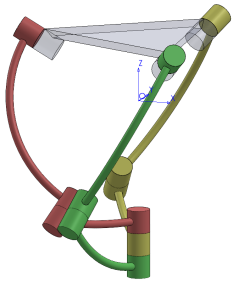

(g) *r-l-l* working mode

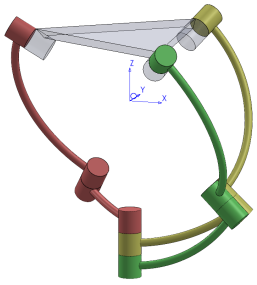

(h) *l-r-r* working mode

Figure 2-6: Solutions to the inverse kinematics (pose taken from Fig. 2-5a)

Algorithm 2: Obtaining a unique solution of the inverse kinematics problem of a coaxial SPM

Input: $\mathbf{v}_i$, $i = 1, 2, 3$, α_1, α_2, η_i
Output: Input joint positions vector $\boldsymbol{\theta}$

for $i \leftarrow 1$ **to** 3 **do**
  Calculate A_i, B_i, C_i using (2.10) given $\mathbf{v}_i$;
  Solve equation (2.8) for T_i;
  Find θ_i using equation (2.9) and select a solution coming from the root with added or subtracted square root of the discriminant for *l-l-l* or *r-r-r* working mode, respectively;
return θ_i, $i = 1, 2, 3$

2.5 Generation of Infinite Rotational Motions

One of the main characteristic features of the coaxial SPM is that it can infinitely rotate the mobile platform around its normal vector as shown in Fig. 2-4. To implement such a rotation at the specific pose of the mobile platform a particular sequence of input joint positions, $\boldsymbol{\theta}_{traj}$, has to be applied to the actuators.

The rotational motion of the mobile platform around its normal vector $\mathbf{n}$ can be interpreted as the rotation of the unit vectors $\mathbf{v}_i$, $i = 1, 2, 3$, around the same vector $\mathbf{n}$, which is computed as:

$$\begin{cases} \mathbf{n} = \dfrac{\mathbf{v}_1 + \mathbf{v}_2 + \mathbf{v}_3}{\|\mathbf{v}_1 + \mathbf{v}_2 + \mathbf{v}_3\|}, & \beta \neq 90^\circ, \\ \mathbf{n} = \dfrac{\mathbf{v}_1 \times \mathbf{v}_2}{\|\mathbf{v}_1 \times \mathbf{v}_2\|}, & \beta = 90^\circ. \end{cases} \tag{2.11}$$

The instantaneous orientation of the mobile platform during the rotational motion is defined by the unit vectors $\mathbf{v}_{i,rot}$, $i = 1, 2, 3$, and is computed following Equation (2.3). Angle σ is a rotation angle measured from the starting configuration till a rotational instant of interest as shown in Fig. 2-4.

Given the orientation of the coaxial SPM, its input joint positions, $\boldsymbol{\theta}$, are computed by solving the inverse kinematic problem, i.e., by following Algorithm 2. The rotational motion is sampled into a sequence of S instants with the rotation angles as:

$$\boldsymbol{\sigma} = \{\sigma_1,\ \sigma_2,\ \ldots\ \sigma_S\}. \tag{2.12}$$

For the simplicity of the numerical analysis, a uniform sampling interval of the rotation is used, i.e., $\delta_\sigma \triangleq \sigma_{j+1} - \sigma_j$, $j = 1, 2, ... S-1$, is constant.

The inverse kinematic problem is solved at each instant. Since Algorithm 2 returns results in the closed interval $-180°$ $(-\pi)$ to $+180°$ $(+\pi)$, appropriate adjustments should be implemented to the results to ensure smooth motion of the manipulator.

In case of reaching $+180°$ $(+\pi)$ side by one of the input joint positions θ_i, $i = 1, 2, 3$, while its sampled rotation, Algorithm 2 results will start from the $-180°$ $(-\pi)$ side at the next sampling instant. An extra $360°$ (2π) has to be to the joint having such value jump starting from the sampling instant it happened $\theta_{i,j}$, $j = 2, 3, ... S$, till the end of the rotational motion input trajectory $\theta_{i,S}$. Consequently, the input joints trajectory $\boldsymbol{\theta}_{traj}$ that leads to a full $360°$ rotation of the mobile platform around the vector $\mathbf{n}$ is generated. The infinite rotational motion of the coaxial SPM is achieved by applying the obtained input sequence $\boldsymbol{\theta}_{traj}$ repeatedly. However, each following rotation has to be accounted for by adding an extra $360°$ (2π) to the input sequence $\boldsymbol{\theta}_{traj}$ at the time when the ongoing rotation is finished, again, to ensure motion continuity.

Before applying the generated motion trajectories on the manipulator itself, it is necessary to verify that none of the input joint positions require any proximal links to surpass the neighboring ones by going through them to achieve corresponding orientation. An example of such link surpass is the input joints positions
$\boldsymbol{\theta} = \left[100°, 200°, 150°\right]^T$, which will be obtained as $\boldsymbol{\theta} = \left[100°, -160°, 150°\right]^T$ by Algorithm 2. In this case, the calculated input joint positions require the *proximal link 2* to move in the opposite direction compared to the other two proximal links, resulting in its collision with the *proximal link 3* while trying to surpass it. In general, link surpass happens when one of the input joint positions is greater than the following input joint position in the positive (clockwise) direction of SPM movement, i.e., $\theta_3 - \theta_2$, $\theta_2 - \theta_1$, or $\theta_1 - \theta_3$ is not greater than $120°$ (the thickness of SPM links is ignored). To solve this issue an extra $360°$ (2π) needs to be added for the entire motion trajectory to the proximal link being the earliest in the positive (clockwise) direction.

The presented approach for the infinite rotational motion generation is summarized in Algorithm 3. It applies to the rotational motions at the desired locations that do not lead to singularities or link collisions. Details on how to check for singularities and link collisions are presented in Chapter 4.

Algorithm 3: Generation of an input joints trajectory for a full-circle rotational motion of a coaxial SPM

Input: $\mathbf{v}_i$, $i = 1, 2, 3$, α_1, α_2, η_i, $\boldsymbol{\sigma}$
Output: Input joints trajectory $\boldsymbol{\theta}_{traj}$

Calculate $\mathbf{n}$ using (2.11) given $\mathbf{v}_i$;
for $j \leftarrow 1$ **to** S **do**
    Calculate $\mathbf{v}_{i,j}$, $i = 1, 2, 3$, using (2.3) with σ_j and $\mathbf{n}$;
    Calculate input joint positions $\boldsymbol{\theta}_j$ for each $\mathbf{v}_{i,j}$, $i = 1, 2, 3$, using Algorithm 2;
    $\boldsymbol{\theta}_{traj}(j) \leftarrow \boldsymbol{\theta}_j$;
/* check for 360° jumps in $\boldsymbol{\theta}_{traj}$ */
for $k \leftarrow 1$ **to** $S - 1$ **do**
    if $\theta_{1,k} - \theta_{1,k+1} > 0°$ **then**
        $\theta_{1,k+1} = \theta_{1,k+1} + 360°$;
    if $\theta_{2,k} - \theta_{2,k+1} > 0°$ **then**
        $\theta_{2,k+1} = \theta_{2,k+1} + 360°$;
    if $\theta_{3,k} - \theta_{3,k+1} > 0°$ **then**
        $\theta_{3,k+1} = \theta_{3,k+1} + 360°$;
/* check for link surpass */
if $\theta_{3,1} - \theta_{2,1} > 120°$ **then**
    $\theta_{2,1\ldots S} = \theta_{2,1\ldots S} + 360°$;
if $\theta_{2,1} - \theta_{1,1} > 120°$ **then**
    $\theta_{1,1\ldots S} = \theta_{1,1\ldots S} + 360°$;
if $\theta_{1,1} - \theta_{3,1} > 120°$ **then**
    $\theta_{3,1\ldots S} = \theta_{3,1\ldots S} + 360°$;
return $\boldsymbol{\theta}_{traj}$

Chapter 3

Mechanical Prototype and Simulation Model

To facilitate the experimental studies on robotic manipulators it is often desirable to have a mechanical prototype and a simulation model. Virtual simulations of the experiments can help to discover any flaws in the mechanical design before its manufactured, or in control algorithms before they are tested on the manufactured prototype. They can also be used to perform additional studies on the manipulators such as link collision detection while estimating its workspace. A mechanical prototype is necessary to verify that the developed methodology for the analysis and control works in real-world settings.

This chapter describes the mechanical prototype of the coaxial SPM under study designed using SolidWorks CAD software and manufactured using rapid prototyping technologies such as 3D printing. It also reports the methods used to create a simulation model of the coaxial SPM in CoppeliaSim (formerly known as *V-REP*) [289] robotic simulator software. The simulation model developed here is used in Chapter 4 to detect the configurations leading to link collisions.

The content presented in this chapter was published in a conference paper titled *"Modeling and simulation of spherical parallel manipulators in CoppeliaSim (V-REP) robot simulator software"* [290], and presented at the 2020 International Conference Nonlinearity, Information and Robotics (NIR).

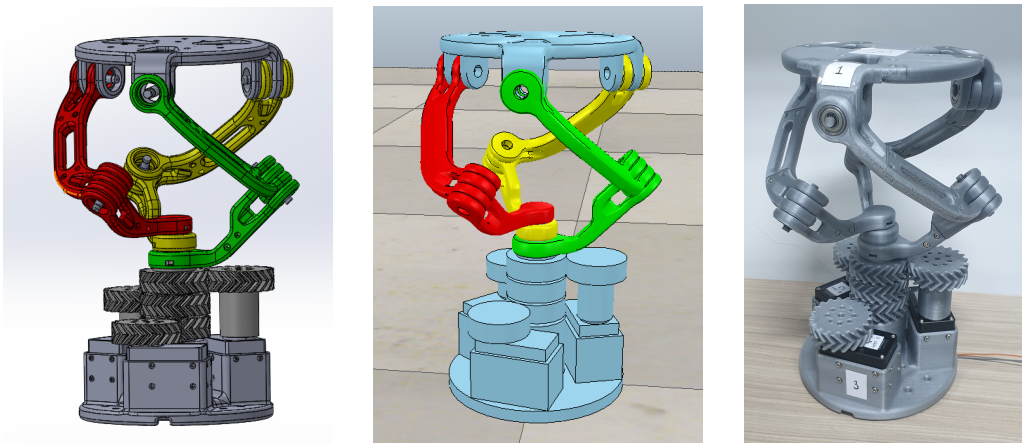

(a) (b) (c)

Figure 3-1: Coaxial SPM: (a) CAD model, (b) simulation model, (c) 3D-printed prototype

3.1 Mechanical Prototype

Before the mechanical design process of a manipulator starts, firstly its geometry parameters have to be selected. It was decided to model the coaxial SPM with $\alpha_1 = 45°$, $\alpha_2 = 90°$, $\beta = 90°$, similar to the ones from Figs. A-1, A-3, B-1, and B-3. The values for these parameters were selected to approximately match one of the Pareto-optimal SPM design solutions (Table 5, Design ID I: $\alpha_1 = 47.2°$, $\alpha_2 = 91.7°$, $\beta = 88.4°$) presented in [239], where a multi-objective design optimization problem was formulated to determine the configuration of a coaxial SPM with minimum mass and increased dexterity. These values also almost match numerically optimized design parameters (Table 2, Design ID I: $\alpha_1 = 48°$, $\alpha_2 = 90°$, $\beta = 90°$) presented in [235]. The selection of such geometry will allow conducting of future comparison studies with the coaxial SPM prototypes presented in the referenced works, which is outside of the scope of this thesis. It was also desirable to have $\alpha_1 \neq \alpha_2$ to avoid II and III singularity types discussed later in Section 4.1.

Next, a CAD model with the selected geometric parameters was designed in SolidWorks CAD software and is depicted in Fig. 3-1a. The *l*-*l*-*l* assembly mode was selected for the model. Fig. 3-2 illustrates a cross-sectional view of the designed coaxial SPM. The central vertical planes of the proximal links coincide with planes formed between the z-axis and the symmetry axes of the links' corresponding actuator gears. This orientation is considered as the home configuration

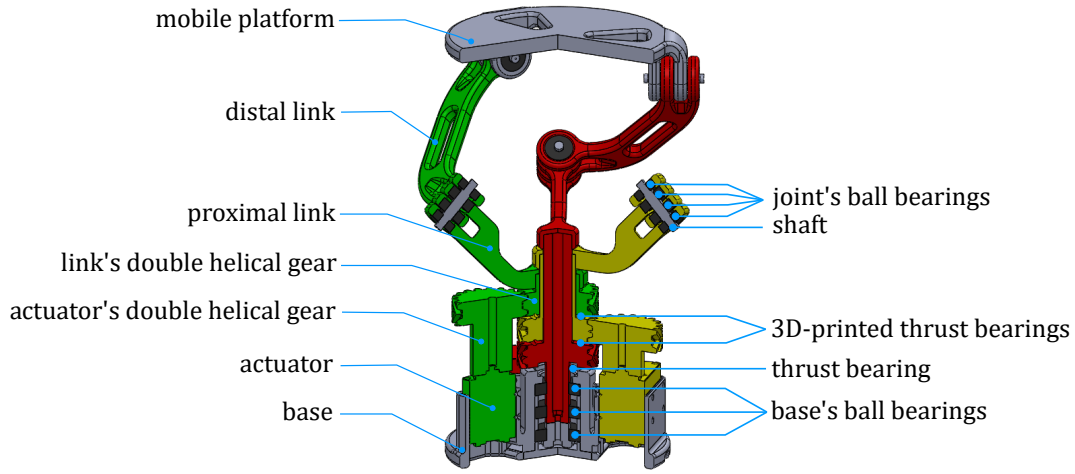

Figure 3-2: Cross-sectional view of the coaxial SPM CAD model

of the manipulator.

Three ball bearings are used in the base to decrease input joints axes play (backlash) and mitigate the effects of a single bearing's internal radial clearance. Following a similar reasoning, all intermediate and platform joints were equipped with four ball bearings (two per link). Since the bearing used in the real prototype were not very expensive, and thus of less precision accuracy, such measures were required to have a stiffer structure. The metal thrust bearing between *proximal link 3*'s gear (red-colored on Fig. 3-2) and the base, and two 3D-printed thrust bearings between link gears (bearing washers are integrated into the design of the gears) are included to provide smoother motion with less friction. The double helical gears (herringbone gears) with gear ratio 1:1 are used to transmit the actuator's motion to the input joints providing smooth motion with reduced backlash [291].

The parts of the prototype (links, mobile platform, base, gears) were manufactured using 3D printing technology with PLA plastic filament on Ultimaker Extended 2+ 3D printer. The assembled experimental prototype is shown in (Fig. 3-1c). Its dimensions are L 200 mm x W 200 mm x H 290 mm (bounding box at the home configuration). Actuation of the input joints is performed by three equidistantly located Dynamixel XM540-W150 servomotors from ROBOTIS. The servomotors are controlled via MATLAB using Dynamixel SDK (Protocol 2.0) API. They also can be controlled in ROS with the ROBOTIS Dynamixel

SDK package.

3.2 Simulation Model

Simulation tools are widely used for modeling manipulator's kinematics and dynamics, path planning and trajectory optimizations, performance evaluation, and verification of control algorithms with simulations performed prior to the real-world experiments on the manufactured prototypes. There exist plenty of simulation tools that allow visualization and performing kinematic and/or dynamic analyses of PMs. Most of them are created to solve a particular problem or tailored to a specific type of robot [292–297]. Among the general-purpose simulators, *Gazebo* simulator [298] developed by Open Source Robotics Foundation is the most well-known example. It is ROS [299] compatible, supports multiple physics engines, and can provide realistic 3D rendering. It can also work with dynamic robot bodies with C++-based scripting. Another known simulator example is *Webots* tool [300] developed by Cyberbotics Ltd mainly to simulate mobile wheeled robots. Robots in *Webots* can be programmed with C/C++, Python, Java, MATLAB or ROS through an API. The other examples include: *RoboDK* [301] for simulating industrial robot-manipulators, *Adams* capable of multibody dynamics simulation of closed-loop kinematic chains, etc. Analysis of the listed simulators revealed that they are not well suited for simulating PMs and require advanced knowledge of the software.

It was decided to use *CoppeliaSim* [289] general-purpose robot simulation tool developed by Coppelia Robotics. It is available for research and academic purposes for free. CoppeliaSim is compatible with ROS, and it supports internal and external scripting with C/C++, Python, MATLAB through external API. Physics engines such as ODE, Bullet, Vortex, Newton, and MuJoCo are integrated in CoppeliaSim. The main reason for selecting this tool was the fact that it can handle the inverse/forward kinematics of any type of mechanism with workspace visualization, sensor simulation, distance calculation, and collision detection. It also has built-in examples of several PMs that helped to model the coaxial SPM under study. CoppeliaSim is also useful for the future dynamic analysis as it

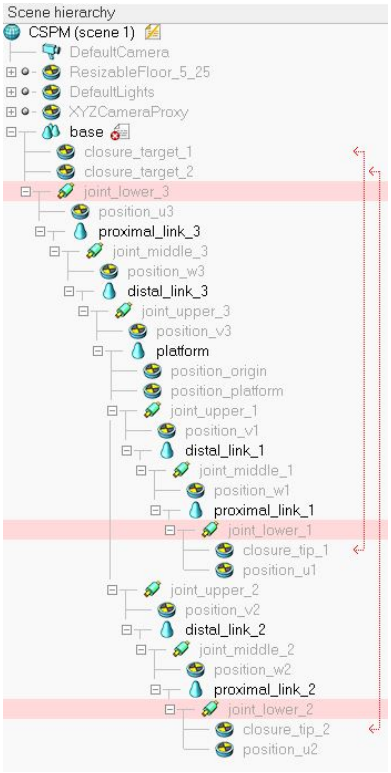

Figure 3-3: CoppeliaSim scene hierarchy

can include the inertia of all manipulator parts, actuators, gears, etc. Using the external API and Python or MATLAB scripts it will be useful to generate various test-scenarios for the coaxial SPM's dynamic analysis. The limitations of the CoppeliaSim robot simulator include limited physics simulation accuracy for very complex objects in real-time control settings. Thus, the simulation model of the manipulator has to be simple and without unnecessary details such as screws, bolts, etc.

To prepare the created CAD model for import into CoppeliSim, it is necessary to simplify its model by removing non-crucial design details such as fixtures, interior holes, and gear teeth. It will help to speed up calculations for the software, for example, for link collision detection. Afterward, it was imported to CoppeliaSim in STL format as a combined assembly and divided inside into several parts corresponding to the manipulator's links. The resulting model of the coaxial SPM, shown in Fig. 3-1b, consists of 8 shapes: the base, 3 distal links, 3 proximal links, and the mobile platform. Actuators and gears were combined with the base and do not play a role in the manipulator's actuation in the developed simulation model. Actuation is implemented through proximal links by applying

angular displacement directly on them from the central rotational axis. It is also necessary to assemble the parts in a way that resembles the closed-loop kinematic architecture of the manipulator as shown in Fig. 3-3. So, two closed loops were constructed in the simulation model. The specific settings are described in detail in [290] and included in Appendix C.

As was mentioned earlier, the CoppeliaSim simulator has a built-in link collision detection module that allows for fast interference checking between any manipulator part or collection of parts. It uses data structures based on a binary tree of oriented bounding boxes [289, 302] for accelerations. Colliding links are visually flagged by changing their color as pictured with the black color in Fig. 3-4. In this figure, the collision between four SPM links, i.e., proximal link 2, distal link 2, proximal link 3, and distal link 3, is observed. In this thesis, CoppeliaSim was used to detect link collision while estimation of its Cartesian workspace and configuration space (C-space) as detailed in Section 4.2.

A numerical example demonstrating the correspondence between the coaxial SPM's orientation obtained in CoppeliaSim and the calculated one is given below. As an example, the input joint positions $\boldsymbol{\theta} = \left[60^\circ, 90^\circ, 120^\circ\right]^T$ are considered (as in Table A.3). To determine the orientation of the mobile platform, i.e., the unit vectors $\mathbf{v}_i$, $i = 1, 2, 3$, the approach from Algorithm 1 is used. Using MATLAB,

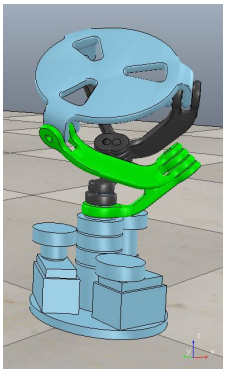

Figure 3-4: Simulation model of the coaxial SPM with detected link collision

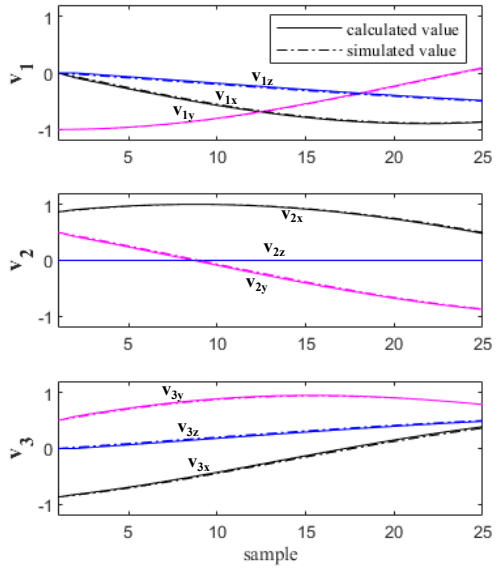

Figure 3-5: Calculated and simulated orientations of the coaxial SPM

the resulting orientation of the coaxial SPM is obtained as:

$$\begin{aligned} \mathbf{v}_{1,calc} &= \Big[-0.8626,\ 0.0790,\ -0.4997\Big]^T, \\ \mathbf{v}_{2,calc} &= \Big[0.5002,\ -0.8659,\ 0.0003\Big]^T, \\ \mathbf{v}_{3,calc} &= \Big[0.3618,\ 0.7866,\ 0.5003\Big]^T. \end{aligned} \tag{3.1}$$

The simulated orientation of the mobile platform has the following unit vectors:

$$\begin{aligned} \mathbf{v}_{1,sim} &= \Big[-0.8623,\ 0.0794,\ -0.5001\Big]^T, \\ \mathbf{v}_{2,sim} &= \Big[0.5001,\ -0.8660,\ 0.0000\Big]^T, \\ \mathbf{v}_{3,sim} &= \Big[0.3622,\ 0.7866,\ 0.5001\Big]^T. \end{aligned} \tag{3.2}$$

Time evaluations of the mobile platform orientation vectors $\mathbf{v}_i$, $i = 1, 2, 3$, during the SPM motion from the home configuration to the configuration corresponding to $\boldsymbol{\theta} = \Big[60°, 90°, 120°\Big]^T$ are shown in Fig. 3-5. The unit vectors $\mathbf{v}_i$, $i = 1, 2, 3$, are represented individually by their x, y, and z components. The simulated motion of the coaxial SPM closely matches the expected numerically pre-calculated behavior. This comparison is made based on 25 samples and interpolation values between them.

Based on the presented and the other numerous computation results and experimental trials on placing the manipulator in various arbitrary configurations, it was observed that CoppeliaSim was able to accurately simulate the coaxial SPM model, supported by numerical calculations using Algorithm 1.

Chapter 4

Configuration Space and Workspace Analyses

Before a manipulator finds its real-world applications, it is necessary to study its Cartesian workspace and joint space to detect singular configurations and avoid link collisions. The singularity- and collision-free motion planning between any two manipulator configurations have to be performed. This is specifically true for PMs due to their complex architecture, which can require a deeper link collision study than their serial counterparts. Examples of performed trajectory planning for PMs include: [303] for the Stewart platform, [304] for a planar 3-DOF PM, [305] for a 3-DOF parallel wrist based on the general SPM model, [124] for a 3-UPU wrist manipulator for sun tracking, etc.

For the coaxial SPM, it is also necessary to ensure that it has no near-singularity configurations and link collisions while its rotational movement around the normal vector of the mobile platform. This chapter presents a method for the numerical analysis of configuration space and the Cartesian workspace of the coaxial SPM for the case of singularity and link collision-free infinite rotational motions.

The results presented in this chapter were published in advance of the thesis in a journal paper titled *"Infinite rotational motion generation and analysis of a spherical parallel manipulator with coaxial input axes"* [306], and available online at Mechatronics journal at ScienceDirect web-portal.

4.1 Singularity Detection

PMs, similarly to SMs, are also prone to singularities. A singular configuration of a manipulator is pose at which it gains or loses some of its DOFs. One of the first research works that considered singularities of PMs was [307]. Three types of singularities were identified, and their physical interpretations were explained. As described in [72], some singularities correspond to the set of input joint positions for which the finite number of assembly modes changes. An example of such a case is when the mobile platform can be slightly moved while the manipulator's links are fixed. This type of singularity happens within the workspace of a parallel manipulator and is called *second type* in [307] and *parallel singularities* in [308]. In overall, such singular configurations are not reachable due to the physical interference of the links. Bonev and Gosselin published the work dedicated to this type of SPM singularities [71] since they can appear inside the Cartesian workspace and require more attention. Other types of singularities correspond to the set of manipulator orientations for which the finite number of working modes changes. In these configurations, the mobile platform is fixed but the input joint can be moved. It happens when the leg links are fully unfolded or folded. It is the boundary of a particular working mode's workspace, so this type of singularities happens on the boundary of the workspace and is called *first type* in [307] and *serial singularities* in [308]. There also exists the *third type* [307] happening only for specific link parameters, and for the cases when one of the previously mention singularity type occurs. For control purposes, it is necessary to keep a manipulator away from singular and near-singular configurations as its controllability is weak at these locations.

Singularity analysis of the coaxial SPM is based on the analysis of the relationship between the input joint rates and output angular velocity of the mobile platform as follows [307]:

$$\mathbf{J}_1\omega + \mathbf{J}_2\dot{\theta} = \mathbf{0}, \tag{4.1}$$

that can be equivalently represented as:

$$\dot{\boldsymbol{\theta}} = \mathbf{J}\omega, \tag{4.2}$$

where ω is the angular velocity of the mobile platform, $\dot{\boldsymbol{\theta}}$ is the input joint rates, and $\mathbf{J}$ is the Jacobian matrix that maps the angular velocity ω to the vinput joint rates $\dot{\boldsymbol{\theta}}$.

The Jacobian matrix can be defined as [77]

$$\mathbf{J} = -\mathbf{J}_2^{-1}\mathbf{J}_1, \tag{4.3}$$

$\mathbf{J}_1$ and $\mathbf{J}_2$ are both $n \times n$ Jacobian matrices ($n = 3$ for coaxial SPM), and configuration dependent, i.e., $\mathbf{J}_1 = \mathbf{J}_1(\mathbf{v}_i, \boldsymbol{\theta})$ and $\mathbf{J}_2 = \mathbf{J}_2(\mathbf{v}_i, \boldsymbol{\theta})$. For the 3-RRR type SPMs, these matrices are expressed as [307]:

$$\mathbf{J}_1 = \begin{bmatrix} (\mathbf{w}_1 \times \mathbf{v}_1)^T \\ (\mathbf{w}_2 \times \mathbf{v}_2)^T \\ (\mathbf{w}_3 \times \mathbf{v}_3)^T \end{bmatrix}, \tag{4.4}$$

$$\mathbf{J}_2 = diag(\mathbf{w}_1 \times \mathbf{u}_1 \cdot \mathbf{v}_1, \mathbf{w}_2 \times \mathbf{u}_2 \cdot \mathbf{v}_2, \mathbf{w}_3 \times \mathbf{u}_3 \cdot \mathbf{v}_3). \tag{4.5}$$

Singular configurations happen when either $\mathbf{J}_1$ or $\mathbf{J}_2$ or both simultaneously singular, i.e., $\det(\mathbf{J}_1) = 0$ and/or $\det(\mathbf{J}_2) = 0$. There exist three types of singularity cases for PMs as was mentioned earlier, and they can be detected mathematically based on values of $\det(\mathbf{J}_1)$ and $\det(\mathbf{J}_2)$. The first singularity type occurs when $\det(\mathbf{J}_2) = 0$. The second singularity type occurs when $\det(\mathbf{J}_1) = 0$. The third singularity type occurs when $\det(\mathbf{J}_1) = 0$ and $\det(\mathbf{J}_2) = 0$, simultaneously.

In this thesis, conditioning index $\zeta(\mathbf{J}) \in (0, 1)$ is used to estimate the proximity of a particular SPM configuration to singularity. It is is defined as [77]:

$$\zeta(\mathbf{J}) = \frac{1}{\|\mathbf{J}\| \, \|\mathbf{J}^{-1}\|}, \tag{4.6}$$

where $\|\mathbf{J}\|$ is estimated as:

$$\|\mathbf{J}\| = \sqrt{tr\left(\mathbf{J}^T \frac{1}{3} I \mathbf{J}\right)}, \tag{4.7}$$

and $\mathbf{I}$ denotes a 3×3 identity matrix.

Depending on the value of the conditioning index, $\zeta(\mathbf{J})$, a configuration of

an SPM can be treated as non-singular, near-singular, and singular. Singular configurations have values of $\zeta(\mathbf{J})$ equal to 0, near-singular configurations have values of $\zeta(\mathbf{J})$ close to 0, whereas non-singular configurations have $\zeta(\mathbf{J})$ equal to 1. This index is commonly used for design optimization, and dexterity analysis of SPMs such as in [27,154,265,309]. To distinguish between near-singular and non-singular configurations, a threshold value $\zeta(\mathbf{J})_{min}$ is defined. The same definition of the near-singularity based on a condition number of the Jacobian matrix is exploited in [310] to determine the near-singular configurations of the Stewart platform. The methodology based on the computation of the conditioning index, $\zeta(\mathbf{J})$, was previously applied by the thesis supervisors to compute the workspace of the Agile Wrist model used in [91].

For a sampled rotational motion of the mobile platform around its normal axis, $\zeta(\mathbf{J})$ has to be computed at each rotational instant. If any of $\zeta(\mathbf{J})$ values during the rotation is below $\zeta(\mathbf{J})_{min}$ threshold value, this rotational motion's trajectory is considered to be not singularity-free and is avoided.

4.2 Link Collision Detection

Analysis for link collisions of PMs is a very time-consuming and complex task. It is complicated by the fact that usually lots of simplifications are accepted to ease the analysis, and it usually is specific to a particular geometry of a manipulator. Multiple approaches to link collision detection exist. One of the methods is based on the approximate estimation of the shape of the manipulator's links by enclosing them into bounding boxes, or ellipsoids as in [90]. The drawback of this method is that it gives only a rough estimate of the collision due to the link approximation that also reduces the overall computed feasible configuration space. Another method is based on the pre-calculated configuration space obtained from the experiment with the real prototype as in [91]. The experimental Agile Wrist setup was set to go through a set of possible input joint positions at a slow speed from the home configuration, and the real collisions were recorded by reading the motor's current. In the event of a collision, the electric current in at least one of the actuators was sharply increasing. This method detects link collisions more

accurately than the first one, but it requires the availability of the operational SPM prototype. Another issue with this method is that it disregards orientations achievable in general, but not reachable from the home configuration directly. As a result of these methods, a configuration space with all feasible input joint positions can be generated and compared as in [91] showing that the second method outperforms the first.

In this thesis, the link collision detection methodology is based on a different approach. It uses virtual simulation tools such as CoppelieSim, described in Chapter 3. This approach ensures more accurate link collision detection at all possible configurations without approximating link shapes and is a faster process as it does not require the availability of an experimental manipulator prototype with implemented motion control. Using CAD or simulation software to determine the manipulator's workspace was also considered in [311, 312].

In case of link collision, the simulator's link collision module signals that visually by coloring collided links and can send collision flag data with the IDs of the collided links to a remote client, such as MATLAB or Python-based script, upon request. CoppeliaSim's collision detection module implements the algorithm for efficient and exact interference detection amongst complex polygonal models, e.g. SPM links, based on a hierarchical representation of the models using tight-fitting oriented bounding box trees. At run-time, the algorithm traverses two such trees and tests for overlaps between oriented bounding boxes [302, 313].

A CoppeliaSim-based collision check routine is repeated at each rotational instant of the sampled rotational motion of the mobile platform around its normal vector. If any of the manipulator's links collide during the rotational motion, this motion is treated as not safe and is avoided.

4.3 Configuration Space

A set of all attainable input joint positions is the configuration space or C-space that provides information on which input commands can or can not be applied to the manipulator's actuators. Its computation is necessary to generate feasible, smooth, and optimal input reference trajectories as a part of the motion planning

process.

The feasibility of an input joint position, $\boldsymbol{\theta}$, is determined based on the singularity analysis described in Section 4.1 and link collision detection with a simulation model of the coaxial SPM described in Section 4.2. A feasible trajectory can not bring a manipulator to the configuration that is singular, near-singular, and (or) has links colliding. An input trajectory can be sampled, and each sampling instant is checked to satisfy the feasibility test.

For the purposes of fast real-time control, the configuration space can be pre-calculated offline for a manipulator to verify its input joint position without the need to go through the feasibility test each time. A full joint space available for a manipulator has to be pre-tested in this case.

For coaxial SPM, its joint space is described by the cube with the sides defined by the input joint positions, $\theta_i, i = 1, 2, 3$. The space can be sampled to obtain a 3D grid of nodes independently checked for singularity and link collisions. Test nodes that pass the test are included in the feasible configuration space, whereas the nodes that do not pass this test are excluded and must be avoided by the manipulator.

Coordinates of the generated 3D grid of nodes belong to the sets

$$\boldsymbol{\phi}_i = \{\theta_{i,1},\ \theta_{i,2},\ \ldots\ \theta_{i,N_i}\}, \quad i = 1, 2, 3, \tag{4.8}$$

where N_i is the size of the set to which an input joint position θ_i belongs. For simplicity and symmetry, set sizes used are made equal, and a uniform sampling interval is used, i.e., $N_1 = N_2 = N_3$, and $\delta_\phi \triangleq \theta_{i,j+1} - \theta_{i,j}$, $j = 1, 2, \ldots N_i - 1$ is constant.

As mentioned in Section 2.5, there exist input joint positions that result in links surpassing each other, meaning that the order of the links is violated. Given a physical prototype of the coaxial SPM, there is a specific sequence of its distal links, i.e., *distal link 1* - *distal link 2* - *distal link 3*, if viewed from the top. This order of the distal links can not be broken in real-world settings as it will require the links to pass through each other; however, it is possible in simulations such as in CoppeliaSim since it is just a simulation model. To decrease computational burden, input joint positions having such effect, and thus their

corresponding nodes from the 3D grid, are excluded from the analysis without any tests performed with them. The remaining nodes are subjects of singularity and link collision checks.

Let a set $\mathcal{V}$ represent the union of all feasible input joint positions of the coaxial SPM. A procedure to estimate the set $\mathcal{V}$ is outlined in the Algorithm 4. Having set $\mathcal{V}$ helps to evaluate the control limits of a manipulator and detect any dependencies between actuators, e.g., safety margins for actuators' operation. This set can also be used while generating optimal motion trajectories, such as trajectories with the shortest path in the joint space.

Algorithm 4: Numerical computation of the configuration space

Input: α_1, α_2, β, $\boldsymbol{x}_0$, η_i, ϕ_i, $i = 1, 2, 3$
Output: Set $\mathcal{V}$

$\mathcal{V} \leftarrow \emptyset$;
for $a_1 \leftarrow 1$ **to** N_1 **do**
  for $a_2 \leftarrow 1$ **to** N_2 **do**
    for $a_3 \leftarrow 1$ **to** N_3 **do**
      $singularity \leftarrow false$;
      $collision \leftarrow false$;
      `/* link surpass check */`
      if $\theta_3(a_3) - \theta_2(a_2) > 120°$ **or** $\theta_2(a_2) - \theta_1(a_1) > 120°$ **or** $\theta_1(a_1) - \theta_3(a_3) > 120°$ **then**
        $collision \leftarrow true$
        break
      $\boldsymbol{\theta} \leftarrow \begin{bmatrix}\theta_1(a_1) & \theta_2(a_2) & \theta_3(a_3)\end{bmatrix}^T$;
      `/* forward kinematics */`
      Calculate $\mathbf{w}_i$ and $\mathbf{v}_i$, $i = 1, 2, 3$, given $\boldsymbol{\theta}$ using Algorithm 1;
      `/* singularity detection */`
      Calculate $\mathbf{J}$ given $\mathbf{u}_i$, $\mathbf{w}_i$ and $\mathbf{v}_i$, $i = 1, 2, 3$,using (4.3)-(4.5);
      Calculate $\zeta(\mathbf{J})$ given $\mathbf{J}$, using (4.6) and (4.7);
      if $\zeta(\boldsymbol{J}) < \zeta(\boldsymbol{J})_{min}$ **then**
        $singularity \leftarrow true$
        break
      `/* link collision detection */`
      Send $\boldsymbol{\theta}$ to the coaxial SPM motion simulator;
      if *collision handle* $== 1$ **then**
        $collision \leftarrow true$
        break
      `/* update the space */`
      if $singularity == false$ **and** $collision == false$ **then**
        $\mathcal{V} \leftarrow \mathcal{V} \cup \{\boldsymbol{\theta}\}$
return $\mathcal{V}$

For the coaxial SPM, the 3D grid of nodes is bounded by input joint values ranging between 0° and 360° with the sampling interval $\delta_\phi = 5°$. A grid of 373,248 test nodes ($N_1 = N_2 = N_3 = 72$, 72x72x72 = 373,248) is generated in the result. The set $\mathcal{V}$ has 0 test nodes in it at the beginning.

The computation process of the feasible configuration space at its various stages is illustrated in Fig. 4-1. The first intermediate set was obtained by excluding nodes resulting in link surpass and is shown in Fig. 4-1a. While observing the 3D shape of this set, it was noticed that it has a triangular cross-section profile throughout the diagonal axis of the 3D grid, as depicted in a shaded circle underneath the first figure. The diagonal axis is a line stretching from the node $\boldsymbol{\theta} = \begin{bmatrix}0°, & 0°, & 0°\end{bmatrix}^T$ till the node $\boldsymbol{\theta} = \begin{bmatrix}360°, & 360°, & 360°\end{bmatrix}^T$ in the grid. This line also corresponds to the trajectory of the infinite rotational motion of the mobile platform around z-axis, as will be shown in Section 4.5. Following this trajectory, coaxial SPM rotates around itself with zero tilt of the mobile platform.

The nodes from the first intermediate set were checked for singularity. The threshold conditioning index was chosen as $\zeta(\mathbf{J})_{min} = 0.2$. This value can be set lower to obtain a larger configurations space, or higher to be more conservative with singular configurations. In this thesis, this value was selected to be more conservative on the obtained C-space. After performing a singularity detection routine on all of these test nodes, several smaller disconnected subsets appeared as shown in Fig. 4-1b on the cross-sectional view part of the figure. Computed subsets belong to different working modes of the coaxial SPM, with the central one (the largest one) corresponding to the current *l-l-l* working mode. It complies with the fact that coaxial SPM's working modes can be switched by passing singularity points, which happen when the manipulator legs' links are fully folded or unfolded.

Afterward, a collision detection routine was implemented in CoppeliaSim with MATLAB integration for the remaining test nodes that correspond to singularity-free configurations. The final set of the feasible input joint positions, $\mathcal{V}$, i.e., the configuration space (C-space) of the coaxial SPM's prototype under study was obtained and is available in Fig. 4-1c. The cross-section profiles of the sets in Figs. 4-1b and 4-1c also have their shapes constant throughout the diagonal axis

of the grid.

Analysis of the obtained set of the feasible configurations $\mathcal{V}$ reveals that it stretches from the node $\boldsymbol{\theta} = \begin{bmatrix} 0^\circ, & 0^\circ, & 0^\circ \end{bmatrix}^T$ to the node $\boldsymbol{\theta} = \begin{bmatrix} 360^\circ, & 360^\circ, & 360^\circ \end{bmatrix}^T$ with a maximum offset of each input joint position being not larger than 100° from the diagonal line mentioned before. Based on this, it is concluded that actuators' input positions can not vary from each other by more than $\pm 100^\circ$ for the coaxial SPM under study. Otherwise, some of the links will collide.

It is worth mentioning that the computed set $\mathcal{V}$ expands infinitely in the negative and positive directions following the $\begin{bmatrix} 0^\circ, & 0^\circ, & 0^\circ \end{bmatrix}^T$ - $\begin{bmatrix} 360^\circ, & 360^\circ, & 360^\circ \end{bmatrix}^T$ diagonal axis and having a same-shaped cross-sectional profile along this axis. This result confirms that coaxial SPMs are capable of infinite rotational motion, and input trajectories leading to it are not bounded, i.e., can go beyond the tested 3D grid bounded by $\theta_i \subseteq [0^\circ, 360^\circ], i = 1, 2, 3$.

4.4 Cartesian Workspace

Computation of the Cartesian workspace (or simply workspace) is necessary to find spatial limitations for the movement of the manipulator. For the coaxial SPM case, its workspace corresponds to all reachable locations by the mobile platform where it can perform infinite rotational motions.

For a numerical estimate of the workspace of the coaxial SPM, a grid of points $\mathcal{W}_{temp}$ is generated. In this thesis, an icosahedral grid [314] normalized to a unit sphere is selected as the base grid. It has almost equally-distributed test points. The interval between test points is calculated based on the applied g-level (grid division level). The number of test points is $N = 2 \times 10^{2m} + 2$, where $m = \{0, 1, 2, 3, 4, ...\}$ is the g-level. The average interval is equal to $\frac{1}{2^m}\sqrt{\frac{2\pi}{5}}$. If a lower precision of the workspace is acceptable, it is worth increasing the interval between points by selecting lower g-level values to reduce computation time.

Since the orientation of the mobile platform is described in terms of the unit vectors $\mathbf{v}_i,\ i = 1, 2, 3$ in our case, it is necessary to reconstruct those vectors at each test point. It can start by selecting unit vector $\mathbf{v}_1$ to be defined by the cross product of the test point (i.e., its coordinates as normal vector $\mathbf{n}$) and the vector

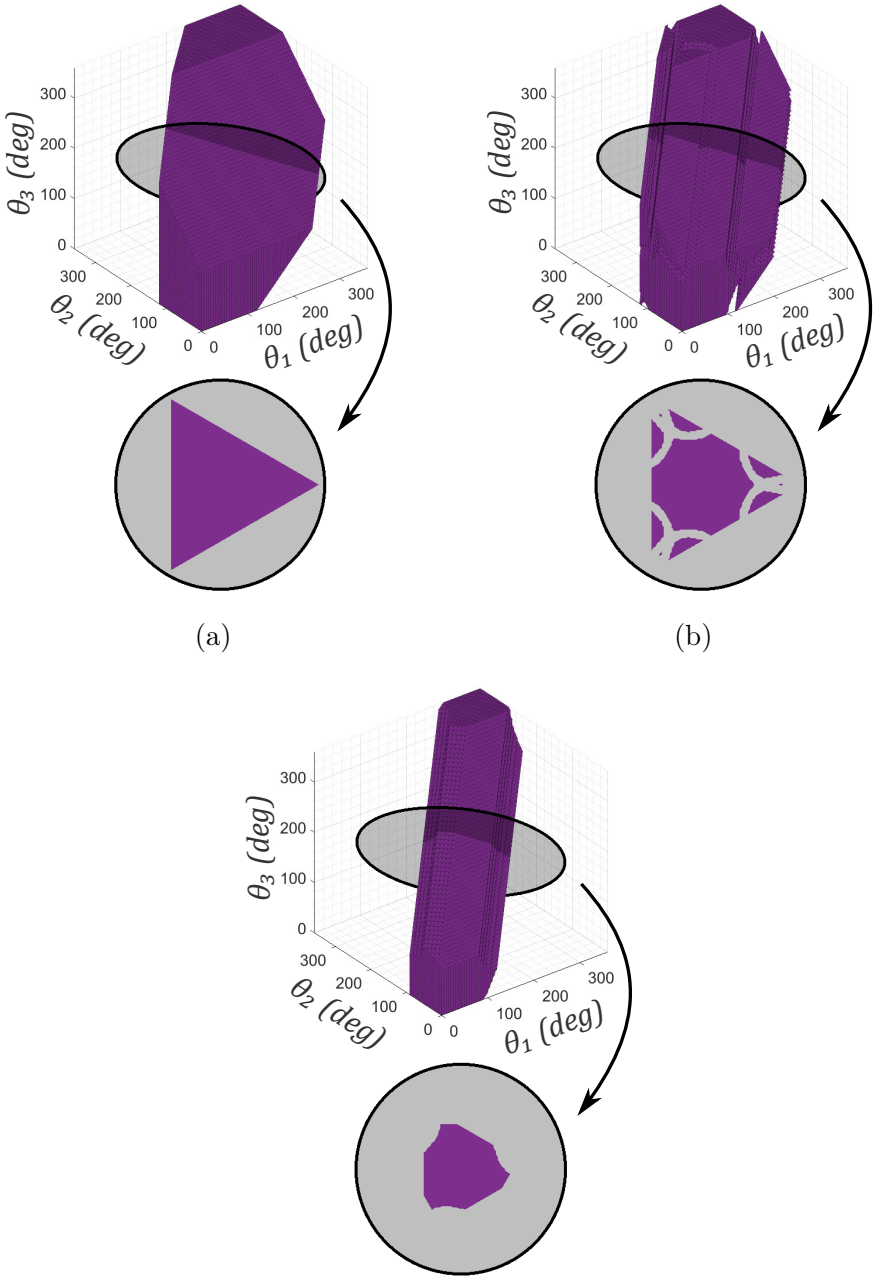

(a) (b)

(c)

Figure 4-1: Sets with cross-sectional views from different stages of the feasible configuration computation process: (a) set of nodes with no link surpass, (b) set of singularity-free nodes, (c) set of link collision-free nodes

pointing in the positive z direction:

$$\mathbf{v}_1 = \frac{\mathbf{n} \times \begin{bmatrix} 0, 0, 1 \end{bmatrix}^T}{\|\mathbf{n} \times \begin{bmatrix} 0, 0, 1 \end{bmatrix}^T\|}. \tag{4.9}$$

This is a somewhat random selection, however, it does not play a significant role since the coaxial SPM will be tested for all sampled rotational instants at this test point. The remaining vectors $\mathbf{v}_2$ and $\mathbf{v}_3$ are found using the Rodrigues' rotation formula as follows:

$$\mathbf{v}_2 = \mathbf{v}_1 \cos 120^\circ + (\mathbf{n} \times \mathbf{v}_1) \sin 120^\circ + \mathbf{n}(\mathbf{n} \cdot \mathbf{v}_1)(1 - \cos 120^\circ), \tag{4.10}$$

$$\mathbf{v}_3 = \mathbf{v}_1 \cos 240^\circ + (\mathbf{n} \times \mathbf{v}_1) \sin 240^\circ + \mathbf{n}(\mathbf{n} \cdot \mathbf{v}_1)(1 - \cos 240^\circ). \tag{4.11}$$

After that, an input joint sequence $\boldsymbol{\theta}_{traj}$ resulting in a 360° rotation is calculated from the unit vectors $\mathbf{v}_{i,rot}$, $i = 1, 2, 3$ using (2.3) and Algorithm 2 for obtaining unique inverse kinematics solutions. All sampled rotational instants are checked for singularity and link collision using the methods outlined in the previous subsections (Sections 4.1 and 4.2). After evaluating the feasibility of each test point from the set $\mathcal{W}_{temp}$, and selecting singularity and collision-free test points, a final set $\mathcal{W}$, representing the union of all points belonging to the Cartesian workspace is obtained. Algorithm 5 details the procedure for determining set $\mathcal{W}$.

For the numerical workspace estimation for the coaxial SPM, an icosahedral grid of test points assigned to the set $\mathcal{W}_{temp}$ was generated with g-level $l = 5$ or $factor = 32$, meaning that each triangle of the icosahedron is subdivided into 32×32 sub-triangles. It resulted in a total of 10,242 test points around the whole unit sphere. At each point, rotation of the unit vectors $\mathbf{v}_i$, $i = 1, 2, 3$, was sampled into 360 instants ($\delta_\sigma = 1^\circ$), and at each instant, unique input joint positions were calculated using Algorithm 2. Following this approach, the input joint sequences $\boldsymbol{\theta}_{traj}$ providing a 360° rotation of the mobile platform at each test point were generated. During the process of numerical estimation, it was found that some input joint sequences contained values with imaginary parts, i.e., non-existing

Algorithm 5: Numerical computation of the Cartesian workspace

Input: l, $\boldsymbol{\sigma}$, α_1, α_2, β, $\boldsymbol{x}_0$, η_i, $i = 1, 2, 3$
Output: Set $\mathcal{W}$

$\mathcal{W} \leftarrow \emptyset$;
$\mathcal{W}_{temp} \leftarrow$ icosahedral grid generated using [314];
for $j \leftarrow 1$ **to** N **do**
  $singularity \leftarrow false$;
  $collision \leftarrow false$;
  Set test node coordinates as $\mathbf{n} = \mathcal{W}_{temp}(j)$;
  Reconstruct $\mathbf{v}_{i,j}$, $i = 1, 2, 3$, following (4.9)-(4.11);
  Generate rotational motion trajectory $\boldsymbol{\theta}_{traj}$ for a single rotation given $\mathbf{v}_{i,j}$, $i = 1, 2, 3$, using Algorithm 3;
  `/* singularity detection */`
  for $k \leftarrow 1$ **to** S **do**
    Calculate $\mathbf{w}_{i,j,k}$ and $\mathbf{v}_{i,j,k}$, $i = 1, 2, 3$, given $\boldsymbol{\theta}_{traj}(k)$ using Algorithm 1;
    Calculate $\mathbf{J}$ given $\mathbf{u}_{i,j,k}$, $\mathbf{w}_{i,j,k}$ and $\mathbf{v}_{i,j,k}$, $i = 1, 2, 3$, using (4.3)-(4.5);
    Calculate $\zeta(\mathbf{J})$ given $\mathbf{J}$, using (4.6) and (4.7);
    if $\zeta(\boldsymbol{J}) < \zeta(\boldsymbol{J})_{min}$ **then**
      $singularity \leftarrow true$
      break
  if $singularity == true$ **then**
    break
  `/* link collision detection */`
  Send $\boldsymbol{\theta}_{\boldsymbol{traj}}$ to robot simulator;
  if *collision handle* $== 1$ **then**
    $collision \leftarrow true$
    break
  `/* update the workspace */`
  if $singularity == false$ **and** $collision == false$ **then**
    $\mathcal{W} \leftarrow \mathcal{W} \cup \mathbf{n}$
return $\mathcal{W}$

solutions, so the test points resulting in it were excluded from the rest of the analysis as they correspond to an unattainable region. Furthermore, test points on the negative side of the unit sphere were also excluded from the analysis as it is expected that the manipulator cannot operate in that region (physical limitation).

A conditioning index $\zeta(\mathbf{J})_{min} = 0.2$ was used to detect near-singular configuration for the remaining test points. It is expected that during the rotational motion, the conditioning index $\zeta(\mathbf{J})$ will not remain to be the same, as some of the links are moving to cause the manipulator to come closer or further from near-singular configurations. And as was observed from Figs. 4-7b and 4-7a,

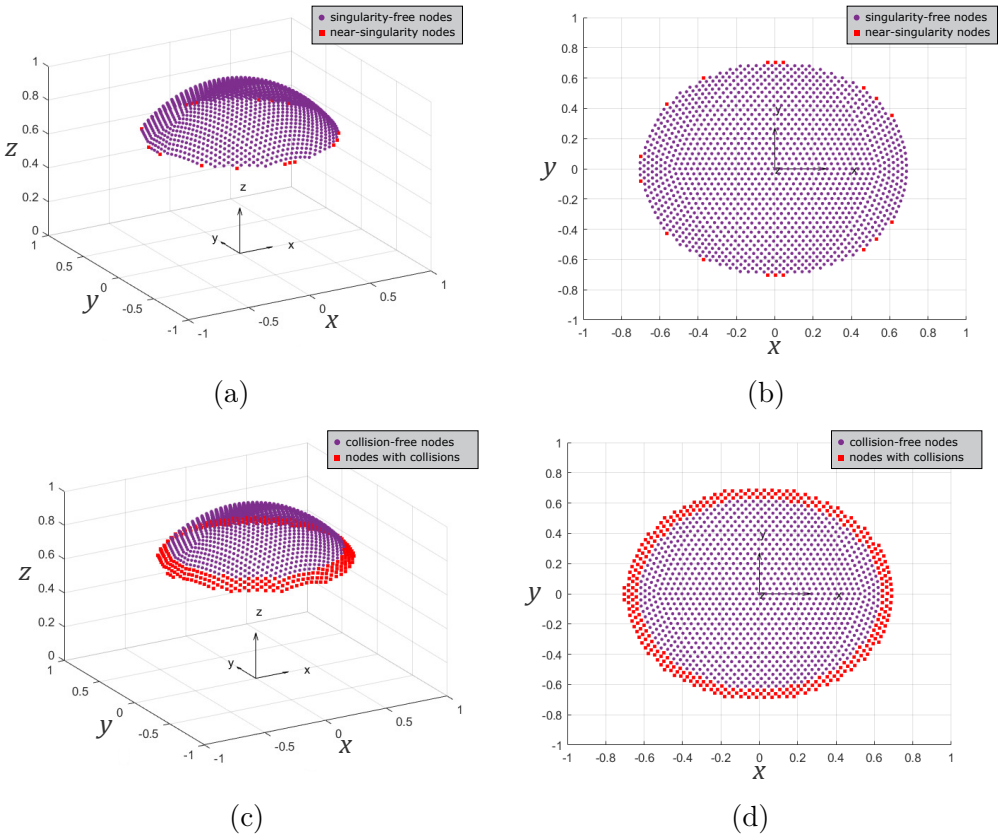

Figure 4-2: Test sets from different stages of the Cartesian workspace computation: (a) set near-singular and singularity-free and test points; (b) top view of (a); (c) set of link collision-free test points; (d) top view of (c)

conditioning index is indeed changing. So, at each of the test points a single rotational motion was sampled, and all test points having at least when near-singular configuration while rotation were disregarded, such as the ones shown in red in Fig. 4-2a and 4-2b.

Similarly to this approach, link collision checks were performed for all sampling instants of the rotational motion at each test point. The resulting set is shown in Figs. 4-2c and 4-2d. The red points represent locations with link collisions present, so they are disregarded and not included in the final set $\mathcal{W}$ corresponding to the coaxial SPM's Cartesian workspace. The resultant set $\mathcal{W}$ contains data points normalized to a unit circle, that can be easily multiplied by some correction value depending on the real radius of the manipulator's workspace, usually the distance from the center of rotation till the to central point of the mobile platform. Analysis of the obtained workspace reveals that for the coaxial SPM under study can achieve 39° as the lowest tilt angle of its mobile platform. So, within this

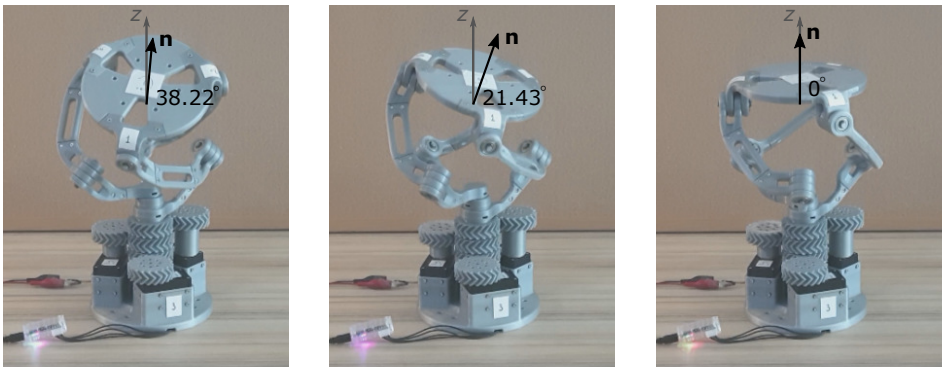

(a) (b) (c)

Figure 4-3: Case studies of the infinite rotational motion generation

tilt angle, it is expected that the coaxial SPM can perform full rotations of the mobile platform with no singularities and link collision present.

4.5 Infinite Rotational Motion Generation

To demonstrate the application of the proposed methods to estimate the workspace and configuration space of the coaxial SPM, three numerical examples with infinite rotational motion are given below.

Example 1: Infinite Rotational Motion at Worspace's Edge Region

An orientation of the coaxial SPM, corresponding to the node $\mathbf{n} = \begin{bmatrix} -0.274, & -0.555, & 0.786 \end{bmatrix}^T$ is used in the first example. It results in 38.22° tilt angle of the mobile platform as illustrated in Fig. 4-3a, where arrow $\mathbf{z}$ represents z-axis of the coordinate system and vector $\mathbf{n}$ is the mobile platform's normal vector shown from the center of rotation. The unit vectors $\mathbf{v}_i$, $i = 1, 2, 3$, describing one of the possible orientations of the manipulator at this test node are calculated following (4.9)-(4.11):

$$\begin{aligned} \mathbf{v}_1 &= \begin{bmatrix} -0.8967, & 0.4427, & 0.0000 \end{bmatrix}^T, \\ \mathbf{v}_2 &= \begin{bmatrix} 0.1471, & -0.8314, & -0.5358 \end{bmatrix}^T, \\ \mathbf{v}_3 &= \begin{bmatrix} 0.7495, & 0.3887, & 0.5358 \end{bmatrix}^T. \end{aligned} \tag{4.12}$$

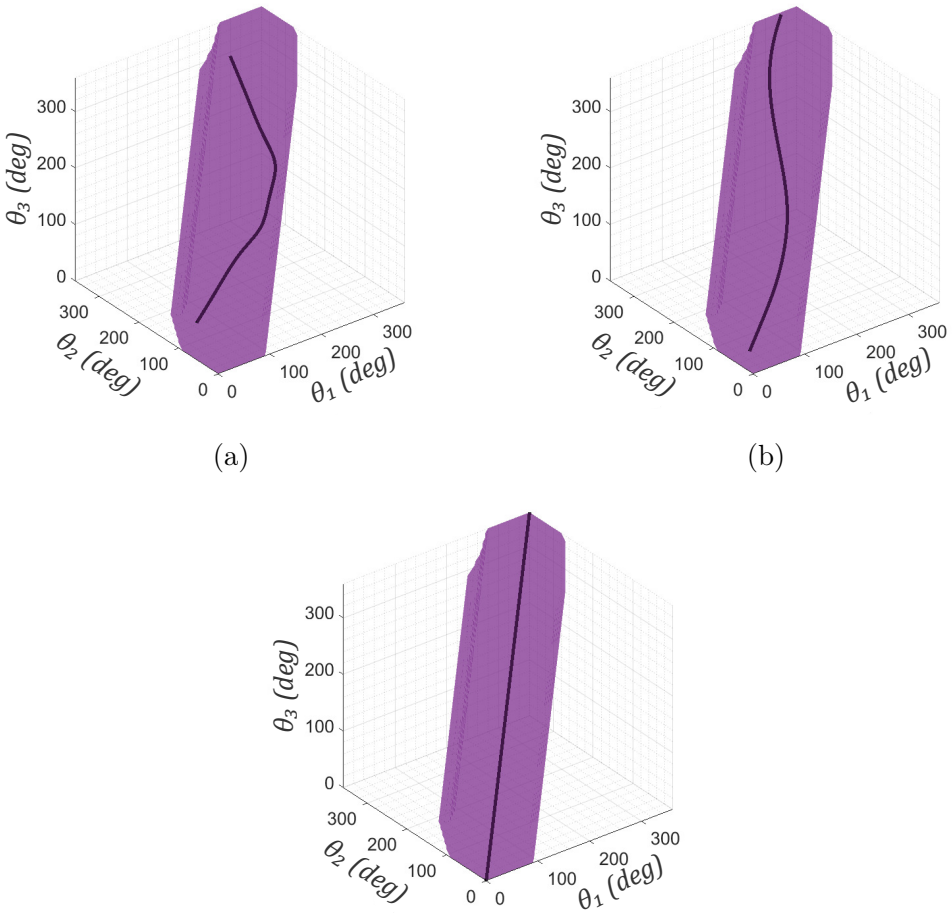

(a) (b)

(c)

Figure 4-4: Generated rotational motion joint trajectories

Once these unit vectors are obtained, the procedure is continued with Algorithm 3. Rotational instants of the unit vectors (4.12), $\mathbf{v}_{i,rot}$, $i = 1, 2, 3$, are calculated by applying (2.3) for a single 360° rotation cycle with $\delta_\sigma = 1°$. The input joint positions $\boldsymbol{\theta}$ are then calculated using Algorithm 2 at each rotational instant. The generated input joint trajectory $\boldsymbol{\theta}_{traj}$ is shown in Fig. 4-4a in the form of a helix-shaped path inside the feasible configurations space, previously computed. The generated trajectory almost reaches the side edges of the C-space, indicating that the coaxial SPM operates near the edge of its workspace. For consistency, all generated trajectories are shown within the feasible configuration space bounded by input joint positions 0° and 360°.

Figure 4-5a illustrates the evolution sequence of the generated input joint positions $\boldsymbol{\theta}_{traj}$ for the three actuators of the SPM prototype, whereas Fig. 4-6a presents the input joint rates of change, calculated as $\theta_{i,j+1}$ - $\theta_{i,j}$. Input joint rates

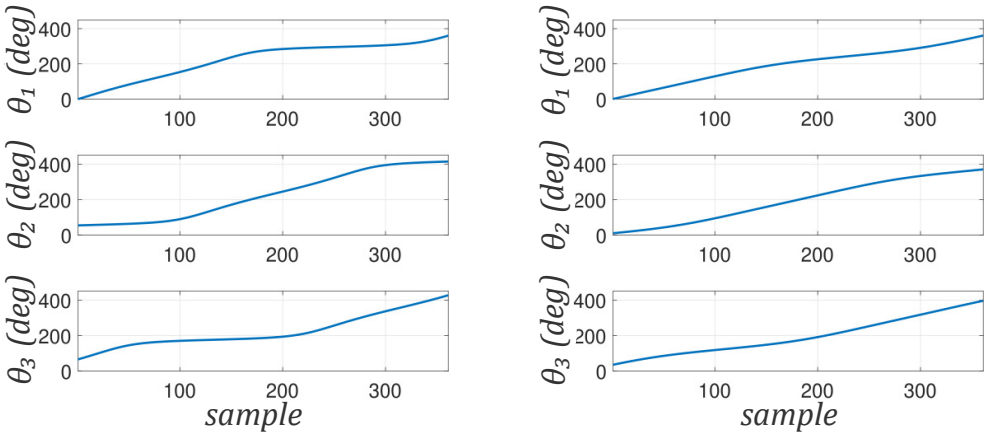

(a)

(b)

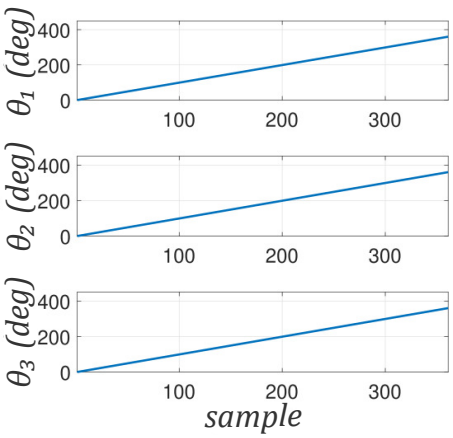

(c)

Figure 4-5: Evolution of input joint positions

of change are periodic and identical to each other with 120° phase shifts between them. It means that only one input joint position can be generated for simplicity and ease of calculations; the remaining input joint positions are obtained by adding 120° and 240° phase shifts. These values are coming from the location of mobile platform joints with respect to each other. If they are not equally distributed, then these values will not be true. A similar periodic behavior during the rotational motion is observed in the sample evolution of the conditioning index $\zeta(\mathbf{J})$ shown in Fig. 4-7a. It implies that during the infinite rotational motion of the coaxial SPM the conditioning index is not constant and can go beyond the threshold value, which indicates that the motion can be unfeasible.

The generated input joint trajectories, before being applied on the SPM prototype, were tested on the simulation model in CoppeliaSim resulting in dynamic visualization of the expected infinite rotation as presented in Fig. 4-8 as six sam-

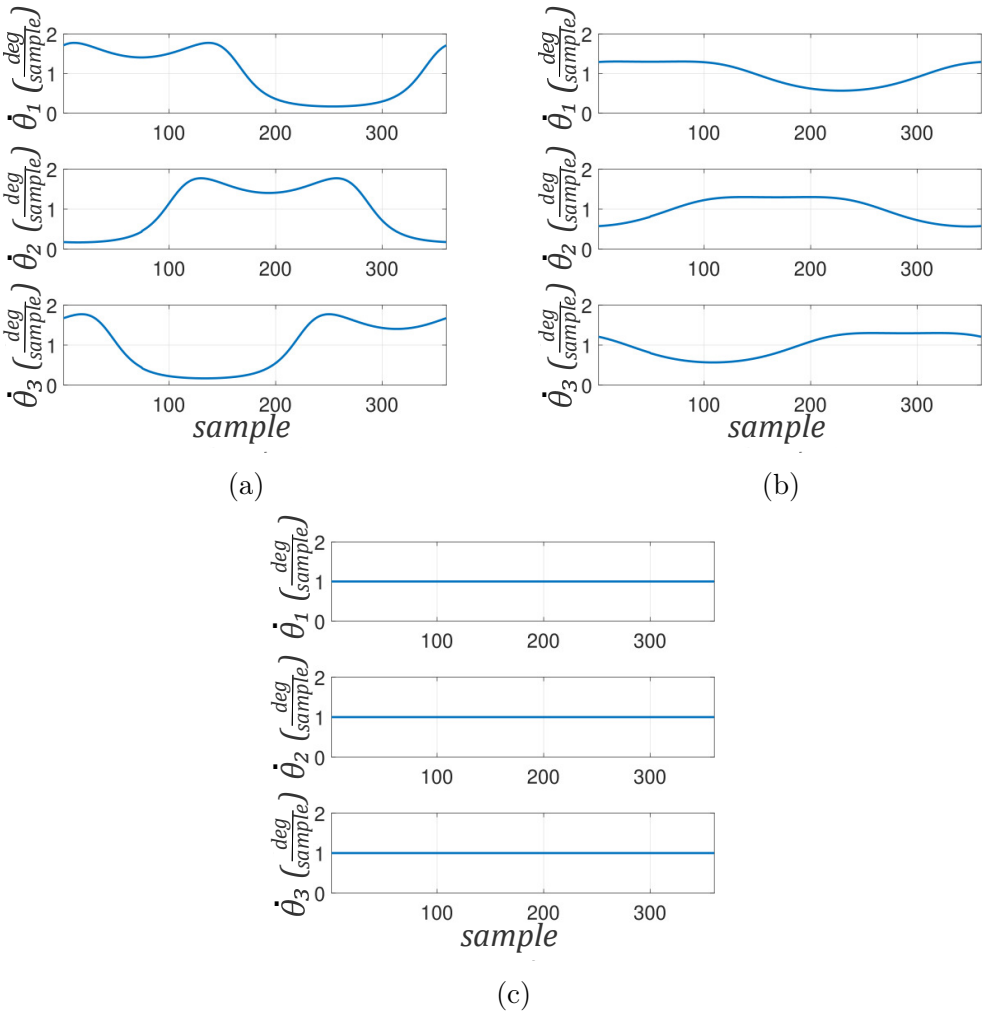

Figure 4-6: Evolution of input joint rates of change

pling instants. Time evolution of the unit vectors $\mathbf{v}_i$, $i = 1, 2, 3$, characterizing the instantaneous orientation of the coaxial SPM during the rotational motion, were compared with the numerically computed reference unit vectors $\mathbf{v}_{i,rot}$, $i = 1, 2, 3$, similarly to the procedure presented in Chapter 3.2, Fig. 3-5. The matching of the simulated and pre-computed desired rotational motion trajectories verifies the correctness and pointing accuracy of the proposed numerical framework for generating input joint trajectories used for realizing infinite rotational motion of the mobile platform around its normal vector at the desired orientation.

The input trajectories were also applied on the experimental prototype of the coaxial SPM as shown in Fig. 4-9 in the same format. The visual evaluation of the experimental prototype behavior confirmed the overall correctness of the proposed framework assuming an open-loop control approach. Design of a closed loop orientation control system for eliminating the effects of the manipulator's

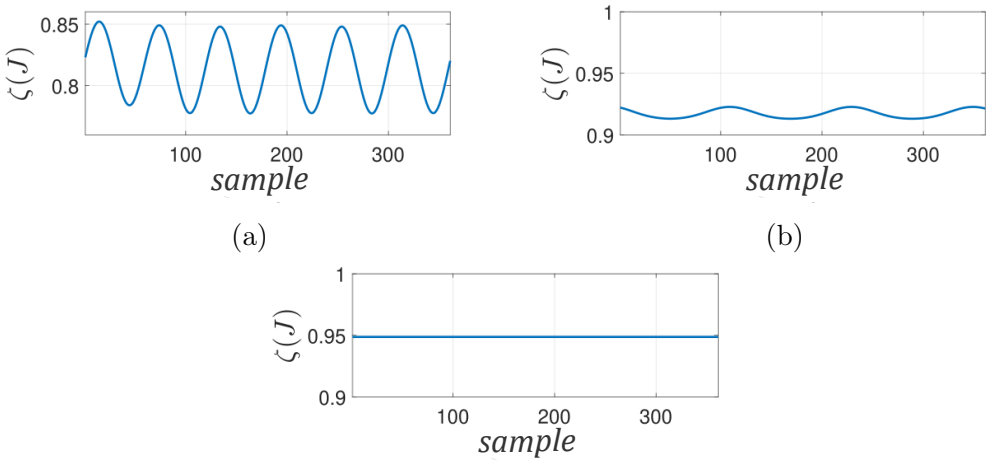

Figure 4-7: Evolution of conditioning index $\zeta(\mathbf{J})$

dynamics, potential frictions in transmission gears and joints, and mechanical inaccuracies in the physical SPM prototype on its pointing accuracy is beyond the scope of the thesis work and can be a part of future research.

Example 2: 360° **Rotational Motion at Workspace's Middle Region**

An orientation of the coaxial SPM, corresponding to the point $\mathbf{n} = \begin{bmatrix} 0.165, & -0.326, & 0.931 \end{bmatrix}^T$ is used in the second example. It results in 21.43° tilt angle of the mobile platform as illustrated in Fig. 4-3b. Similarly to Example 1, the generated input trajectory, input joint positions and rates of change, conditioning index $\zeta(\mathbf{J})$ computed for this example are presented in Figs. 4-4b, 4-5b, 4-6b, 4-7b, respectively. The snapshots of the resulting rotation of the simulation model and experimental prototype are given in Fig. 4-10 and Fig. 4-11, respectively.

Example 3: 360° **Rotational Motion in Workspace's Central Region**

An orientation of the coaxial SPM, corresponding to the point $\mathbf{n} = \begin{bmatrix} 0, & 0, & 1 \end{bmatrix}^T$ is used in the third example. It results in 0° tilt angle (i.e., no tilt) of the mobile platform as illustrated in Fig. 4-3c. Similarly to Examples 1 and 2, the generated input trajectory, input joint positions and rates of change, conditioning index $\zeta(\mathbf{J})$ computed for this example are presented in Figs. 4-4c, 4-5c, 4-6c, 4-7c, respectively. In this case study, input joint rates of change and conditioning index

$\zeta(\mathbf{J})$ are constant values. The input trajectory is a straight line connecting nodes $\left[0°,\ 0°,\ 0°\right]^T$ and $\left[360°,\ 360°,\ 360°\right]^T$. The snapshots of the resulting rotation of the simulation model and experimental prototype are given in Fig. 4-12 and Fig. 4-13, respectively.

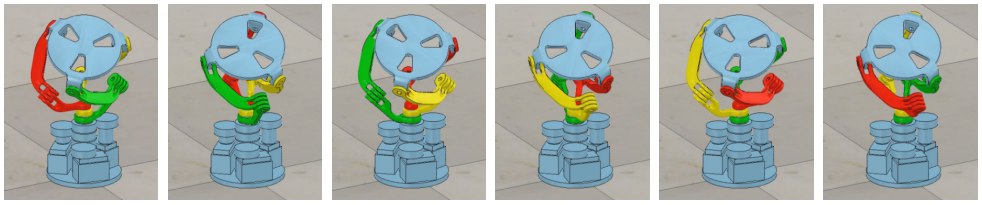

(a) $\sigma = 0°$ (b) $\sigma = 60°$ (c) $\sigma = 120°$ (d) $\sigma = 180°$ (e) $\sigma = 240°$ (f) $\sigma = 300°$

Figure 4-8: Simulated rotational instants around $\mathbf{n} = [-0.274, -0.555, 0.786]^T$

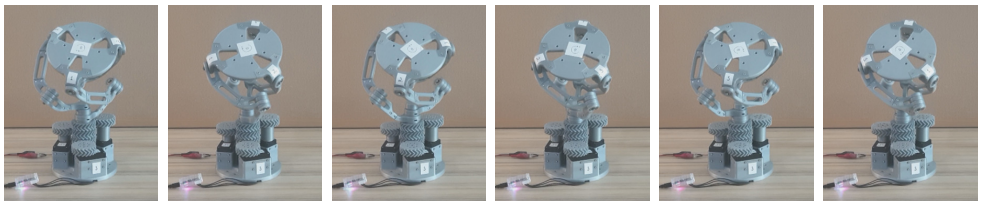

(a) $\sigma = 0°$ (b) $\sigma = 60°$ (c) $\sigma = 120°$ (d) $\sigma = 180°$ (e) $\sigma = 240°$ (f) $\sigma = 300°$

Figure 4-9: Experimental rotational instant around $\mathbf{n} = [-0.274, -0.555, 0.786]^T$

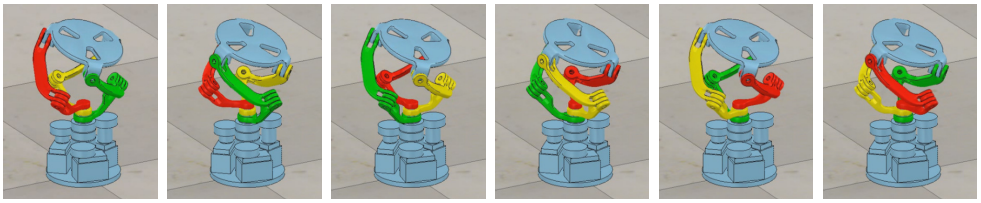

(a) $\sigma = 0°$ (b) $\sigma = 60°$ (c) $\sigma = 120°$ (d) $\sigma = 180°$ (e) $\sigma = 240°$ (f) $\sigma = 300°$

Figure 4-10: Simulated rotational instants around $\mathbf{n} = [0.165, -0.326, 0.931]^T$

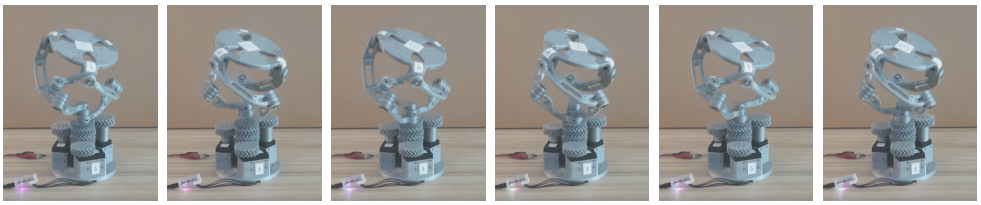

(a) $\sigma = 0°$ (b) $\sigma = 60°$ (c) $\sigma = 120°$ (d) $\sigma = 180°$ (e) $\sigma = 240°$ (f) $\sigma = 300°$

Figure 4-11: Experimental rotational instants around $\mathbf{n} = [0.165, -0.326, 0.931]^T$

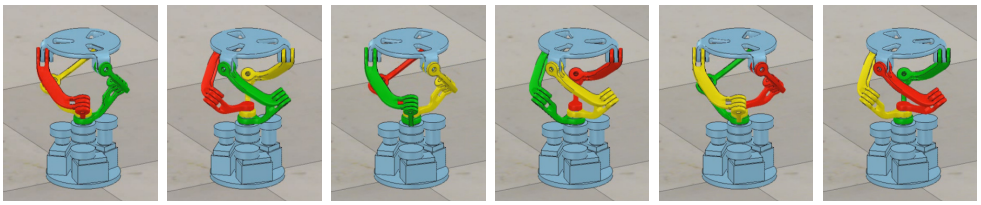

(a) $\sigma = 0°$ (b) $\sigma = 60°$ (c) $\sigma = 120°$ (d) $\sigma = 180°$ (e) $\sigma = 240°$ (f) $\sigma = 300°$

Figure 4-12: Simulated rotational instants around $\mathbf{n} = [0, 0, 1]^T$

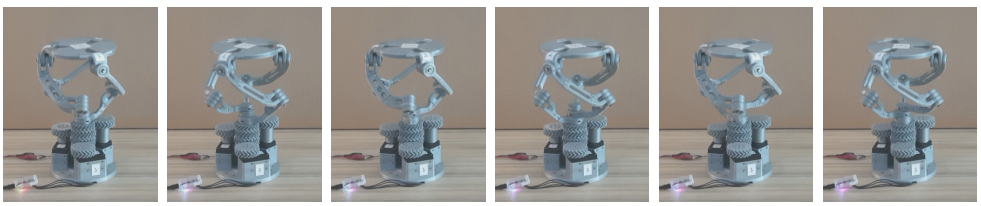

(a) $\sigma = 0°$ (b) $\sigma = 60°$ (c) $\sigma = 120°$ (d) $\sigma = 180°$ (e) $\sigma = 240°$ (f) $\sigma = 300°$

Figure 4-13: Experimental rotational instants around $\mathbf{n} = [0, 0, 1]^T$

Chapter 5

Orientation Control

To generate motion trajectories including the optimal ones for a manipulator it is required to compute its configurations space (also called C-space), as was done in Section 4.3. However, storing the data with all the feasible configurations and checking whether the specific trajectory is feasible is computationally expensive and can not be done in real-time. For fast and optimal calculations it is necessary to have C-space in the form of a convex set. One can generate an inner convex approximation from the non-convex configuration space, and use it for real-time control of the manipulator. In this chapter, a methodology for obtaining such estimation is presented making it offline, i. e., pre-calculating it , such that the results can be used in real-time. Having this convex set can allow to detect if the input configuration is feasible or not without making all the necessary checks presented so far. It can be done simply by quick estimation if the input configuration of some trajectory is within the boundaries of the convex approximation. This can be used in the case of the external reference tracking control example such as following the joystick command which sometimes can lead to input configurations outside of C -space. It is also possible to bring the manipulator to the closest feasible orientation.

The final experimental system was developed in the ROS framework, which allows easy communication between sensors and actuators in the form of rostopic and rosnodes. An example of motion planning of a robot in ROS can be found in [315].

5.1 Convex Approximation of the C-Space

As estimated in Section 4.3, configuration space of a coaxial SPM is a 3D-space in which each axis corresponds to one of the input joint positions, i.e., θ_1, θ_2, or θ_3. There exist regions in the joint space that represent sets with unfeasible configurations which have to be avoided by the manipulator. Unfeasible configurations are defined as the ones that lead to singular or near-singular configurations or result in link collisions. The obtained configuration space is not bounded by the planes parallel to the planes formed by axes corresponding to θ_1-θ_2, θ_1-θ_3, or θ_2-θ_3, it stretches infinitely in the diagonal direction, i.e., in the direction of the vector between $\boldsymbol{\theta} = [0°, 0°, 0°]^T$ and $\boldsymbol{\theta} = [360°, 360°, 360°]^T$, in both positive and negative directions. It can also be observed that the obtained space is non-convex meaning that generating quickly optimal trajectories will not be possible unless a convex version of the space is obtained [316]. It can be done by excluding some of the feasible configurations for the sake of obtaining the convex approximation of the configuration space from its inside region, the so-called inner convex approximation.

Different methods to generate internal convex approximations of a non-convex set were proposed when an analytical expression is given for the non-convex set [317–319], with no standard approaches available in the case when an analytical expression of a set is not available. In this thesis, an approach to make a convex estimate of C-space similar to the one described in Algorithm 1 in [91] is used. This approach is based on performing iterative numerical estimates for each node from C-space expanding from its center on by one to detect if its inclusion in the formed convex set does not result in obtaining a non-convex space.

In the remainder of this section, this iterative method for obtaining an inner approximation of C-space is explained. Let set $\mathcal{V}$ denote a set of all feasible nodes of the C-space, and set $\mathcal{F}$ will denote a set of all unfeasible nodes (forbidden area), with set $\mathcal{P}$ denoting nodes that will belong to the obtained convex estimate of the C-space. Then, if a procedure is started from the input configuration $\boldsymbol{\theta}_{start}$, the space is slowly expanded. A simplified graphical representation with some of the parameters is shown in Fig. 5-1

As an initial step, a collection of polytopes $\mathcal{C}$ is defined as a list containing

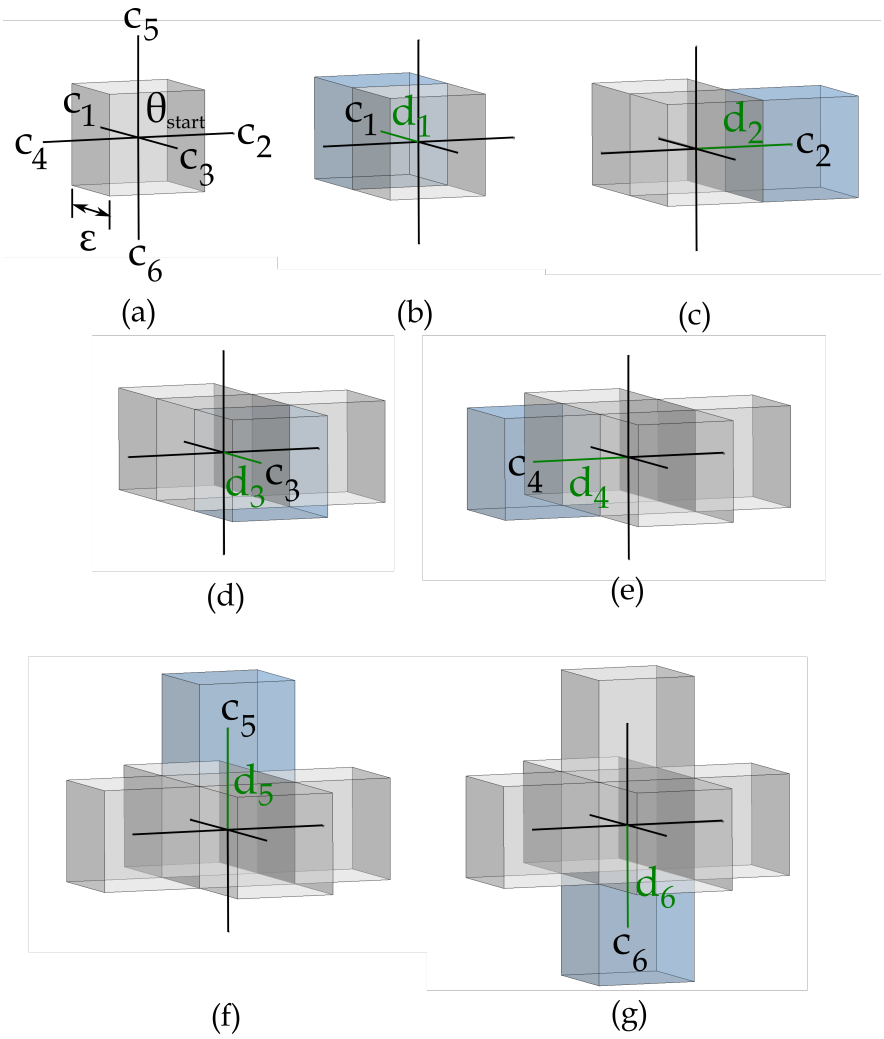

Figure 5-1: Graphical representation of the estimation of the convex approximation of the C-space

all cubes with edge length, ϵ, centered around the nodes of $\mathcal{F}$, namely $\mathcal{C}_k$, $k = 1, ..., |\mathcal{F}|$, with $|\cdot|$ standing for the cardinality of a set. Then, the starting node $\boldsymbol{\theta}_{start}$, which can be the home configuration, is assigned to a temporary convex approximation $\mathcal{P}_{temp}$. The idea is that at each iteration the nearest unchecked points to $\mathcal{P}_{temp}$ from the grid will be checked to satisfy convexity and if they pass the checks are added to $\mathcal{P}_{temp}$. In the beginning, there is only one node in this set, namely $\boldsymbol{\theta}_{start}$. A set $\mathcal{V}_N$ is the set containing nodes with the smallest distance to $\mathcal{P}_{temp}$. At the first iteration, the nodes of this set of six nodes from non-diagonal directions of $\boldsymbol{\theta}_{start}$.

At each iteration, a distance, d_k, is measured from the updated polytope $\mathcal{P}_{temp}$ towards all k nodes that are inside set $\mathcal{V}$ but were not included in the list of nodes forming a convex set $\mathcal{V}_\mathcal{P}$, altogether such set is denoted as $\mathcal{V} \setminus \mathcal{V}_\mathcal{P}$ with its size

being k. For all nodes $\mathbf{v}_k \in \mathcal{V} \setminus \mathcal{V}_{\mathcal{P}}$, the distance is defined as:

$$\text{dist}(\mathbf{v}_k, \mathcal{P}_{temp}) \triangleq \inf\{\|\mathbf{v}_k - \boldsymbol{\theta}\|_2 : \boldsymbol{\theta} \in \mathcal{P}_{temp}\}. \tag{5.1}$$

It can be determined numerically by solving the following Quadratic Program (QP) [316]:

$$\begin{aligned} (\text{dist}(\mathbf{v}_k, \mathcal{P}_{temp}))^2 = \min_{\boldsymbol{\theta}} \quad & \|\mathbf{v}_k - \boldsymbol{\theta}\|_2^2 \\ \text{s.t.} \quad & \mathbf{A}_p\boldsymbol{\theta} \leq \mathbf{b}_p \end{aligned} \tag{5.2}$$

where $\mathbf{A}_p\boldsymbol{\theta} \leq \mathbf{b}_p$ is the H-representation of polytope $\mathcal{P}_{temp}$.

The nodes with the minimal distance d_{min} are included in the set of the nodes to be checked at this iteration, namely $\mathcal{V}_N$, with the size j. Using the H-representation, a temporary version of a polytope with each node $\mathbf{v}_j$ being added one by one to define it as $\mathcal{P}'_{temp} = \text{co}(\mathcal{P}_{temp}, \mathbf{v}_j)$ is sequentially checked against all sets of $\mathcal{C}$ for any intersections. If the intersection does not happen, then $\mathcal{P}'_{temp}$ is treated as $\mathcal{P}'_{temp}$ and the convex set $\mathcal{V}_{\mathcal{P}}$ is amended by one more node $\mathbf{v}_j$. If the intersection exists, then from the set of the feasible nodes $\mathcal{V}$, the node $\mathbf{v}_j$ is eliminated. This iterative procedure is repeated until no nodes are left in $\mathcal{V}$. In the result, the polytope $\mathcal{P}$ from the final version of $\mathcal{P}_{temp}$ is defined using H-representation as:

$$\mathcal{P} = \{\boldsymbol{\theta} \in \mathbb{R}_3 : \mathbf{A}_p\boldsymbol{\theta} \leq \mathbf{b}_p\}. \tag{5.3}$$

The procedure described above is recorded as Algorithm 6 below. This Algorithm is the same as Algorithm 1 from [91]. However, in this thesis, the configuration space analyzed is larger and can be extended to account for the infinite roll rotation feature of the coaxial SPM. As a part of future work, a faster method has to be considered such as inscribing a cylinder inside the C-space, and compared with the C-space obtained with the given algorithm. In this thesis, it is believed that using this specific approach is conservative and allows to increase in the size of the C-space, however a thorough comparison needs to be conducted. The configurations space obtained in Fig. 4-1c was convex-approximated using this algorithm. The resultant C-space is shown in Fig. 5-2. Due to the heavy computational burden of Algorithm 6, not all nodes from the original C-space were considered. A step of 20° was used to select the nodes used in the initial

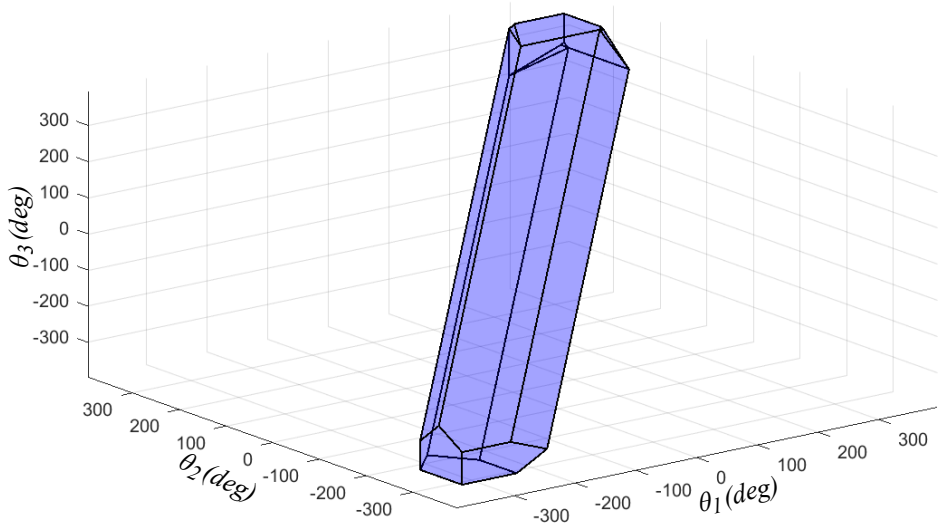

Figure 5-2: Convex Configuration Space

sets $\mathcal{V}$ and $\mathcal{F}$. The remaining points were disregarded in the current stage of the research. It also should be noted that because coaxial SPM has infinite rotations, its configuration space is not bounded, and to account for this the previously reported C-space (from Section 4.3) was modified to include some configuration exceeding the original 3D grid and it was also center at $\left[0°, 0°, 0°\right]$, i.e., the home configuration. It has the H-representation described by $\mathbf{A}_p$ matrix of the size 42x3, and $\mathbf{b}_p$ matrix of the size 42x1, i.e., it is described with 43 inequalities. The $\mathbf{A}$ and $\mathbf{b}$ matrices are given in Appendix D.

5.2 Constrained Control with Joystick Inputs

Once the new convex estimate of the configuration space is obtained, it is used in the constrained orientation control in real-time. The estimated polytope $\mathcal{P}$ defined in its H-representation form is used to check whether any input configuration is inside the convex C-space or not. The input trajectory is sampled with some time interval, and at each sampling instant, the checks are performed. If it is outside then the closest possible input configuration within the convex C-space is used instead. The value of the closest constrained input joint position vector, $\boldsymbol{\theta}_{constr}$, is obtained as the projection of the reference input position vector, $\boldsymbol{\theta}_{ref}$,

Algorithm 6: Convex approximation of the configuration space

Input: $\mathcal{V}$, $\mathcal{F}$, $\boldsymbol{\theta}_{start}$
Output: Set $\mathcal{P}$

```
/* collection of unfeasible areas                                    */
```
$\mathcal{C} \leftarrow \emptyset$;
for $k \leftarrow 1$ **to** $|\mathcal{F}|$ **do**
  $\mathcal{C} \leftarrow \{\mathcal{C}, \mathcal{C}_k\}$;
```
/* initialization of P_temp                                          */
```
$\mathcal{P}_{temp} \leftarrow \{\boldsymbol{\theta}_{start}\}$;
```
/* initialization of vertex list P_temp                              */
```
$\mathcal{V}_{\mathcal{P}} \leftarrow \{\boldsymbol{\theta}_{start}\}$;
$i \leftarrow 0$;
while $\mathcal{V} \setminus \mathcal{V}_{\mathcal{P}} \neq \emptyset$ **do**
  $i \leftarrow i + 1$;
  for $k \leftarrow 1$ **to** $|\mathcal{V} \setminus \mathcal{V}_{\mathcal{P}}|$ **do**
    $\mathbf{v}_k \leftarrow k$-th element of $\mathcal{V} \setminus \mathcal{V}_{\mathcal{P}}$;
    ```
    /* distance computed as in 5.2                                   */
    ```
    $d_k \leftarrow \text{dist}(\mathbf{v}_k, \mathcal{P}_{temp})$;
  $d_{min} \leftarrow \min\{d_k\}_{k=1}^{\mathcal{V}\setminus\mathcal{V}_{\mathcal{P}}}$;
  $\mathcal{V}_N \leftarrow \{\mathbf{v}_j : d_j == d_{min}\}$;
  for $j \leftarrow 1$ **to** $|\mathcal{V}_N|$ **do**
    $\mathcal{P}'_{temp} = \text{co}(\mathcal{P}_{temp}, \mathbf{v}_j)$;
    intersect$\leftarrow$ false;
    for $k \leftarrow 1$ **to** $|\mathcal{F}|$ **do**
      if $\mathcal{P}_{temp} \cap \mathcal{C}_k \neq \emptyset$ **then**
        intersect$\leftarrow$ true;
        break;
    if *intersect == false* **then**
      $\mathcal{P}_{temp} \leftarrow \mathcal{P}'_{temp}$;
      $\mathcal{V}_{\mathcal{P}} \leftarrow \mathcal{V}_{\mathcal{P}} \cup \{\mathbf{v}_j\}$;
    else
      $\mathcal{V} \leftarrow \mathcal{V} \setminus \{\mathbf{v}_j\}$;
$\mathcal{P} \leftarrow \mathcal{P}_{temp}$;
return $\mathcal{P}$

onto $\mathcal{P}$, solved as the QP in the form:

$$\begin{aligned} \boldsymbol{\theta}_{constr} = \arg\min_{\boldsymbol{\theta}} \quad & \|\boldsymbol{\theta} - \boldsymbol{\theta}_{ref}\|_2^2 \\ \text{s.t.} \quad & \mathbf{A}_p\boldsymbol{\theta} \leq \mathbf{b}_p \end{aligned} \tag{5.4}$$

The input joint position vector, $\boldsymbol{\theta}_{constr}$, is within the C-space and ensures that the manipulator will not have singularities and link collisions. To test the

proposed constrained orientation control via external reference tracking the developed coaxial SPM prototype was equipped with a UM7 IMU sensor from CHRobotics. The sensor was mounted on top of the mobile platform with its reference frame parallel to the coaxial SPM's reference frame, but with an offset on the z-axis. This sensor combines triaxial accelerator, rate gyro, and magnetometer data using an extended Kalman filter to produce an estimate of the orientation of the mobile platform in the form of an orientation quaternion at each sampling instant, $\mathbf{q}_{mp}$, where subscript mp stands for the mobile platform. The quaternions were converted to the vector form using the following equation:

$$\mathbf{v}_{mp,i} = \mathbf{q}\mathbf{v}_{home,i}\mathbf{q}^*, \quad i = 1, 2, 3, \tag{5.5}$$

using the Hamilton product, where $\mathbf{q}^*$ is the quaternion conjugate, $\mathbf{v}_{home,i}$ is the home configuration.

The sensor readings were sent wirelessly to the control computer similar to the approach in [320]. This was required to ensure that sensor wires are not screwed up by the manipulator's motions/rotations; it can affect the quality of sensor measurements. The external reference position is provided by the gamepad joystick from Microsoft Xbox, whose orientation can also be described in the form of quaternion, $\mathbf{q}_{ref}$. It has two tracked buttons that can provide orientation input, however, the data is given in the form of x and y components of their location on a unit circle. The z component is found as:

$$joystick_z = \sqrt{1 - joystick_x^2 - joystick_y^2} \tag{5.6}$$

Control of the coaxial SPM was implemented using the Robot Operating System (ROS) framework. It allows the integration of different parts of the developed system together and provides easy communication between the sensors and actuators UM7 IMU, Xbox joystick, and Dynamixel XM540-W150 servomotors). To communicate with the joystick, the *joy* package was used (http://wiki.ros.org/joy). The *UM7* package (http://wiki.ros.org/um7) was used to communicate with the IMU sensor. The actuators were controlled with Dynamixel Workbench API from ROS. The control algorithm was implemented in C code and included the

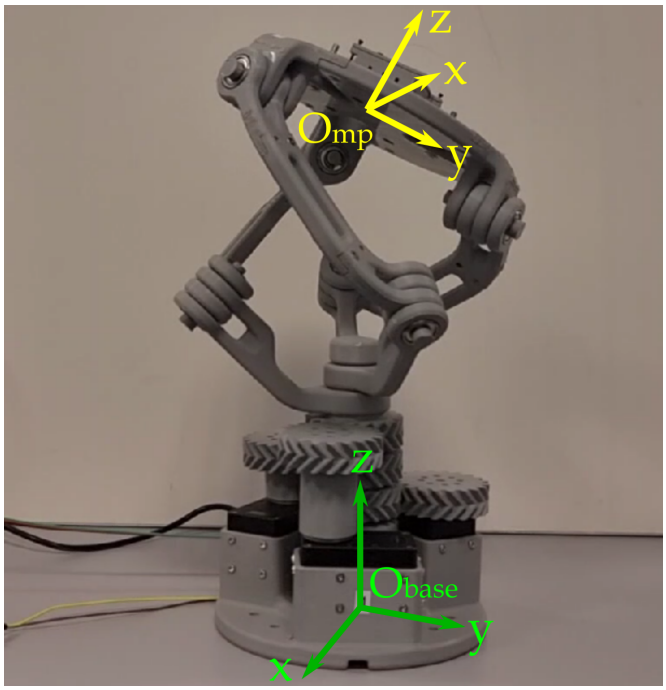

Figure 5-3: External reference position set by the joystick (joystick is not shown)

calculation of inverse kinematic problem from the joystick's reference input, and QP solver for finding the closest constrained input joint position vector, $\boldsymbol{\theta}_{constr}$. In particular, the CVXGEN tool [321] for embedded convex optimizations was used to obtain the C code implementation of the QP solver routine (based on interior point methods). These calculations were made in real-time, based on the previously offline-generated convex C-space $\mathcal{P}$.

An example of external reference tracking is shown in Fig. 5-3. This reference position was set externally by the joystick, and an extended rotational motion of the mobile platform was executed in this position. The referenced input joint positions, $\boldsymbol{\theta}_{ref}$, were obtained by solving the inverse kinematic problem for the joystick's position $\mathbf{q}_{ref}$. The constrained input joint positions $\boldsymbol{\theta}_{constr}$ were also calculated by solving the inverse kinematic problem for the IMU sensor position data $\mathbf{q}_{mp}$. A comparison of the resultant input joint position is presented in Fig. 5-4. These positions can also be viewed on the C-space in the form of 3D trajectory as depicted in Fig. 5-5. Based on these figures, it can be concluded that the developed coaxial SPM's external reference tracking framework is fully operational and functional.

5.3 Inertial Stabilization

Since it was confirmed that the developed control framework is capable of external reference tracking, inertial stabilization based on the same constrained control approach can be implemented. The coaxial SPM-based stabilization system has to hold the object in the reference position while ensuring the absence of singularities and link collisions. In this scenario, the base is not stationary, but rather goes through some motions, and the stabilization control has to balance the mobile platform. To obtain the data about the base position, an additional UM7-LT IMU sensor was installed in the base of the coaxial SPM. The orientation of the base platform is provided in the form of an orientation quaternion at each sampling instant, $\mathbf{q}_{base}$. Employing the quaternion-based rotation sequence rule [322], the resulting quaternion for calculation input joint position to achieve stabilization of the mobile platform is calculated as:

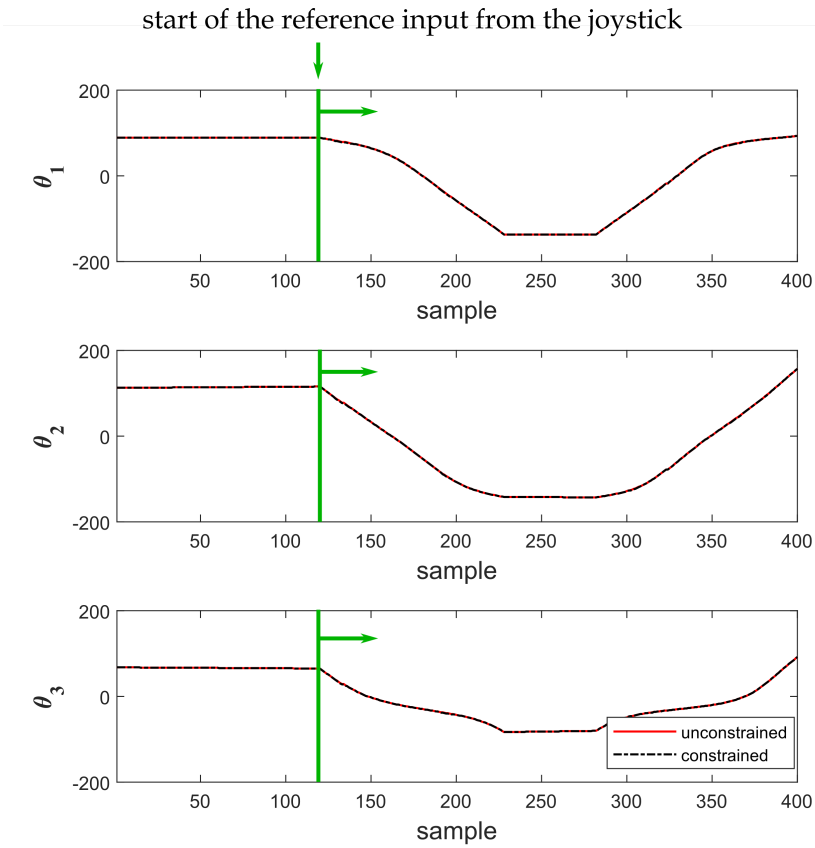

Figure 5-4: Comparison of the referenced input joint positions, $\boldsymbol{\theta}_{ref}$, obtained using inverse kinematics from $\mathbf{q}_{ref}$ with the constrained input joint positions $\boldsymbol{\theta}_{constr}$ as calculated from the IMU sensor data $\mathbf{q}_{mp}$

$$\mathbf{q} = \mathbf{q}_{base}^{-1} \times \mathbf{q}_{ref} \tag{5.7}$$

The inertial stabilization control algorithm was implemented using the ROS framework and C programming language, similar to the external reference tracking scenario. The resulting list of nodes and topics is given in Fig. 5-6. To test the inertial stabilization framework, a home configuration was used as the reference position, and the coaxial SPM's base was moved as shown in Figs. 5-7a and 5-7b. The sampling frequency from the orientation IMU sensors was set to 50 Hz (the sampling frequency with which the given IMU sensor was stably working). Orientations (in the form of quaternions) of the coaxial SPM's mobile platform, $\mathbf{q}_{mp}$, and base platform $\mathbf{q}_{base}$ are depicted in Fig. 5-8. The resulting input joint positions, $\boldsymbol{\theta}_{constr}$ are shown with a black dashed line in Fig. 5-9. From the figure, it is seen that when the coaxial SPM is tilted too much it results in the input joint position vector going out of the convex C-space as illustrated with a red trajectory in Fig. 5-10. In this figure, the red trajectory is the unconstrained one, $\boldsymbol{\theta}_{ref}$, obtained from the $\mathbf{q}$ quaternion. In contrast, the black trajectory, $\boldsymbol{\theta}_{constr}$, is constrained and is obtained as a result of the constrained orientation control framework. As seen in the left view, the constrained trajectory does not leave the boundaries of the C-Space, ensuring the safe stabilization of the coaxial SPM. A part of the red trajectory outside the convex configuration space corresponds to the input angle positions at samples approximately 300-425. In this part of the manipulator's motion, the mobile platform can no longer stay in the referenced home position, but rather stays in the closest one at each sampling instant, demonstrated in Fig. 5-7c.

Overall, this chapter demonstrated the application examples of the final motion control system based on the coaxial SPM model with implemented trajectory tracking and stabilization control.

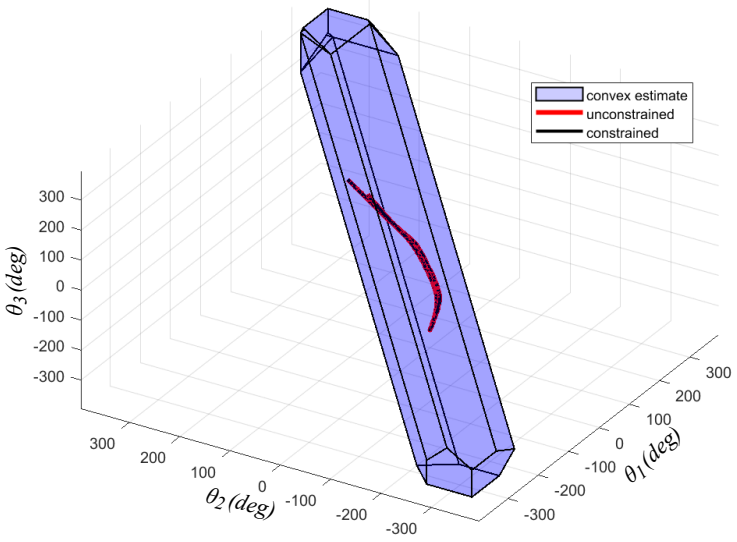

(a)

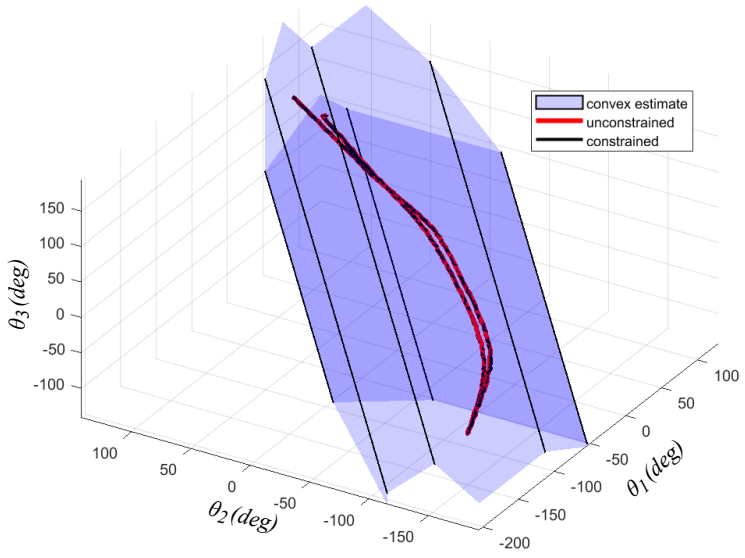

(b)

Figure 5-5: Trajectory for motion from Fig. 5-3: (a) full view, (b) zoomed-in view

Figure 5-6: List of rostopics and rosnodes

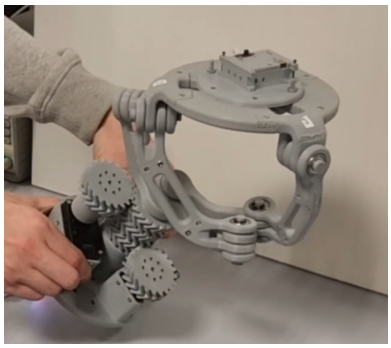

(a) Stabilized orientation, at one of the sampling instants

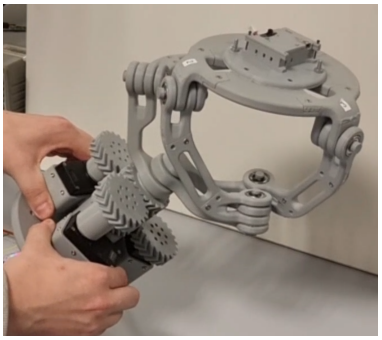

(b) Stabilized orientation, at another sampling instant

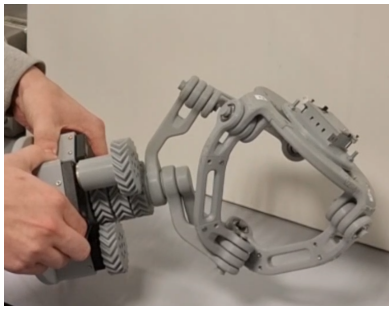

(c) Stabilized orientation outside of the constrained configuration space

Figure 5-7: Inertial stabilization example

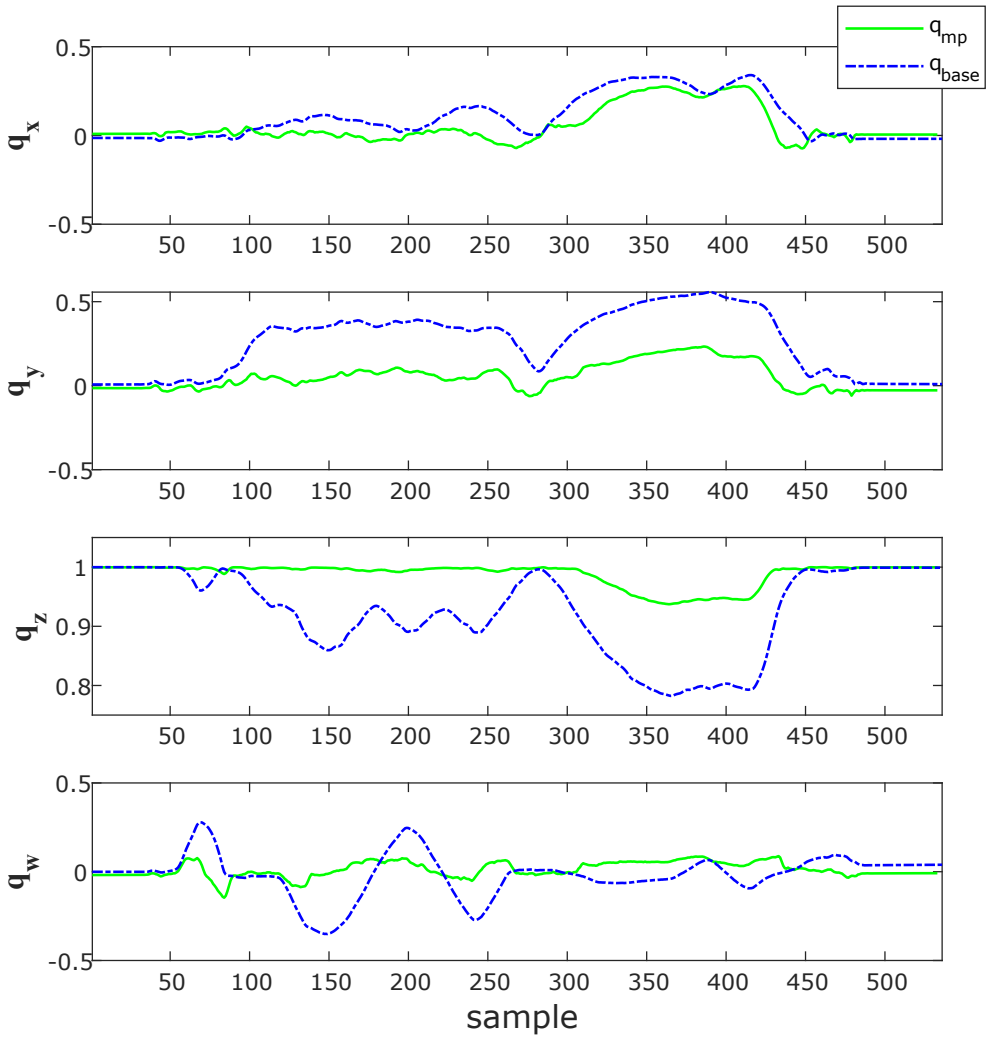

Figure 5-8: Orientations of the coaxial SPM's mobile platform, $\mathbf{q}_{mp}$, and base platform $\mathbf{q}_{base}$

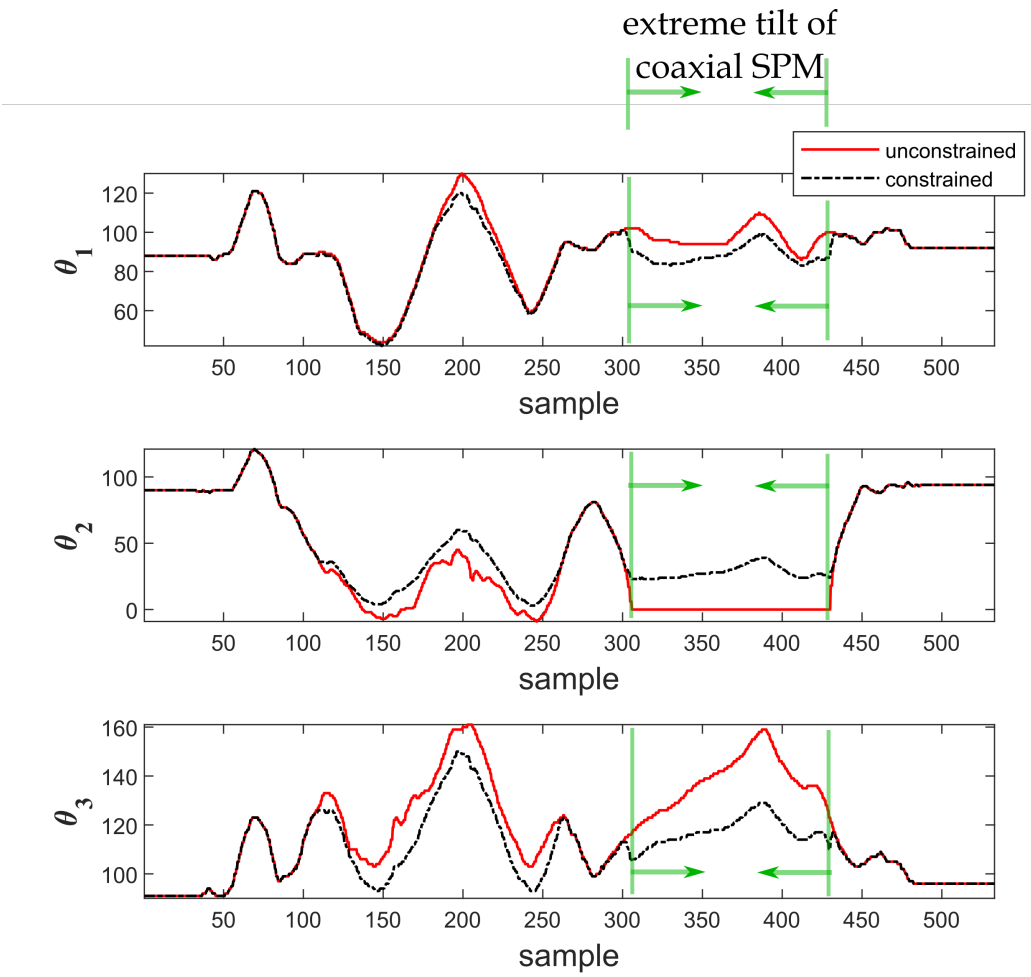

Figure 5-9: Constrained input joint positions $\boldsymbol{\theta}_{constr}$ as calculated from $\mathbf{q}$ using Equation (5.7)

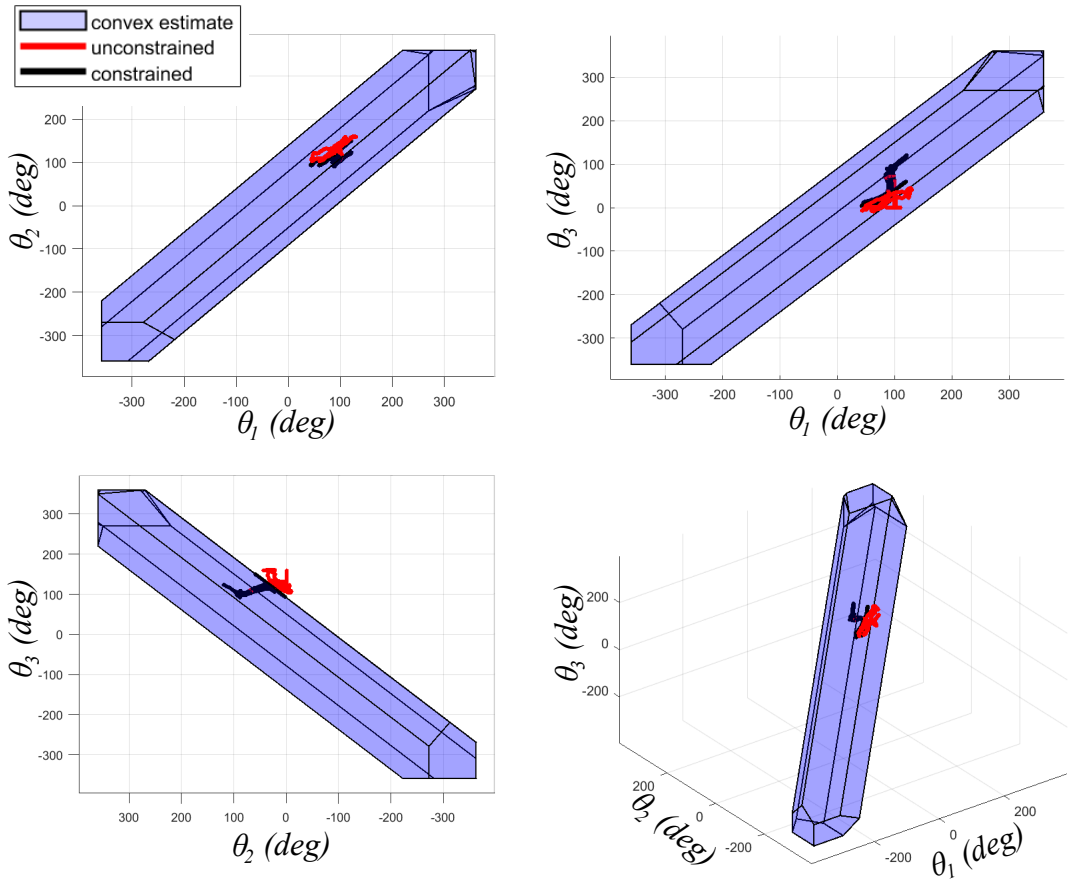

Figure 5-10: Trajectory for motion from Fig. 5-7 from different view angles, from left to right: top view, right view, left view, view from an angle

Chapter 6

Conclusions and Future Work

6.1 Summary

In this thesis, it was investigated if motion control platforms can be developed based on the coaxial SPM with capabilities to infinitely rotate its mobile platform and achieve target tracking and object stabilization.

To test the thesis hypothesis, forward and inverse kinematics of a coaxial SPM was studied at the beginning. Algorithms to obtain unique solutions to the forward and inverse kinematic problems were presented. Next, the extended and (or) infinite rotational motion of the presented manipulator was analyzed with one more algorithm to generate such motions presented.

The results of the kinematic analysis of the coaxial SPM were applied in estimating the Cartesian workspace and feasible configuration space. While obtaining these spaces using a numerical approach, singular configurations and configurations leading to link collisions were excluded, ensuring the safe operation of the coaxial SPM.

Afterward, coaxial SPM's configuration space was used to generate motion trajectories for external reference tracking and stabilization. For this purpose, the C-space previously obtained was convex-approximated to be used in real-time application examples. IMU orientation sensors were used to measure the orientations of the mobile and base platforms, and the joystick gamepad was used to provide external reference commands. The final motion control system was developed using the ROS framework and C programming language.

As the result of the work conducted in the scope of this thesis, it was shown that coaxial SPMs could be used as 3-DOF motion control platforms with target tracking and object stabilization, and the operational physical prototype of the system was developed. Overall concluding that the hypothesis was true.

Potential applications of the developed manipulator and its developed real-time control framework include rehabilitation devices where a wider range of rotations is required, surgical robotics where full-circle rotation of the tools is required (e.g., laparoscopic surgeries), motion control systems and stabilization platforms, as well as some machining devices (e.g., turning and milling machines).

6.2 Contributions

The main contributions of this thesis are:

- Developed algorithms for obtaining unique kinematic solutions to the forward and inverse kinematic problems of the coaxial SPM
- Developed simulation model of the coaxial SPM in CoppeliaSim and utilized it for link collision estimations helping to foster PM analysis in this simulator software
- Found that for the given SPM geometry its maximum tilt is equal to 39°
- Developed an orientation control framework with infinite rotation capability using IMU feedback and joystick control in the ROS framework

6.3 Limitations of the Reported Research

During the research related to the thesis, one of the obstacles was the accuracy of the manufactured prototype since it was 3D printed. A better approach would be to manufacture it using CNC milling with metal. However, that would increase the cost of the prototype, and at the current stage having a 3D printed version is enough, since some design modifications can be introduced easier and faster. Another issue was the poor accuracy of the IMU sensor used (UM7 from

CHRobotics); the measurements provided were not stable, and the effect of sensor drifting was present.

Since a numerical approach was used in obtaining the configuration space, its representation cannot be the most precise one. A higher sampling of the tested 3D space would be desirable, however, it would come at the expense of the increased computation time.

6.4 Future Work

For future research in the direction of this thesis, an optimization of the manipulator's design to obtain a larger configuration space is possible, since the current geometric parameters were selected to match other works in this field, and optimized for other performance parameters.

Velocity control for the actuators can be investigated for the generation of infinite rotational motions as it was observed that there is some dependency between such rotations and input joint position rates.

Dynamic analysis can also be conducted to be incorporated into the overall stabilization control framework, taking the effect of external forces into effect.

A less conservative convex approximation of the configuration space can be obtained by inscribing a cylindrical shape inside the C-space. This can potentially simplify the computational burden on the control system and increase the response rate required for fast real-time control.

BLANK

Appendix A

Example of the Solutions to the Forward Kinematics Problem

Table A.1: Solutions to the forward kinematics using CAD (Example 2).

Solution	$\mathbf{v}_1^T$	$\mathbf{v}_2^T$	$\mathbf{v}_3^T$
Fig. A-1a	$[0.000, -1.000, 0.000]$	$[0.866, 0.500, 0.000]$	$[-0.866, 0.500, 0.000]$
Fig. A-1b	$[0.000, 1.000, 0.000]$	$[-0.866, -0.500, 0.000]$	$[0.866, -0.500, 0.000]$
Fig. A-1c	$[0.000, -1.000, 0.000]$	$[-0.520, 0.500, -0.693]$	$[0.520, 0.500, -0.693]$
Fig. A-1d	$[0.000, 1.000, 0.000]$	$[0.520, -0.500, -0.693]$	$[-0.520, -0.500, 0.693]$
Fig. A-1e	$[-0.693, -0.200, -0.693]$	$[-0.173, 0.700, 0.693]$	$[0.866, -0.500, 0.000]$
Fig. A-1f	$[0.693, 0.200, 0.693]$	$[0.173, -0.700, -0.693]$	$[-0.866, 0.500, 0.000]$
Fig. A-1g	$[0.693, -0.200, 0.693]$	$[-0.866, -0.500, 0.000]$	$[0.173, 0.700, -0.693]$
Fig. A-1h	$[-0.693, 0.200, -0.693]$	$[0.866, 0.500, 0.000]$	$[-0.173, -0.700, 0.693]$

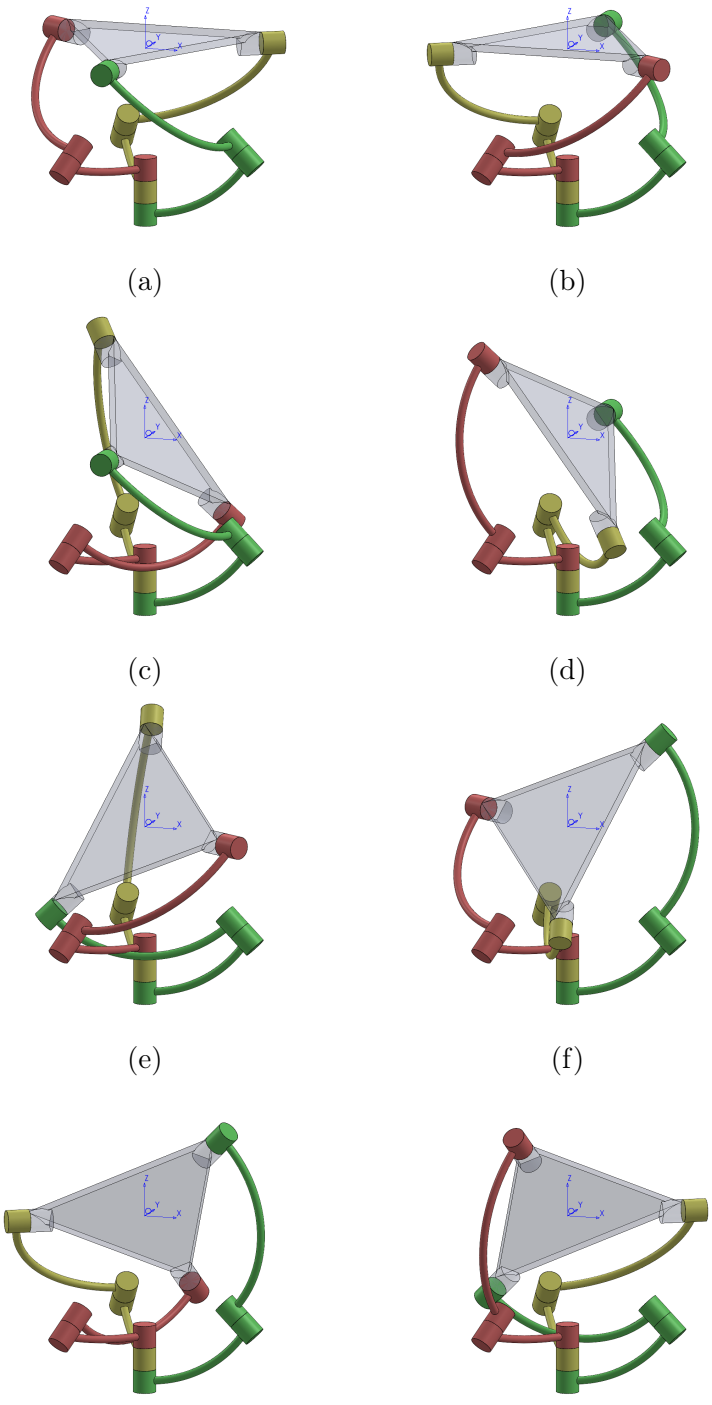

(a) (b) (c) (d) (e) (f) (g) (h)

Figure A-1: Solutions to the forward kinematics for zero input (Example 2)

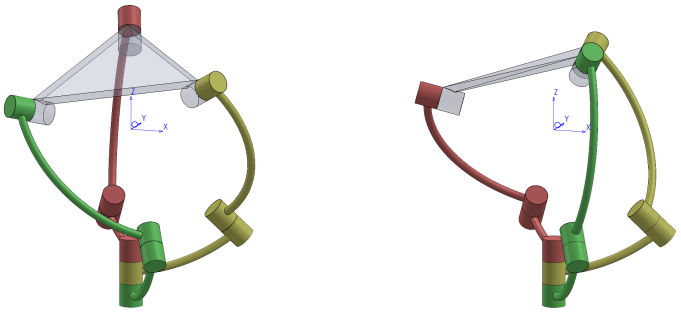

(a)

(b)

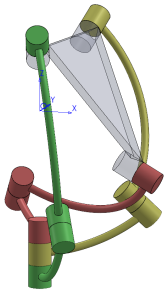

(c)

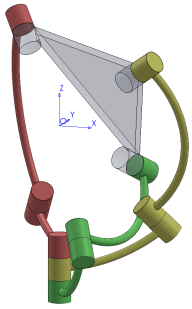

(d)

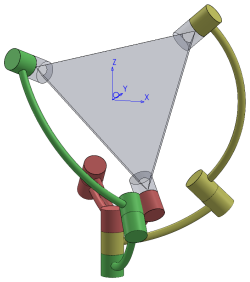

(e)

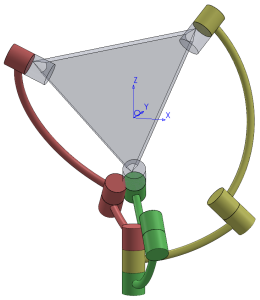

(f)

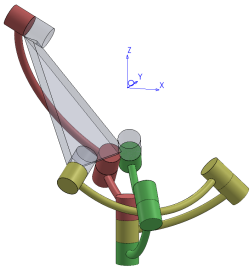

(g)

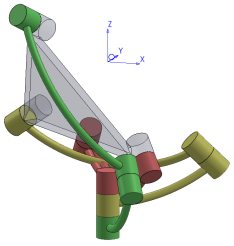

(h)

Figure A-2: Solutions to the forward kinematics for non-zero input (Example 3)

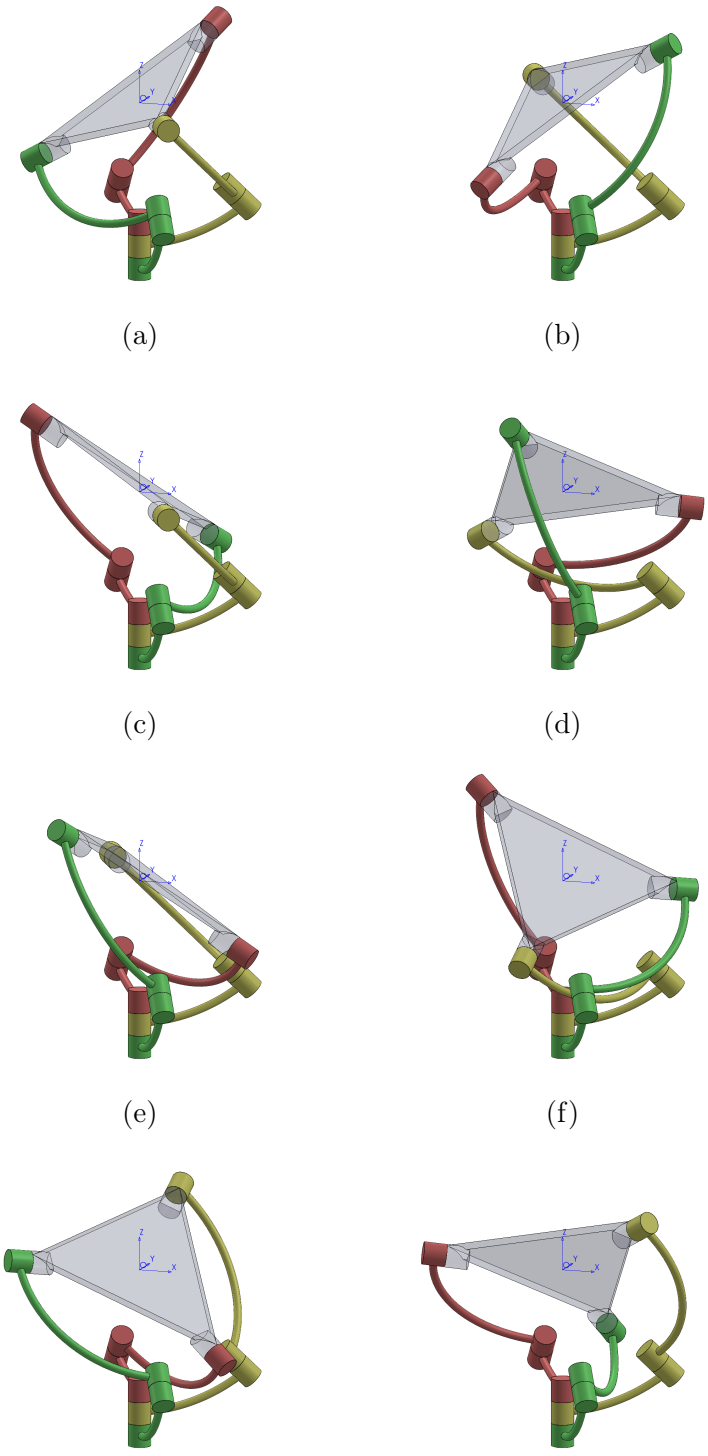

(a) (b) (c) (d) (e) (f) (g) (h)

Figure A-3: Solutions to the forward kinematics for non-zero input (Example 4)

Table A.2: Solutions to the forward kinematics using CAD (Example 3).

Solution	$\mathbf{v}_1^T$	$\mathbf{v}_2^T$	$\mathbf{v}_3^T$
Fig. A-2a	$[-0.676, -0.690, 0.259]$	$[0.781, -0.406, 0.473]$	$[-0.234, 0.674, 0.701]$
Fig. A-2b	$[0.467, -0.540, 0.701]$	$[0.039, 0.880, 0.473]$	$[-0.935, -0.240, 0.259]$
Fig. A-2c	$[0.204, -0.687, 0.697]$	$[0.183, 0.807, 0.562]$	$[0.883, -0.030, -0.468]$
Fig. A-2d	$[0.416, 0.780, -0.468]$	$[0.790, -0.245, 0.562]$	$[-0.493, 0.520, 0.697]$
Fig. A-2e	$[-0.497, -0.764, 0.413]$	$[0.746, 0.038, 0.665]$	$[0.483, -0.528, -0.699]$
Fig. A-2f	$[-0.216, 0.682, -0.699]$	$[0.406, 0.627, 0.665]$	$[-0.909, -0.048, 0.413]$
Fig. A-2g	$[-0.204, 0.687, -0.697]$	$[-0.183, -0.807, -0.562]$	$[-0.883, 0.030, 0.468]$
Fig. A-2h	$[-0.416, -0.780, 0.468]$	$[-0.790, 0.245, -0.562]$	$[0.493, -0.520, -0.697]$

Table A.3: Solutions to the forward kinematics using CAD (Example 4).

Solution	$\mathbf{v}_1^T$	$\mathbf{v}_2^T$	$\mathbf{v}_3^T$
Fig. A-3a	$[-0.862, 0.079, -0.500]$	$[0.500, -0.866, 0.000]$	$[0.362, 0.787, 0.500]$
Fig. A-3b	$[0.862, -0.079, 0.500]$	$[-0.500, 0.866, 0.000]$	$[-0.362, -0.787, -0.500]$
Fig. A-3c	$[0.362, 0.787, -0.500]$	$[0.500, -0.866, 0.000]$	$[-0.862, 0.079, 0.500]$
Fig. A-3d	$[-0.137, -0.782, 0.608]$	$[-0.781, 0.410, -0.471]$	$[0.918, 0.372, -0.137]$
Fig. A-3e	$[-0.362, -0.787, 0.500]$	$[-0.500, 0.866, 0.000]$	$[0.862, -0.079, -0.500]$
Fig. A-3f	$[0.781, 0.609, -0.137]$	$[-0.036, -0.881, -0.471]$	$[-0.746, 0.272, 0.608]$
Fig. A-3g	$[-0.781, -0.609, 0.137]$	$[0.036, 0.881, 0.471]$	$[0.746, -0.272, -0.608]$
Fig. A-3h	$[0.137, 0.782, -0.608]$	$[0.781, -0.410, 0.471]$	$[-0.918, -0.372, 0.137]$

Table A.4: Comparison of the forward kinematics solutions (Examples 2-4).

Orientation	$\mathbf{v}_1^T$	$\mathbf{v}_2^T$	$\mathbf{v}_3^T$
Fig. A-1a CAD	$[0.000, -1.000, 0.000]$	$[0.866, 0.500, 0.000]$	$[-0.866, 0.500, 0.000]$
Fig. A-1a calculated	$[0.0003, -1.0000, 0.0003]$	$[0.8659, 0.5003, 0.0003]$	$[-0.8662, 0.4997, 0.0003]$
Fig. A-1b CAD	$[0.000, 1.000, 0.000]$	$[-0.866, -0.500, 0.000]$	$[0.866, -0.500, 0.000]$
Fig. A-1b calculated	$[0.0003, 1.0000, 0.0003]$	$[-0.8662, -0.4997, 0.0003]$	$[0.8659, -0.5003, 0.0003]$
Fig. A-2a CAD	$[-0.676, -0.690, 0.259]$	$[0.781, -0.406, 0.473]$	$[-0.234, 0.674, 0.701]$
Fig. A-2a calculated	$[-0.6759, -0.6898, 0.2594]$	$[0.7814, -0.4064, 0.4735]$	$[-0.2340, 0.6740, 0.7007]$
Fig. A-2b CAD	$[0.467, -0.540, 0.701]$	$[0.039, 0.880, 0.473]$	$[-0.935, -0.240, 0.259]$
Fig. A-2b calculated	$[0.4667, -0.5396, 0.7007]$	$[0.0387, 0.8799, 0.4735]$	$[-0.9353, -0.2405, 0.2594]$
Fig. A-3a CAD	$[-0.862, 0.079, -0.500]$	$[0.500, -0.866, 0.000]$	$[0.362, 0.787, 0.500]$
Fig. A-3a calculated	$[-0.8625, 0.0791, -0.4998]$	$[0.5001, -0.8659, 0.0002]$	$[0.3620, 0.7866, 0.5002]$
Fig. A-3b CAD	$[0.862, -0.079, 0.500]$	$[-0.500, 0.866, 0.000]$	$[-0.362, -0.787, -0.500]$
Fig. A-3b calculated	$[0.8622, -0.0798, 0.5002]$	$[-0.4999, 0.8661, 0.0002]$	$[-0.3627, -0.7865, -0.4998]$

Appendix B

Example of the Solutions to the Inverse Kinematics Problem

Table B.1: Comparison of the inverse kinematics solutions (Examples 2-4).

Orientation	$\mathbf{v}$	$\boldsymbol{\theta}_{CAD}$	$\boldsymbol{\theta}_{calculated}$
Fig. B-1a	$\begin{bmatrix} 0.000 & 0.866 & -0.866 \\ -1.000 & 0.500 & 0.500 \\ 0.000 & 0.000 & 0.000 \end{bmatrix}$	$\begin{bmatrix} 0.00° \\ 0.00° \\ 0.00° \end{bmatrix}$	$\begin{bmatrix} 0.0000° \\ -0.0007° \\ 0.0007° \end{bmatrix}$
Fig. B-1b	$\begin{bmatrix} 0.000 & 0.866 & -0.866 \\ -1.000 & 0.500 & 0.500 \\ 0.000 & 0.000 & 0.000 \end{bmatrix}$	$\begin{bmatrix} 180.00° \\ 180.00° \\ 180.00° \end{bmatrix}$	$\begin{bmatrix} -180.0000° \\ 179.9993° \\ -179.9993° \end{bmatrix}$
Fig. B-2a	$\begin{bmatrix} -0.676 & 0.781 & -0.234 \\ -0.690 & -0.406 & 0.674 \\ 0.259 & 0.473 & 0.701 \end{bmatrix}$	$\begin{bmatrix} 60.00° \\ 90.00° \\ 120.00° \end{bmatrix}$	$\begin{bmatrix} 59.9657° \\ 89.9718° \\ 120.1282° \end{bmatrix}$
Fig. B-2b	$\begin{bmatrix} -0.676 & 0.781 & -0.234 \\ -0.690 & -0.406 & 0.674 \\ 0.259 & 0.473 & 0.701 \end{bmatrix}$	$\begin{bmatrix} 208.84° \\ 204.96° \\ 141.71° \end{bmatrix}$	$\begin{bmatrix} -151.1401° \\ -155.0368° \\ 141.5797° \end{bmatrix}$
Fig. B-3a	$\begin{bmatrix} -0.862 & 0.500 & 0.362 \\ 0.079 & -0.866 & 0.787 \\ -0.500 & 0.000 & 0.500 \end{bmatrix}$	$\begin{bmatrix} 60.00° \\ 90.00° \\ 120.00° \end{bmatrix}$	$\begin{bmatrix} 59.9527° \\ 89.9993° \\ 119.9545° \end{bmatrix}$
Fig. B-3b	$\begin{bmatrix} -0.862 & 0.500 & 0.362 \\ 0.079 & -0.866 & 0.787 \\ -0.500 & 0.000 & 0.500 \end{bmatrix}$	$\begin{bmatrix} 310.53° \\ 270.00° \\ 229.47° \end{bmatrix}$	$\begin{bmatrix} -49.4799° \\ -90.0007° \\ -130.5520° \end{bmatrix}$

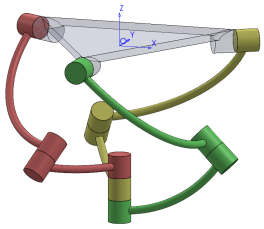

(a) *l-l-l* working mode

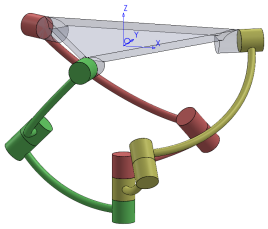

(b) *r-r-r* working mode

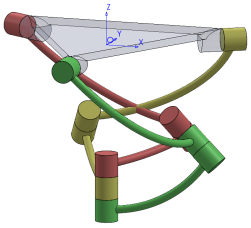

(c) *l-l-r* working mode

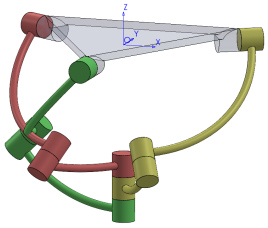

(d) *r-r-l* working mode

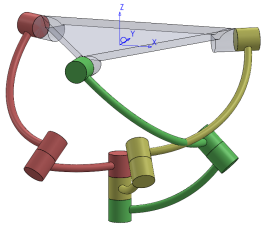

(e) *l-r-l* working mode

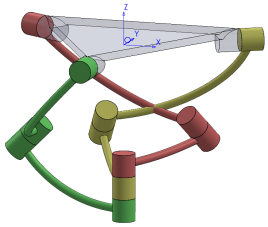

(f) *r-l-r* working mode

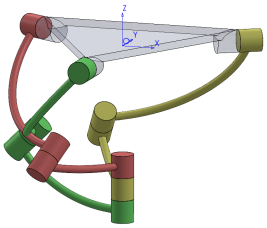

(g) *r-l-l* working mode

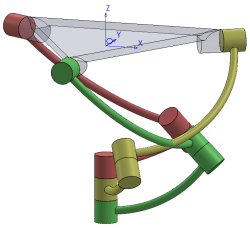

(h) *l-r-r* working mode

Figure B-1: Solutions to the inverse kinematics (pose taken from Fig. A-1a)

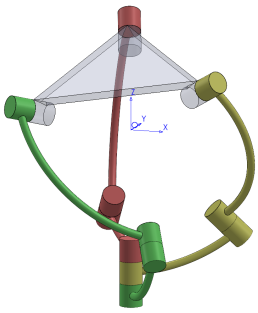

(a) *l-l-l* working mode

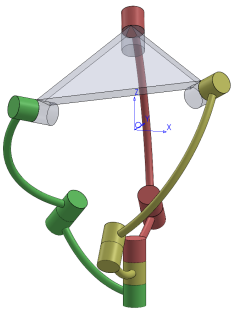

(b) *r-r-r* working mode

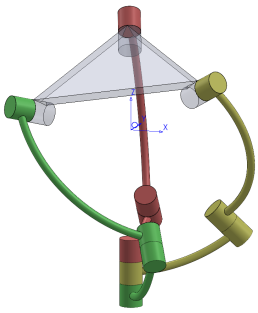

(c) *l-l-r* working mode

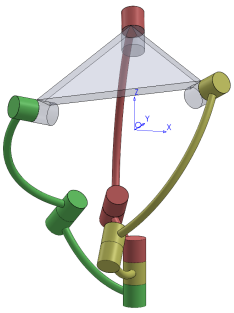

(d) *r-r-l* working mode

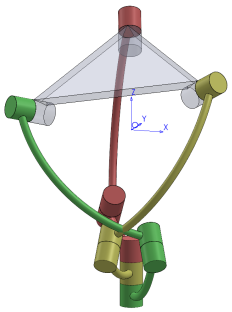

(e) *l-r-l* working mode

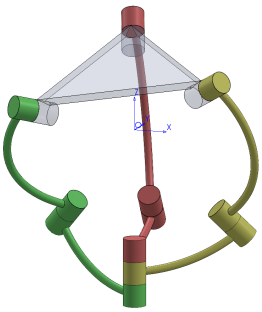

(f) *r-l-r* working mode

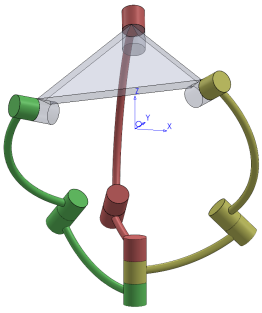

(g) *r-l-l* working mode

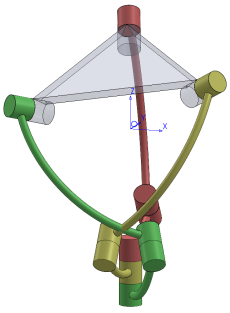

(h) *l-r-r* working mode

Figure B-2: Solutions to the inverse kinematics (pose taken from Fig. A-2a)

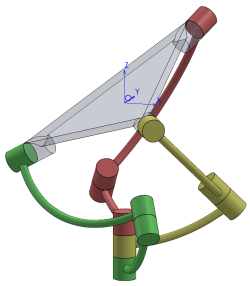

(a) *l-l-l* working mode

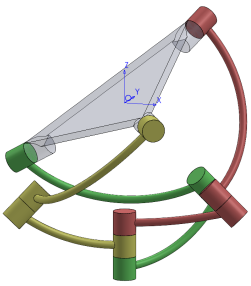

(b) *r-r-r* working mode

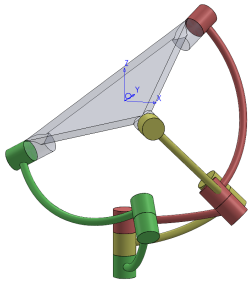

(c) *l-l-r* working mode

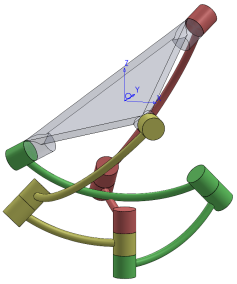

(d) *r-r-l* working mode

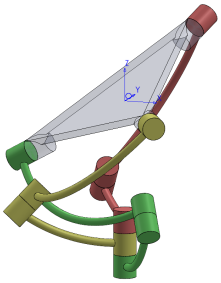

(e) *l-r-l* working mode

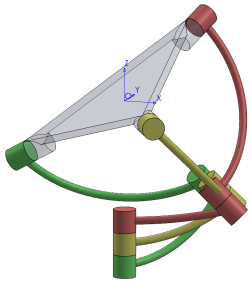

(f) *r-l-r* working mode

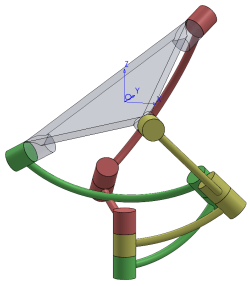

(g) *r-l-l* working mode

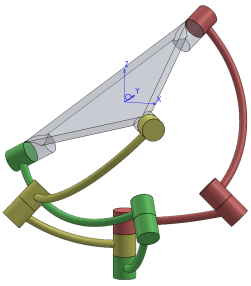

(h) *l-r-r* working mode

Figure B-3: Solutions to the inverse kinematics (pose taken from Fig. A-3a)

Appendix C

Setting CoppeliaSim

C.1 Creating Coaxial SPM Model in CoppeliaSim

The initial stage of simulating a robot involves creating a manipulator model in CoppeliaSim that adheres to all mechanical constraints, ensuring that the model's motion simulation mirrors that of the physical prototype. The first step was to import the SolidWorks-designed manipulator model into CoppeliaSim, ensuring that the CAD model isn't too heavy, or else it could negatively affect visualization and calculation modules in CoppeliSim. Therefore, the CAD model was simplified by removing insignificant design features like holes and small details. Afterward, the whole assembly was imported as a single mesh in STL format, with the number of triangles being reduced using the "`decimate the mesh`" function, followed by splitting the manipulator model into separate links using the "`automatic mesh division`" function. The stationary base link was created by merging the base platform, actuators, and gears. The imported CAD model was then reoriented to match the coordinate system of the kinematic model discussed Chapter 2. The model of the coaxial SPM in CoppeliaSim consists of seven shapes representing the manipulator links: the base, 6 mobile links, and mobile platform. The legs were colored differently to improve visual aspects of the simulation model. Finally, the model was ready to be assembled, similar to the closed-loop chain kinematic architecture of the manipulator as shown in Fig. 3-3.

There are 2 closed loops in this scene. The first one is *base - proximal link 3 - distal link 3 - mobile platform - distal link 1 - proximal link 1*, and the second one

is *base - proximal link 3 - distal link 3 - mobile platform - distal link 2 - proximal link 2*. In order to close the loop it is necessary to use *dummy* objects that are connected to the base and the last elements in the loops; all of them should be located in the center of the base. It is due to those dummy objects the simulator can simulate PMs.

In order to make the *kinematics* calculation module to work properly the *IK groups* have to be enabled, added, and activated in the simulator settings. In the case of the coaxial SPM it is necessary to have 2 *IK groups* with 2 *IK elements* in each (*closure-tip-1* linked to *closure-target-1*, and *closure-tip-2* linked to *closure-target-2*, also shown in Fig. 3-3 with dashed arrows). All constraints (*X, Y, Z, Alpha-Beta, Gamma*) have to be enabled in the settings of *IK groups*.

The Damped Least Squares (DLS) calculation method with the damping coefficient equal to 0.0001 was selected for the *kinematics* calculation module. It should also be noted that all joints used are revolute and are also used as the intermediate elements in the above-mentioned loops. The actuated joints are set to the *inverse kinematic mode* in *Scene Object Properties* menu, whereas remaining joints are set to the *passive* mode.

One of the important features of CoppeliaSim robot simulator is its built-in *collision detection* module that allows fast interference checking between any *shape* or collection of *shapes*. To have this feature in the simulation of the coaxial SPM it is necessary to enable all *collision detections* under *calculation module* settings. Afterward, new *collision objects* have to be added without enabling *explicit handling* mode. In this thesis, collision checks between each link versus all other links (entities) have been implemented, resulting in 8 *collision objects*. Whenever the link collision happens CoppeliaSim changes link colours to indicate the collision event, and sends his information to an external client.

Each link in CoppeliaSim has a position and an orientation in the 3D space. In order to determine the position and the orientation of the link we can use either absolute coordinates or joint coordinates. Due to the fact that the origin of the global coordinate system is located in the center of the bottom surface of the base, *dummy* objects were added to the center of rotation and all joints. In this way, the vectors representing these joints, i.e. $\mathbf{u}_i$, $\mathbf{w}_i$, and $\mathbf{v}_i$, are calculated

as the difference between each link *dummy* and the center of rotation *dummy*.

C.2 Model Interfacing with MATLAB and Motion Control

The first step in linking MATLAB to CoppeliaSim is to copy **vrchk.m**, **remoteApiProto.m**, **remApi.m**, and **remoteApi.dll** files from CoppeliaSim installation folder or website (`www.coppeliarobotics.com`) to MATLAB working folder. These files contain necessary API information and functions. After establishing communication with the simulator using *vrep.simxStart* function, the motion control of the simulated coaxial SPM can be realized. In order to be able to control simulated joints via MATLAB, at first, joint *handles* have to be obtained from the simulator using
vrep.simxGetObjectHandle function. Afterward, a joint position can be read or varied using *vrep.simxGetJointPosition* and *vrep.simxSetJointPosition* functions, respectively. If collision detection *handle* is required to be returned to MATLAB, this is done using *vrep.simxGetCollisionHandle* and *vrep.simxReadCollision* functions. *Handles* are returned from CoppeliaSim in the form of unique numbers assigned to each object, joint positions are returned as angle values in radians, collision events variable takes values 1 when indicating the collision and 0 if no collision occurs.

The coaxial SPM simulation model is actuated via MATLAB commands sent to actuated joints (highlighted in red in Fig. 3-3). Before sending any commands to the simulator it is also necessary to verify that input joint vector $\boldsymbol{\theta}$ does not lead to a singular configuration. It is done in MATLAB using the approach for computing the coaxial SPM unique kinematic solutions and verifying that the Jacobian matrix at this specific SPM configuration is full-rank.

Appendix D

A_p and b_p Matrices of the Convex C-Space

matrix A_p

42x3 double

	1	2	3
1	0.0023	0.0023	-0.0023
2	0.0026	0.0033	-0.0040
3	0.0033	-0.0040	0.0026
4	0.0023	-0.0023	0.0023
5	-0.0023	0.0023	0.0023
6	-0.0040	0.0026	0.0033
7	0.0047	-0.0116	0.0070
8	0.0047	-0.0116	0.0070
9	-2.4966e-18	-0.0111	0.0111
10	2.8184e-18	-0.0111	0.0111
11	-2.0998e-18	-0.0111	0.0111
12	-0.0116	0.0070	0.0047
13	-0.0116	0.0070	0.0047
14	-3.8565e-18	0.0028	-1.3306e-19
15	3.5059e-19	0.0028	-5.7226e-20
16	-1.4024e-18	0.0028	-1.5974e-18
17	-3.2134e-19	0.0028	9.6190e-20
18	0.0028	-1.8658e-19	8.6627e-19
19	0.0028	-2.9950e-18	-8.1563e-18
20	0.0028	-2.2377e-20	-5.7343e-18
21	0.0028	-2.1753e-18	1.2548e-16
22	1.8835e-19	2.9278e-19	0.0028
23	6.4515e-21	-1.4690e-18	0.0028
24	-6.5369e-20	7.8696e-20	0.0028
25	-1.2308e-19	-4.0080e-18	0.0028
26	6.3687e-19	-0.0028	-4.2807e-19
27	-1.5922e-18	-0.0028	1.5528e-19
28	-3.1843e-19	-0.0028	1.4838e-19
29	-0.0111	0.0111	-4.3315e-18
30	-0.0111	0.0111	-4.6815e-18
31	-0.0111	0.0111	-2.0708e-17
32	-0.0028	3.5075e-18	4.8507e-19
33	-0.0028	-1.5335e-18	1.3219e-18
34	-0.0028	-5.7626e-19	-3.5942e-19
35	0.0111	9.6465e-18	-0.0111
36	0.0111	-4.4152e-18	-0.0111
37	0.0111	1.7886e-17	-0.0111
38	-1.9712e-19	2.3170e-19	-0.0028
39	-1.5620e-18	5.5136e-19	-0.0028
40	1.0439e-20	7.3267e-19	-0.0028
41	0.0070	0.0047	-0.0116
42	0.0070	0.0047	-0.0116

matrix b_p

42x1 double

	1
1	1.0000
2	1.0000
3	1.0000
4	1.0000
5	1.0000
6	1.0000
7	0.9999
8	0.9999
9	0.9999
10	0.9999
11	0.9999
12	0.9999
13	0.9999
14	1.0000
15	1.0000
16	1.0000
17	1.0000
18	1.0000
19	1.0000
20	1.0000
21	1.0000
22	1.0000
23	1.0000
24	1.0000
25	1.0000
26	1.0000
27	1.0000
28	1.0000
29	0.9999
30	0.9999
31	0.9999
32	1.0000
33	1.0000
34	1.0000
35	0.9999
36	0.9999
37	0.9999
38	1.0000
39	1.0000
40	1.0000
41	0.9999
42	0.9999

Figure D-1: $\mathbf{A}_p$ and $\mathbf{b}_p$ matrices

Bibliography

[1] J.-P. Merlet, *Parallel Robots*. Springer, 2006.

[2] S. Sadeqi, S. P. Bourgeois, E. J. Park, and S. Arzanpour, "Design and performance analysis of a 3-RRR spherical parallel manipulator for hip exoskeleton applications," *Journal of Rehabilitation and Assistive Technologies Engineering*, vol. 4, pp. 1–11, 2017.

[3] J. Hunt and H. Lee, "A new parallel actuated architecture for exoskeleton applications involving multiple degree-of-freedom biological joints," *Journal of Mechanisms and Robotics*, vol. 10, no. 5, 2018.

[4] V. E. Gough and S. G. Whitehall, "Universal tyre test machine," *Proc. FISITA 9th Int. Technical Congr., London, 1962*, pp. 117–137, 1962.

[5] D. Stewart, "A platform with six degrees of freedom," *Proceedings of the Institution of Mechanical Engineers*, vol. 180, no. 1, pp. 371–386, 1965.

[6] D. Stewart, "A platform with six degrees of freedom," *Aircraft Engineering and Aerospace Technology*, vol. 38, no. 4, pp. 30–35, 1966.

[7] H. Chanal, E. Duc, and P. Ray, "A study of the impact of machine tool structure on machining processes," *International Journal of Machine Tools and Manufacture*, vol. 46, no. 2, pp. 98–106, 2006.

[8] J. Allen, D. Axinte, P. Roberts, and R. Anderson, "A review of recent developments in the design of special-purpose machine tools with a view to identification of solutions for portable in situ machining systems," *The International Journal of Advanced Manufacturing Technology*, vol. 50, no. 9, pp. 843–857, 2010.

[9] M. Petko and G. Karpiel, "Mechatronic design of a parallel manipulator for milling," in *2005 IEEE/ASME International Conference on Advanced Intelligent Mechatronics*, pp. 759–764, 2005.

[10] A. Pashkevich, A. Klimchik, S. Briot, and C. Damien, "Performance evaluation of parallel manipulators for milling application," *Global Product Development - Proceedings of the 20th CIRP Design Conference*, pp. 619–629, 2011.

[11] D. A. Axinte, J. M. Allen, R. Anderson, I. Dane, L. Uriarte, and A. Olara, "Free-leg Hexapod: a novel approach of using parallel kinematic platforms for developing miniature machine tools for special purpose operations," *CIRP Annals*, vol. 60, no. 1, pp. 395–398, 2011.

[12] A. Olarra, J. M. Allen, and D. A. Axinte, "Experimental evaluation of a special purpose miniature machine tool with parallel kinematics architecture: free leg hexapod," *Precision Engineering*, vol. 38, no. 3, pp. 589–604, 2014.

[13] G. Wu and B. Niu, "Dynamic stability of a tripod parallel robotic wrist featuring continuous end-effector rotation used for drill point grinder," *Mechanism and Machine Theory*, vol. 129, pp. 36–50, 2018.

[14] H. Saied, A. Chemori, M. Michelin, M. El-Rafei, C. Francis, and F. Pierrot, "A redundant parallel robotic machining tool: design, control and real-time experiments," in *New Developments and Advances in Robot Control*, pp. 39–79, Springer, 2019.

[15] F. Pierrot, C. Reynaud, and A. Fournier, "DELTA: a simple and efficient parallel robot," *Robotica*, vol. 8, no. 2, pp. 105–109, 1990.

[16] T. Huang, Z. Li, M. Li, D. G. Chetwynd, and C. M. Gosselin, "Conceptual design and dimensional synthesis of a novel 2-DOF translational parallel robot for pick-and-place operations," *Journal of Mechanical Design*, vol. 126, no. 3, pp. 449–455, 2004.

[17] G. S. Natal, A. Chemori, and F. Pierrot, "Dual-space control of extremely fast parallel manipulators: payload changes and the 100G experiment," *IEEE Transactions on Control Systems Technology*, vol. 23, no. 4, pp. 1520–1535, 2014.

[18] C. M. Gosselin and J.-F. Hamel, "The Agile Eye: a high-performance three-degree-of-freedom camera-orienting device," in *Proceedings of the 1994 IEEE International Conference on Robotics and Automation (ICRA)*, pp. 781–786, 1994.

[19] C. M. Gosselin, E. St. Pierre, and M. Gagne, "On the development of the Agile Eye," *IEEE Robotics & Automation Magazine*, vol. 3, no. 4, pp. 29–37, 1996.

[20] C. M. Gosselin and E. St-Pierre, "Development and experimentation of a fast 3-DOF camera-orienting device," *The International Journal of Robotics Research*, vol. 16, no. 5, pp. 619–630, 1997.

[21] M. Shoham, M. Burman, E. Zehavi, L. Joskowicz, E. Batkilin, and Y. Kunicher, "Bone-mounted miniature robot for surgical procedures: concept and clinical applications," *IEEE Transactions on Robotics and Automation*, vol. 19, no. 5, pp. 893–901, 2003.

[22] Y. Li and Q. Xu, "Design and development of a medical parallel robot for cardiopulmonary resuscitation," *IEEE/ASME Transactions on Mechatronics*, vol. 12, no. 3, pp. 265–273, 2007.

[23] T. Essomba, M. A. Laribi, L. Nouaille, S. Zeghloul, G. Poisson, and P. Vieyres, "A specific performances comparative study of two spherical robots for tele-echography application," *Proceedings of the Institution of*

Mechanical Engineers, Part C: Journal of Mechanical Engineering Science, vol. 228, no. 18, pp. 3419–3429, 2014.

[24] T. Essomba, M. A. Laribi, S. Zeghloul, and G. Poisson, "Optimal synthesis of a spherical parallel mechanism for medical application," *Robotica*, vol. 34, no. 3, pp. 671–686, 2016.

[25] T. Essomba, Y. Hsu, J. S. Sandoval Arevalo, M. A. Laribi, and S. Zeghloul, "Kinematic optimization of a reconfigurable spherical parallel mechanism for robotic-assisted craniotomy," *Journal of Mechanisms and Robotics*, vol. 11, no. 6, 2019.

[26] A. Ma and S. Payandeh, "Analysis and experimentation of a 4-DOF haptic device," in *2008 Symposium on Haptic Interfaces for Virtual Environment and Teleoperator Systems*, pp. 351–356, 2008.

[27] A. Chaker, A. Mlika, M. A. Laribi, L. Romdhane, and S. Zeghloul, "Synthesis of spherical parallel manipulator for dexterous medical task," *Frontiers of Mechanical Engineering*, vol. 7, no. 2, pp. 150–162, 2012.

[28] H. Saafi, M. A. Laribi, and S. Zeghloul, "Optimal haptic control of a redundant 3-RRR spherical parallel manipulator," in *2015 IEEE/RSJ International Conference on Intelligent Robots and Systems (IROS)*, pp. 2591–2596, 2015.

[29] H. Saafi, M. A. Laribi, and S. Zeghloul, "Redundantly actuated 3-RRR spherical parallel manipulator used as a haptic device: improving dexterity and eliminating singularity," *Robotica*, vol. 33, no. 5, pp. 1113—-1130, 2015.

[30] H. Saafi, M. A. Laribi, and S. Zeghloul, "Optimal torque distribution for a redundant 3-RRR spherical parallel manipulator used as a haptic medical device," *Robotics and Autonomous Systems*, vol. 89, pp. 40–50, 2017.

[31] W. Shang, S. Cong, and Y. Zhang, "Nonlinear friction compensation of a 2-dof planar parallel manipulator," *Mechatronics*, vol. 18, no. 7, pp. 340–346, 2008.

[32] Y.-X. Zhang, S. Cong, W.-W. Shang, Z.-X. Li, and S.-L. Jiang, "Modeling, identification and control of a redundant planar 2-DOF parallel manipulator," *International Journal of Control, Automation, and Systems*, vol. 5, no. 5, pp. 559–569, 2007.

[33] J. Wu, J. Wang, L. Wang, and T. Li, "Dynamics and control of a planar 3-DOF parallel manipulator with actuation redundancy," *Mechanism and Machine Theory*, vol. 44, no. 4, pp. 835–849, 2009.

[34] J. Wu, J. Wang, L. Wang, and Z. You, "Performance comparison of three planar 3-DOF parallel manipulators with 4-RRR, 3-RRR and 2-RRR structures," *Mechatronics*, vol. 20, no. 4, pp. 510–517, 2010.

[35] J. Wu, Y. Gao, B. Zhang, and L. Wang, "Workspace and dynamic performance evaluation of the parallel manipulators in a spray-painting equipment," *Robotics and Computer-Integrated Manufacturing*, vol. 44, pp. 199–207, 2017.

[36] S. Caro, D. Chablat, R. Ur-Rehman, and P. Wenger, "Multiobjective design optimization of 3-PRR planar parallel manipulators," in *Global Product Development*, pp. 373–383, Springer, 2011.

[37] E. F. Fichter, "A Stewart platform-based manipulator: general theory and practical construction," *The International Journal of Robotics Research*, vol. 5, no. 2, pp. 157–182, 1986.

[38] R. Clavel, "Delta a fast robot with parallel geometry," in *Proc. Int. Symposium on Industrial Robots*, pp. 91–100, 1988.

[39] R. Clavel, "Conception d'un robot parallèle rapide à 4 degrés de liberté," 1991.

[40] N. M. Bajaj, A. J. Spiers, and A. M. Dollar, "State of the art in artificial wrists: a review of prosthetic and robotic wrist design," *IEEE Transactions on Robotics*, vol. 35, no. 1, pp. 261–277, 2019.

[41] S. Bai, X. Li, and J. Angeles, "A review of spherical motion generation using either spherical parallel manipulators or spherical motors," *Mechanism and Machine Theory*, vol. 140, pp. 377–388, 2019.

[42] M. Callegari, L. Carbonari, G. Palmieri, and M.-C. Palpacelli, "Parallel wrists for enhancing grasping performance," in *Grasping in Robotics*, pp. 189–219, Springer, 2013.

[43] G. Wu and S. Caro, "U-joint induced torsional instabilities of a family of 3-DOF partially-decoupled spherical parallel manipulators," in *IFToMM International Conference on Mechanisms, Transmissions and Applications*, pp. 332–343, 2019.

[44] T. Li and S. Payandeh, "Design of spherical parallel mechanisms for application to laparoscopic surgery," *Robotica*, vol. 20, no. 2, pp. 133–138, 2002.

[45] J. M. Sabater-Navarro, N. Garcia, J. Rodriguez, R. Morales, F. J. Badesa, and J. M. de Paco, "A simple and compact parallel robotic wrist for laparoscopy," in *2012 4th IEEE RAS & EMBS International Conference on Biomedical Robotics and Biomechatronics (BioRob)*, pp. 835–840, 2012.

[46] M. Malosio, S. P. Negri, N. Pedrocchi, F. Vicentini, M. Caimmi, and L. M. Tosatti, "A spherical parallel three degrees-of-freedom robot for ankle-foot neuro-rehabilitation," in *2012 Annual International Conference of the IEEE Engineering in Medicine and Biology Society*, pp. 3356–3359, 2012.

[47] Y. Du, R. Li, D. Li, and S. Bai, "An ankle rehabilitation robot based on 3-RRS spherical parallel mechanism," *Advances in Mechanical Engineering*, vol. 9, no. 8, pp. 1–8, 2017.

[48] F. Patanè and P. Cappa, "A 3-DOF parallel robot with spherical motion for the rehabilitation and evaluation of balance performance," *IEEE Transactions on neural systems and rehabilitation engineering*, vol. 19, no. 2, pp. 157–166, 2010.

[49] J.-A. Leal-Naranjo, M. Wang, J.-C. Paredes-Rojas, and H. Rostro-Gonzalez, "Design and kinematic analysis of a new 3-DOF spherical parallel manipulator for a prosthetic wrist," *Journal of the Brazilian Society of Mechanical Sciences and Engineering*, vol. 42, no. 63, pp. 1–12, 2019.

[50] R. J. Saltaren, J. M. Sabater, E. Yime, J. M. Azorin, R. Aracil, and N. Garcia, "Performance evaluation of spherical parallel platforms for humanoid robots," *Robotica*, vol. 25, no. 3, pp. 257–267, 2006.

[51] H. Li, J. Luo, C. Huang, Q. Huang, and S. Xie, "Design and control of 3-DoF spherical parallel mechanism robot eyes inspired by the binocular vestibule-ocular reflex," *Journal of Intelligent & Robotic Systems*, vol. 78, no. 3, pp. 425–441, 2015.

[52] F. Pierrot and E. Dombre, "Parallel structures for robot wrists," in *Advances in Robot Kinematics*, pp. 476–484, Springer, 1991.

[53] G. Gogu, "Fully-isotropic over-constrained parallel wrists with two degrees of freedom," in *Proceedings of the 2005 IEEE International Conference on Robotics and Automation*, pp. 4014–4019, 2005.

[54] G. Gogu, "Fully-isotropic three-degree-of-freedom parallel wrists," in *Proceedings 2007 IEEE International Conference on Robotics and Automation*, pp. 895–900, 2007.

[55] G. Gogu, "Fully-isotropic redundantly-actuated parallel wrists with three degrees of freedom," in *ASME 2007 International Design Engineering Technical Conferences and Computers and Information in Engineering Conference*, pp. 943–950, 2007.

[56] G. Gogu, "Parallel wrists with three degrees of freedom," in *Structural Synthesis of Parallel Robots*, pp. 483—-552, Springer, 2012.

[57] R. Damerla and S. Awtar, "Constraint-based analysis of parallel kinematic articulated wrist mechanisms," *Journal of Mechanisms and Robotics*, vol. 13, no. 3, 2021.

[58] H. Asada and J. Granito, "Kinematic and static characterization of wrist joints and their optimal design," in *Proceedings of the 1985 IEEE International Conference on Robotics and Automation (ICRA)*, pp. 244–250, 1985.

[59] D. J. Cox and D. Tesar, "The dynamic model of a three degree of freedom parallel robotic shoulder module," in *Advanced Robotics: 1989*, pp. 475–487, Springer, 1989.

[60] D. Marco, L. Torfason, and D. Tesar, "Computer simulation and design of a three degree-of-freedom shoulder module," pp. 273–282, 1989.

[61] W. M. Craver, "Structural analysis and design of a three-degree-of-freedom robotic shoulder module," Master's thesis, University of Texas, Austin TX, 1989.

[62] R. I. Alizade, N. R. Tagiyev, and J. Duffy, "A forward and reverse displacement analysis of an in-parallel spherical manipulator," *Mechanism and Machine Theory*, vol. 29, no. 1, pp. 125–137, 1994.

[63] C. M. Gosselin and J. Angeles, "The optimum kinematic design of a planar three-degree-of-freedom parallel manipulator," *Journal of Mechanisms, Transmissions, and Automation in Design*, vol. 110, no. 1, pp. 35–41, 1988.

[64] C. M. Gosselin and J. Angeles, "The optimum kinematic design of a spherical three-degree-of-freedom parallel manipulator," *Journal of Mechanisms, Transmissions, and Automation in Design*, vol. 111, no. 2, pp. 202–207, 1989.

[65] C. M. Gosselin, J. Sefrioui, and M. J. Richard, "On the direct kinematics of spherical three-degree-of-freedom parallel manipulators with a coplanar platform," *Journal of Mechanical Design*, vol. 116, no. 2, pp. 587–593, 1994.

[66] C. M. Gosselin, J. Sefrioui, and M. J. Richard, "On the direct kinematics of spherical three-degree-of-freedom parallel manipulators of general architecture," *Journal of Mechanical Design*, vol. 116, no. 2, pp. 594–598, 1994.

[67] C. Innocenti and V. Parenti-Castelli, "Echelon form solution of direct kinematics for the general fully-parallel spherical wrist," *Mechanism and Machine Theory*, vol. 28, no. 4, pp. 553–561, 1993.

[68] Z. Huang and Y. L. Yao, "A new closed-form kinematics of the generalized 3-DOF spherical parallel manipulator," *Robotica*, vol. 17, no. 5, pp. 475–485, 1999.

[69] X.-J. Liu, Z.-L. Jin, and F. Gao, "Optimum design of 3-DOF spherical parallel manipulators with respect to the conditioning and stiffness indices," *Mechanism and Machine Theory*, vol. 35, no. 9, pp. 1257–1267, 2000.

[70] T. Huang, C. M. Gosselin, D. J. Whitehouse, and D. G. Chetwynd, "Analytical approach for optimal design of a type of spherical parallel manipulator using dexterous performance indices," *Proceedings of the Institution of Mechanical Engineers, Part C: Journal of Mechanical Engineering Science*, vol. 217, no. 4, pp. 447–455, 2003.

[71] I. A. Bonev and C. M. Gosselin, "Singularity loci of spherical parallel mechanisms," in *Proceedings of the 2005 IEEE International Conference on Robotics and Automation (ICRA)*, pp. 2957–2962, 2005.

[72] I. A. Bonev, D. Chablat, and P. Wenger, "Working and assembly modes of the Agile Eye," in *Proceedings of the 2006 IEEE International Conference on Robotics and Automation (ICRA)*, pp. 2317–2322, 2006.

[73] A. Jelassi, A. Chaker, and A. Mlika, "3-RRR spherical parallel robot optimization with minimum of singularities," in *Computational Kinematics*, pp. 299–306, Springer, 2018.

[74] K. A. Arrouk, B. C. Bouzgarrou, and G. Gogu, "Workspace characterization and kinematic analysis of general spherical parallel manipulators revisited via graphical based approaches," *Mechanism and Machine Theory*, vol. 122, pp. 404–431, 2018.

[75] H. Elgolli, A. Houidi, A. Mlika, and L. Romdhane, "Analytical analysis of the dynamic of a spherical parallel manipulator," *The International Journal of Advanced Manufacturing Technology*, vol. 101, no. 1-4, pp. 859–871, 2019.

[76] J. Angeles, A. Morozov, L. Slutski, O. Navarro, and L. Jabre, "The modular design of a long-reach, 11-axis manipulator," in *Romansy 13*, pp. 225–233, Springer, 2000.

[77] C. M. Gosselin and E. Lavoie, "On the kinematic design of spherical three-degree-of-freedom parallel manipulators," *The International Journal of Robotics Research*, vol. 12, no. 4, pp. 394–402, 1993.

[78] C. M. Gosselin and M. Gagne, "A closed-form solution for the direct kinematics of a special class of spherical three-degree-of-freedom parallel manipulators," in *Computational Kinematics*, pp. 231–240, Springer, 1995.

[79] C. M. Gosselin and J. Wang, "Singularity loci of a special class of spherical three-degree-of-freedom parallel mechanisms with revolute actuators," *The International Journal of Robotics Research*, vol. 21, no. 7, pp. 649–659, 2002.

[80] X. Kong and C. M. Gosselin, "A formula that produces a unique solution to the forward displacement analysis of a quadratic spherical parallel manipulator: the Agile Eye," *Journal of Mechanisms and Robotics*, vol. 2, no. 4, 2009.

[81] X. Kong, C. M. Gosselin, and J. M. Ritchie, "Forward displacement analysis of a linearly actuated quadratic spherical parallel manipulator," *Journal of Mechanisms and Robotics*, vol. 3, no. 1, 2011.

[82] J. Hofschulte, M. Seebode, and W. Gerth, "Parallel manipulator hip joint for a bipedal robot," in *Climbing and Walking Robots*, pp. 601–609, Springer, 2005.

[83] M. Daneshmand, M. H. Saadatzi, M. H. F. Kaloorazi, M. T. Masouleh, and G. Anbarjafari, "Optimal design of a spherical parallel manipulator based on kinetostatic performance using evolutionary techniques," *Journal of Mechanical Science and Technology*, vol. 30, no. 3, pp. 1323–1331, 2016.

[84] F. Bidault, C.-P. Teng, and J. Angeles, "Structural optimization of a spherical parallel manipulator using a two-level approach," in *ASME 2001 International Design Engineering Technical Conferences and Computers and Information in Engineering Conference*, pp. 215–224, 2001.

[85] S. Staicu, "Recursive modelling in dynamics of Agile Wrist spherical parallel robot," *Robotics and Computer-Integrated Manufacturing*, vol. 25, no. 2, pp. 409–416, 2009.

[86] E. Abedloo, A. Molaei, and H. D. Taghirad, "Closed-form dynamic formulation of spherical parallel manipulators by Gibbs-Appell method," in *2014 Second RSI/ISM International Conference on Robotics and Mechatronics*, pp. 576–581, 2014.

[87] R. Khezrian, E. Abedloo, M. Farhadmanesh, and S. A. A. Moosavian, "Multi criteria design of a spherical 3-DoF parallel manipulator for optimal dynamic performance," in *2014 Second RSI/ISM International Conference on Robotics and Mechatronics (ICRoM)*, pp. 546–551, 2014.

[88] Y. Jian and J. Angeles, "Kinematics simulation and control design of the Agile Wrist in a dual-arm robotic mechanical systems," in *2012 IEEE International Conference on Computer Science and Automation Engineering*, pp. 39–42, 2012.

[89] A. Niyetkaliyev and A. Shintemirov, "An approach for obtaining unique kinematic solutions of a spherical parallel manipulator," in *2014 IEEE/ASME International Conference on Advanced Intelligent Mechatronics*, pp. 1355–1360, 2014.

[90] A. Shintemirov, A. Niyetkaliyev, and M. Rubagotti, "Numerical optimal control of a spherical parallel manipulator based on unique kinematic solutions," *IEEE/ASME Transactions on Mechatronics*, vol. 21, no. 1, pp. 98–109, 2015.

[91] T. Taunyazov, M. Rubagotti, and A. Shintemirov, "Constrained orientation control of a spherical parallel manipulator via online convex optimization," *IEEE/ASME Transactions on Mechatronics*, vol. 23, no. 1, pp. 252–261, 2017.

[92] L. Birglen, C. M. Gosselin, N. Pouliot, B. Monsarrat, and T. Laliberte, "SHaDe, a new 3-DOF haptic device," *IEEE Transactions on Robotics and Automation*, vol. 18, no. 2, pp. 166–175, 2002.

[93] K. Al-Widyan, X. Q. Ma, and J. Angeles, "The robust design of parallel spherical robots," *Mechanism and Machine Theory*, vol. 46, no. 3, pp. 335–343, 2011.

[94] C.-H. Kuo, J. S. Dai, and G. Legnani, "A non-overconstrained variant of the Agile Eye with a special decoupled kinematics," *Robotica*, vol. 32, no. 6, pp. 889–905, 2014.

[95] M. Karouia and J. M. Hervé, "A family of novel orientational 3-DOF parallel robots," in *Romansy 14*, pp. 359–368, Springer, 2002.

[96] M. Karouia and J. M. Hervé, "New parallel wrists: special limbs with motion dependency," in *On Advances in Robot Kinematics*, pp. 371–380, Springer, 2004.

[97] X. Kong and C. M. Gosselin, "Type synthesis of 3-DOF spherical parallel manipulators based on screw theory," *Journal of Mechanical Design*, vol. 126, no. 1, pp. 101–108, 2004.

[98] X. Kong and C. M. Gosselin, "Type synthesis of three-degree-of-freedom spherical parallel manipulators," *The International Journal of Robotics Research*, vol. 23, no. 3, pp. 237–245, 2004.

[99] R. Di Gregorio, "A new family of spherical parallel manipulators," *Robotica*, vol. 20, no. 4, pp. 353–358, 2002.

[100] Y. Fang and L.-W. Tsai, "Structure synthesis of a class of 3-DOF rotational parallel manipulators," *IEEE Transactions on Robotics and Automation*, vol. 20, no. 1, pp. 117–121, 2004.

[101] T. A. Hess-Coelho, "Topological synthesis of a parallel wrist mechanism," *Journal of Mechanical Design*, vol. 128, no. 1, pp. 230–235, 2006.

[102] Y. Qi, T. Sun, Y. Song, and Y. Jin, "Topology synthesis of three-legged spherical parallel manipulators employing Lie group theory," *Proceedings of the Institution of Mechanical Engineers, Part C: Journal of Mechanical Engineering Science*, vol. 229, no. 10, pp. 1873–1886, 2015.

[103] P. Vischer and R. Clavel, "Argos: a novel 3-DoF parallel wrist mechanism," *The International Journal of Robotics Research*, vol. 19, no. 1, pp. 5–11, 2000.

[104] P. Vischer and R. Clavel, "Kinematic calibration of the parallel Argos mechanism," *Robotica*, vol. 18, no. 6, pp. 589–599, 2000.

[105] M. Karouia and J. M. Hervé, "Non-overconstrained 3-DOF spherical parallel manipulators of type: 3-RCC, 3-CCR, 3-CRC," *Robotica*, vol. 24, no. 1, pp. 85–94, 2006.

[106] A. Chaker, A. Mlika, M. A. Laribi, L. Romdhane, and S. Zeghloul, "Accuracy analysis of non-overconstrained spherical parallel manipulators," *European Journal of Mechanics - A/Solids*, vol. 47, pp. 362–372, 2014.

[107] R. Di Gregorio, "A new parallel wrist using only revolute pairs: the 3-RUU wrist," *Robotica*, vol. 19, no. 3, pp. 305—-309, 2001.

[108] J. M. Hervé and M. Karouia, "The novel 3-RUU wrist with no idle pair," in *Proceedings of the Workshop on Fundamental Issues and Future Research Directions for Parallel Mechanisms and Manipulators*, pp. 3–4, 2002.

[109] R. Di Gregorio, "Kinematics of a new spherical parallel manipulator with three equal legs: the 3-URC wrist," *Journal of Robotic Systems*, vol. 18, no. 5, pp. 213–219, 2001.

[110] M. Callegari, A. Cammarata, A. Gabrielli, and R. Sinatra, "Kinematics and dynamics of a 3-CRU spherical parallel robot," in *ASME 2007 International Design Engineering Technical Conferences and Computers and Information in Engineering Conference*, pp. 933–941, 2007.

[111] M. Callegari, A. Cammarata, A. Gabrielli, M. Ruggiu, and R. Sinatra, "Analysis and design of a spherical micromechanism with flexure hinges," *Journal of Mechanical Design*, vol. 131, no. 5, 2009.

[112] S. Huda and Y. Takeda, "Kinematic analysis and synthesis of a 3-URU pure rotational parallel mechanism with respect to singularity and workspace," *Journal of Advanced Mechanical Design, Systems, and Manufacturing*, vol. 1, no. 1, pp. 81–92, 2007.

[113] M. Karouia and J. M. Hervé, "An orientational 3-DOF parallel mechanism," in *Proceedings of the 3rd Chemnitz Parallel Kinematics Seminar*, pp. 139–150, 2002.

[114] R. Di Gregorio, "The 3-RRS wrist: a new, simple and non-overconstrained spherical parallel manipulator," *Journal of Mechanical Design*, vol. 126, no. 5, pp. 850–855, 2004.

[115] R. Di Gregorio, "Kinematics of the 3-RSR wrist," *IEEE Transactions on Robotics*, vol. 20, no. 4, pp. 750–753, 2004.

[116] R. Deidda, A. Mariani, and M. Ruggiu, "On the kinematics of the 3-RRUR spherical parallel manipulator," *Robotica*, vol. 28, no. 6, pp. 821–832, 2010.

[117] J. J. Lee and S.-L. Chang, "On the kinematics of the UPS wrist for real time control," in *ASME 1992 International Design Engineering Technical Conferences and Computers and Information in Engineering Conference*, pp. 305–312, 1992.

[118] M. Badescu and C. Mavroidis, "Workspace optimization of 3-legged UPU and UPS parallel platforms with joint constraints," *Journal of Mechanical Design*, vol. 126, no. 2, pp. 291–300, 2004.

[119] M. Karouia and J. M. Hervé, "A three-dof tripod for generating spherical rotation," in *Advances in Robot Kinematics*, pp. 395–402, Springer, 2000.

[120] R. Di Gregorio, "Kinematics of the 3-UPU wrist," *Mechanism and Machine Theory*, vol. 38, no. 3, pp. 253–263, 2003.

[121] R. Di Gregorio, "Statics and singularity loci of the 3-UPU wrist," *IEEE Transactions on Robotics*, vol. 20, no. 4, pp. 630–635, 2004.

[122] A. H. Chebbi, Z. Affi, and L. Romdhane, "Modelling and analysis of the 3-UPU spherical manipulator," *European Journal of Computational Mechanics*, vol. 22, no. 2-4, pp. 157–169, 2013.

[123] D. Gan, J. S. Dai, J. Dias, and L. Seneviratne, "Forward kinematics solution distribution and analytic singularity-free workspace of linear-actuated symmetrical spherical parallel manipulators," *Journal of Mechanisms and Robotics*, vol. 7, no. 4, 2015.

[124] R. B. A. Shyam and A. Ghosal, "Path planning of a 3-UPU wrist manipulator for sun tracking in central receiver tower systems," *Mechanism and Machine Theory*, vol. 119, pp. 130–141, 2018.

[125] D. Paganelli, "Avoiding parallel singularities of 3UPS and 3UPU spherical wrists," in *Proceedings 2007 IEEE International Conference on Robotics and Automation*, pp. 1201–1206, 2007.

[126] M. Callegari, P. Marzetti, and B. Olivieri, "Kinematics of a parallel mechanism for the generation of spherical motions," in *On Advances in Robot Kinematics*, pp. 449–458, Springer, 2004.

[127] M. .Callegari, "Design and prototyping of a spherical parallel machine based on 3-CPU kinematics," *Parallel Manipulators: New Developments*, pp. 171–198, 2008.

[128] M. Callegari, L. Carbonari, G. Palmieri, M.-C. Palpacelli, and D. Tina, "Position control of a 3-CPU spherical parallel manipulator," *Journal of Control Science and Engineering*, vol. 2013, 2013.

[129] L. Carbonari, M. Callegari, G. Palmieri, and M.-C. Palpacelli, "Analysis of kinematics and reconfigurability of a spherical parallel manipulator," *IEEE Transactions on Robotics*, vol. 30, no. 6, pp. 1541–1547, 2014.

[130] M.-C. Palpacelli, L. Carbonari, G. Palmieri, and M. Callegari, "Analysis and design of a reconfigurable 3-DoF parallel manipulator for multimodal tasks," *IEEE/ASME Transactions on Mechatronics*, vol. 20, no. 4, pp. 1975–1985, 2014.

[131] M.-C. Palpacelli, L. Carbonari, G. Palmieri, and M. Callegari, "A family of non-overconstrained 3-DoF reconfigurable parallel manipulators," in *Advances in Robot Kinematics 2016*, pp. 191–200, Springer, 2018.

[132] M. Urízar and M. L. Husty, "Assembly mode change of spherical 3-RPR parallel manipulator," *Mechanics Based Design of Structures and Machines*, vol. 40, no. 4, pp. 487–505, 2012.

[133] D. Li, Z. Zhang, and H. Li, "Forward displacement analysis of a 3-RPR spherical parallel mechanism," *Proceedings of the Institution of Mechanical Engineers, Part C: Journal of Mechanical Engineering Science*, vol. 227, no. 8, pp. 1864–1869, 2013.

[134] J. Enferadi and A. A. Tootoonchi, "A novel spherical parallel manipulator: forward position problem, singularity analysis, and isotropy design," *Robotica*, vol. 27, no. 5, pp. 663–676, 2009.

[135] J. Enferadi and A. A. Tootoonchi, "Inverse dynamics analysis of a general spherical star-triangle parallel manipulator using principle of virtual work," *Nonlinear dynamics*, vol. 61, no. 3, pp. 419–434, 2010.

[136] J. Enferadi and A. A. Tootoonchi, "Accuracy and stiffness analysis of a 3-RRP spherical parallel manipulator," *Robotica*, vol. 29, no. 2, pp. 193–209, 2011.

[137] A. Akbarzadeh and J. Enferadi, "A virtual work based algorithm for solving direct dynamics problem of a 3-RRP spherical parallel manipulator," *Journal of Intelligent & Robotic Systems*, vol. 63, no. 1, pp. 25–49, 2011.

[138] A. Akbarzadeh, J. Enferadi, and M. Sharifnia, "Dynamics analysis of a 3-RRP spherical parallel manipulator using the natural orthogonal complement," *Multibody System Dynamics*, vol. 29, no. 4, pp. 361–380, 2013.

[139] S. Zarkandi, "Kinematic analysis and optimal design of a novel 3-PRR spherical parallel manipulator," *Proceedings of the Institution of Mechanical Engineers, Part C: Journal of Mechanical Engineering Science*, vol. 235, no. 4, pp. 693–712, 2021.

[140] S. Zarkandi, "Task-based torque minimization of a 3-PRR spherical parallel manipulator," *Robotica*, vol. 40, no. 3, pp. 475–504, 2022.

[141] R. Li, J. Zhao, D. Fan, S. Liang, S. Song, and S. Bai, "Design and workspace analysis of reconfigurable 3-RPRP spherical parallel mechanisms," in *2018 International Conference on Reconfigurable Mechanisms and Robots (ReMAR)*, pp. 1–8, 2018.

[142] P. Ji and H. Wu, "Algebraic solution to forward kinematics of a 3-DOF spherical parallel manipulator," *Journal of Robotic Systems*, vol. 18, no. 5, pp. 251–257, 2001.

[143] G. Alici and B. Shirinzadeh, "Topology optimisation and singularity analysis of a 3-SPS parallel manipulator with a passive constraining spherical joint," *Mechanism and Machine Theory*, vol. 39, no. 2, pp. 215–235, 2004.

[144] J. Li and J. M. McCarthy, "Singularity variety of a 3SPS-1S spherical parallel manipulator," in *ASME 2016 International Design Engineering Technical Conferences and Computers and Information in Engineering Conference*, 2016.

[145] K. Wohlhart, "Displacement analysis of the general spherical Stewart platform," *Mechanism and Machine Theory*, vol. 29, no. 4, pp. 581–589, 1994.

[146] J. Wang and C. M. Gosselin, "Singularity loci of a special class of spherical 3-DOF parallel mechanisms with prismatic actuators," *Journal of Mechanical Design*, vol. 126, no. 2, pp. 319–326, 2004.

[147] G. Alici and B. Shirinzadeh, "Loci of singular configurations of a 3-DOF spherical parallel manipulator," *Robotics and Autonomous Systems*, vol. 48, no. 2-3, pp. 77–91, 2004.

[148] I. A. Bonev and C. M. Gosselin, "Analytical determination of the workspace of symmetrical spherical parallel mechanisms," *IEEE Transactions on Robotics*, vol. 22, no. 5, pp. 1011–1017, 2006.

[149] R. Vertechy and V. Parenti-Castelli, "Real-time direct position analysis of parallel spherical wrists by using extra sensors," *Journal of Mechanical Design*, vol. 128, no. 1, pp. 288–294, 2006.

[150] J. Enferadi, "A novel approach for obtaining assembly modes of a 3UPS-S fully spherical parallel manipulator," *Journal of Mechanics*, vol. 32, no. 5, pp. 555–563, 2016.

[151] J. Enferadi and R. Nikrooz, "The performance indices optimization of a symmetrical fully spherical parallel mechanism for dimensional synthesis," *Journal of Intelligent & Robotic Systems*, vol. 90, no. 3, pp. 305–321, 2018.

[152] J. S. Navarro, N. Garcia, C. Perez, E. Fernandez, R. Saltaren, and M. Almonacid, "Kinematics of a robotic 3UPS1S spherical wrist designed for laparoscopic applications," *The International Journal of Medical Robotics and Computer Assisted Surgery*, vol. 6, no. 3, pp. 291–300, 2010.

[153] B. Li, S. Chen, and D. Zhang, "Analysis and optimal design of a spherical parallel manipulator with three rotational degrees of freedom," in *International Workshop on Robotics in Smart Manufacturing*, pp. 71–81, 2013.

[154] L. J. Puglisi, R. J. Saltaren, H. A. Moreno, P. F. Cárdenas, C. Garcia, and R. Aracil, "Dimensional synthesis of a spherical parallel manipulator based on the evaluation of global performance indexes," *Robotics and Autonomous Systems*, vol. 60, no. 8, pp. 1037–1045, 2012.

[155] T. Sun, Y. Song, G. Dong, B. Lian, and J. Liu, "Optimal design of a parallel mechanism with three rotational degrees of freedom," *Robotics and Computer-Integrated Manufacturing*, vol. 28, no. 4, pp. 500–508, 2012.

[156] L. J. Puglisi, R. J. Saltaren, G. R. Portolés, H. A. Moreno, P. F. Cárdenas, and C. Garcia, "Design and kinematic analysis of 3PSS-1S wrist for needle insertion guidance," *Robotics and Autonomous Systems*, vol. 61, no. 5, pp. 417–427, 2013.

[157] Y. Hou, X. Hu, D. Zeng, and Y. Zhou, "Biomimetic shoulder complex based on 3-PSS/S spherical parallel mechanism," *Chinese Journal of Mechanical Engineering*, vol. 28, no. 1, pp. 29–37, 2015.

[158] J. Enferadi and K. Jafari, "A Kane's based algorithm for closed-form dynamic analysis of a new design of a 3RSS-S spherical parallel manipulator," *Multibody System Dynamics*, vol. 49, no. 4, pp. 377–394, 2020.

[159] R. Di Gregorio, "Type synthesis of underactuated wrists generated from fully-parallel wrists," *Journal of Mechanical Design*, vol. 134, no. 12, 2012.

[160] R. Di Gregorio, "Kinematic analysis of the (nS)-2SPU underactuated parallel wrist," *Journal of Mechanisms and Robotics*, vol. 4, no. 3, 2012.

[161] R. Di Gregorio, "Instantaneous kinematics and singularities of two types of under-actuated parallel wrists," in *ASME 2012 Engineering Systems Design and Analysis*, pp. 117–125, 2012.

[162] R. Di Gregorio, "Kinetostatics of S-(nS)PU-SPU and S-(nS)PU-2SPU nonholonomic parallel wrists," *Journal of Mechanisms and Robotics*, vol. 5, no. 4, 2013.

[163] M. Battistelli, M. Callegari, and R. Di Gregorio, "Design and performance analysis of an (nS)-2SPU underactuated wrist," in *2014 IEEE/ASME 10th International Conference on Mechatronic and Embedded Systems and Applications (MESA)*, 2014.

[164] M. Callegari, M. Battistelli, and R. Di Gregorio, "Design of a non-holonomic spherical wrist," *Journal of Intelligent & Robotic Systems*, vol. 81, no. 2, pp. 181–194, 2016.

[165] J. Gallardo-Alvarado, M. A. García-Murillo, and L. Pérez-González, "Kinematics of the 3RRRS+S parallel wrist: a parallel manipulator free of intersecting revolute axes," *Mechanics Based Design of Structures and Machines*, vol. 41, no. 4, pp. 452–467, 2013.

[166] J. Enferadi and A. Shahi, "A closed-form solution for the position analysis of a novel fully spherical parallel manipulator," *Robotica*, vol. 33, no. 10, pp. 2114–2136, 2015.

[167] J. Enferadi and A. Shahi, "A closed-form dynamics of a novel fully wrist driven by revolute motors," *Journal of Mechanics*, vol. 32, no. 4, pp. 479–490, 2016.

[168] J. Gallardo-Alvarado, R. Rodriguez-Castro, L. Perez-Gonzalez, and C. R. Aguilar-Najera, "Kinematics of the 3(RPSP)-S fully spherical parallel manipulator by means of screw theory," *Robotics*, vol. 7, no. 2, 2018.

[169] X. L. Shan, G. Cheng, and X. Z. Liu, "Note: Application of a novel 2(3HUS+S) parallel manipulator for simulation of hip joint motion," *Review of Scientific Instruments*, vol. 87, no. 7, 2016.

[170] X. L. Shan and G. Cheng, "Kinematic analysis and parameter optimization for a novel 2(3HUS+S) parallel hip joint simulator," *International Journal of Robotics and Automation*, vol. 32, no. 4, pp. 379–386, 2017.

[171] F. Guo, G. Cheng, Z. Zhao, X. Shan, and X. Liu, "Configuration bifurcation and uncontrolled DOF analysis of 2(3HUS+S) parallel manipulator," in *2017 IEEE International Conference on Robotics and Biomimetics (ROBIO)*, pp. 2191–2196, 2017.

[172] F. Guo, G. Cheng, and Z. Zhao, "Interior singularity analysis for a 2(3HUS+S) parallel manipulator with descending matrix rank method," *International Journal of Advanced Robotic Systems*, vol. 16, no. 1, 2019.

[173] F. Guo, G. Cheng, Z. Qiao, Z. Jin, and Y. Li, "Fatigue life estimation of 2(3HUS+S) parallel manipulator for simulation of hip joint motion," in *2020 6th International Conference on Robotics and Artificial Intelligence*, pp. 271–277, 2020.

[174] H. Zhang, G. Cheng, X. Shan, and F. Guo, "Kinematic accuracy research of 2(3HUS+S) parallel manipulator for simulation of hip joint motion," *Robotica*, vol. 36, no. 9, pp. 1386–1401, 2018.

[175] H. Zhang, G. Cheng, S. Chen, F. Guo, and X. Shan, "Stiffness modeling and performance evaluation of 2(3HUS+S) parallel manipulator," in *2018 3rd International Conference on Advanced Robotics and Mechatronics (ICARM)*, pp. 456–461, 2018.

[176] S. Chen, G. Cheng, and X. Liu, "Dynamic parameter identification method for a 2(3HUS+S) parallel manipulator," in *2021 6th IEEE International Conference on Advanced Robotics and Mechatronics (ICARM)*, pp. 679–686, 2021.

[177] T. A. Hess-Coelho, "Prototype of a redundant parallel robot wrist," in *ASME 2004 International Design Engineering Technical Conferences and Computers and Information in Engineering Conference*, pp. 749–754, 2004.

[178] T. A. Hess-Coelho, "A redundant parallel spherical mechanism for robotic wrist applications," *Journal of Mechanical Design*, vol. 129, no. 8, pp. 891–895, 2007.

[179] S. K. Agrawal, G. Desmier, and S. Li, "Fabrication and analysis of a novel 3 DOF parallel wrist mechanism," *Journal of Mechanical Design*, vol. 117, no. 2A, pp. 343–345, 1995.

[180] D. Chablat and P. Wenger, "Design of a spherical wrist with parallel architecture: application to vertebrae of an eel robot," in *Proceedings of the 2005 IEEE International Conference on Robotics and Automation*, pp. 3336–3341, 2005.

[181] C. Wang, Y. Fang, S. Guo, and Y. Chen, "Design and kinematical performance analysis of a 3-RUS/RRR redundantly actuated parallel mechanism for ankle rehabilitation," *Journal of Mechanisms and Robotics*, vol. 5, no. 4, 2013.

[182] C. Wang, Y. Fang, S. Guo, and C. Zhou, "Design and kinematic analysis of redundantly actuated parallel mechanisms for ankle rehabilitation," *Robotica*, vol. 33, no. 2, pp. 366–384, 2015.

[183] M. Karouia and J. M. Hervé, "Asymmetrical 3-dof spherical parallel mechanisms," *European Journal of Mechanics - A/Solids*, vol. 24, no. 1, pp. 47–57, 2005.

[184] G. Chen, W. Yu, H. Wang, and J. Wang, "Design and kinematic analysis of a spherical parallel manipulator using concurrent planar parallelogram linkages," *Proceedings of the Institution of Mechanical Engineers, Part C: Journal of Mechanical Engineering Science*, vol. 233, no. 7, pp. 2491–2501, 2019.

[185] X. Kong, "Forward displacement analysis of a 2-DOF RR-RRR-RRR spherical parallel manipulator," in *Proceedings of 2010 IEEE/ASME International Conference on Mechatronic and Embedded Systems and Applications*, pp. 446–451, 2010.

[186] K. Wu, J. J. Yu, G. H. Zong, and X. Kong, "Comparison study on motion characteristics of three 2-DOF pointing devices," in *ASME 2014 International Design Engineering Technical Conferences and Computers and Information in Engineering Conference*, 2014.

[187] J. Yu, K. Wu, G. Zong, and X. Kong, "A comparative study on motion characteristics of three two-degree-of-freedom pointing mechanisms," *Journal of Mechanisms and Robotics*, vol. 8, no. 2, 2016.

[188] J. J. Yu, Z. Jin, and X. Kong, "Identification and comparison for continuous motion characteristics of three two-degree-of-freedom pointing mechanisms," *Journal of Mechanisms and Robotics*, vol. 9, no. 5, 2017.

[189] K. Wu, J. Yu, G. Zong, and X. Kong, "A family of rotational parallel manipulators with equal-diameter spherical pure rotation," *Journal of Mechanisms and Robotics*, vol. 6, no. 1, 2014.

[190] M. E. Rosheim and G. F. Sauter, "New high-angulation omni-directional sensor mount," in *SPIE Free-Space Laser Communication and Laser Imaging II*, pp. 163–174, 2002.

[191] J. Sofka, V. A. Skormin, V. V. Nikulin, D. J. Nicholson, and M. E. Rosheim, "New generation of gimbals systems for laser positioning applications," in *SPIE Proceedings Free-Space Laser Communication and Active Laser Illumination III*, pp. 182–191, 2004.

[192] J. Sofka, V. A. Skormin, V. V. Nikulin, and D. J. Nicholson, "Omni-Wrist III - A new generation of pointing devices. Part I: Laser beam steering devices - mathematical modeling," *IEEE Transactions on Aerospace and Electronic Systems*, vol. 42, no. 2, pp. 718–725, 2006.

[193] J. Sofka, V. A. Skormin, V. V. Nikulin, and D. J. Nicholson, "Omni-Wrist III - A new generation of pointing devices. Part II: Gimbals systems - control," *IEEE Transactions on Aerospace and Electronic Systems*, vol. 42, no. 2, pp. 726–734, 2006.

[194] X. Dong, J. Yu, B. Chen, and G. Zong, "Geometric approach for kinematic analysis of a class of 2-DOF rotational parallel manipulators," *Chinese Journal of Mechanical Engineering*, vol. 25, no. 2, pp. 241–247, 2012.

[195] J. J. Yu, X. Dong, X. Pei, G. H. Zong, X. Kong, and Q. Qiu, "Mobility and singularity analysis of a class of 2-DOF rotational parallel mechanisms using a visual graphic approach," in *ASME 2011 International Design Engineering Technical Conferences and Computers and Information in Engineering Conference*, pp. 1027–1036, 2011.

[196] R. Ghaedrahmati and C. M. Gosselin, "Kinematic analysis of a new 2-DOF parallel wrist with a large singularity-free rotational workspace," *Mechanism and Machine Theory*, vol. 175, 2022.

[197] K. Wu, J. J. Yu, G. H. Zong, and X. Kong, "Type synthesis of 2-DOF rotational parallel manipulators with an equal-diameter spherical pure rolling motion," in *ASME 2013 International Design Engineering Technical Conferences and Computers and Information in Engineering Conference*, 2013.

[198] K. Wu, J. J. Yu, S. Z. Li, G. H. Zong, and X. Kong, "Type synthesis of two degrees-of-freedom rotational parallel mechanisms with a fixed center-of-rotation based on a graphic approach," in *ASME 2012 International Design Engineering Technical Conferences and Computers and Information in Engineering Conference*, pp. 647–658, 2012.

[199] L.-J. Zhang, Y.-W. Niu, and Z. Huang, "Analysis of the workspace of spherical 2-DOF parallel manipulator with actuation redundancy," in *2006 International Conference on Mechatronics and Automation*, pp. 153–158, 2006.

[200] L.-J. Zhang, Y.-Q. Li, and W.-Y. Shi, "Parameter optimum design of spherical 2-DOF parallel manipulator with actuation redundancy," in *2009 International Conference on Mechatronics and Automation*, pp. 1499–1504, 2009.

[201] Y. Li, L. Zhang, and Y. Niu, "Dynamic analysis of spherical 2-DOF parallel manipulator with actuation redundancy," in *2011 IEEE International Conference on Mechatronics and Automation*, pp. 1350–1355, 2011.

[202] C. M. Gosselin and F. Caron, "Two degree-of-freedom spherical orienting device," Oct. 19 1999. US Patent 5,966,991.

[203] L.-J. Zhang, Y.-W. Niu, Y.-Q. Li, and Z. Huang, "Analysis of the workspace of 2-DOF spherical 5R parallel manipulator," in *Proceedings 2006 IEEE International Conference on Robotics and Automation*, pp. 1123–1128, 2006.

[204] L.-J. Zhang, Y.-Q. Li, and Y.-Q. Guo, "Dynamic analysis of spherical 5R parallel manipulator," in *2009 International Conference on Mechatronics and Automation*, pp. 1510–1514, 2009.

[205] X. Kong, "Forward displacement analysis and singularity analysis of a 2-DOF 5R spherical parallel manipulator," in *ASME 2009 International Design Engineering Technical Conferences and Computers and Information in Engineering Conference*, pp. 443–447, 2009.

[206] X. Kong, "Forward displacement analysis and singularity analysis of a special 2-DOF 5R spherical parallel manipulator," *Journal of Mechanisms and Robotics*, vol. 3, no. 2, 2011.

[207] J. J. Cervantes-Sánchez, J. C. Hernández-Rodríguez, and E. J. González-Galván, "On the 5R spherical, symmetric manipulator: workspace and singularity characterization," *Mechanism and Machine Theory*, vol. 39, no. 4, pp. 409–429, 2004.

[208] C. Wu, X.-J. Liu, L. Wang, and J. Wang, "Optimal design of spherical 5R parallel manipulators considering the motion/force transmissibility," *Journal of Mechanical Design*, vol. 132, no. 3, 2010.

[209] E. R. J. Bozorgi, I. Yahyapour, A. Karimi, M. T. Masouleh, and M. Yazdani, "Design, development, dynamic analysis and control of a 2-DOF spherical parallel mechanism," in *2014 Second RSI/ISM international conference on robotics and mechatronics (ICRoM)*, pp. 445–450, 2014.

[210] A. Arian, B. Danaei, and M. T. Masouleh, "Kinematics and dynamics analysis of a 2-DOF spherical parallel robot," in *2016 4th International Conference on Robotics and Mechatronics*, pp. 154–159, 2016.

[211] A. Gabrielli, A. Borboni, L. Carbonari, and M.-C. Palpacelli, "Kinematic calibration of a 2-DOF parallel orientation manipulator: theory and simulation results," in *ASME International Mechanical Engineering Congress and Exposition*, 2016.

[212] J. Gallardo-Alvarado, "Two-degree-of-freedom parallel wrist," in *Kinematic Analysis of Parallel Manipulators by Algebraic Screw Theory*, pp. 205–217, Springer, 2016.

[213] B. Danaei, A. Arian, M. T. Masouleh, and A. Kalhor, "Dynamic modeling and base inertial parameters determination of a 2-DOF spherical parallel mechanism," *Multibody System Dynamics*, vol. 41, no. 4, pp. 367–390, 2017.

[214] B. Danaei, M. Alipour, A. Arian, M. T. Masouleh, and A. Kalhor, "Control of a two degree-of-freedom parallel robot as a stabilization platform," in *2017 5th RSI International Conference on Robotics and Mechatronics (ICRoM)*, pp. 232–238, 2017.

[215] S. E. Askarinejad, A. Fahim, M. R. H. Yazdi, and M. T. Masouleh, "Data-driven identification of the Jacobian matrix of a 2-DoF spherical parallel manipulator," in *2019 7th International Conference on Robotics and Mechatronics (ICRoM)*, pp. 229–234, 2019.

[216] A. Alamdar, F. Farahmand, S. Behzadipour, and A. Mirbagheri, "A geometrical approach for configuration and singularity analysis of a new non-symmetric 2DOF 5R spherical parallel manipulator," *Mechanism and Machine Theory*, vol. 147, 2020.

[217] M. Ruggiu, "Kinematic and dynamic analysis of a two-degree-of-freedom spherical wrist," *Journal of Mechanisms and Robotics*, vol. 2, no. 3, 2010.

[218] H. Jeong, H. Shin, and B. Yi, "Development of a new 2-DOF wrist mechanism using reverse motion transmission," *IEEE Robotics and Automation Letters*, vol. 6, no. 4, pp. 6947–6954, 2021.

[219] K. Ueda, H. Yamada, H. Ishida, and S. Hirose, "Design of large motion range and heavy duty 2-DOF spherical parallel wrist mechanism," *Journal of Robotics and Mechatronics*, vol. 25, no. 2, pp. 294–305, 2013.

[220] J. M. Wiitala and M. M. Stanisic, "Design of an overconstrained and dextrous spherical wrist," *Journal of Mechanical Design*, vol. 122, no. 3, pp. 347–353, 2000.

[221] M. Carricato and V. Parenti-Castelli, "A novel fully decoupled two-degrees-of-freedom parallel wrist," *The International Journal of Robotics Research*, vol. 23, no. 6, pp. 661–667, 2004.

[222] X. Duan, Y. Yang, and B. Cheng, "Modeling and analysis of a 2-DOF spherical parallel manipulator," *Sensors*, vol. 16, no. 9, 2016.

[223] A. Cammarata, "Optimized design of a large-workspace 2-DOF parallel robot for solar tracking systems," *Mechanism and Machine theory*, vol. 83, pp. 175–186, 2015.

[224] D. Chablat, G. Michel, P. Bordure, S. Venkateswaran, and R. Jha, "Workspace analysis in the design parameter space of a 2-DOF spherical parallel mechanism for a prescribed workspace: application to the otologic surgery," *Mechanism and Machine Theory*, vol. 157, p. 104224, 2021.

[225] R. Vertechy and V. Parenti-Castelli, "Synthesis of 2-DOF spherical fully parallel mechanisms," in *Advances in Robot Kinematics*, pp. 385–394, Springer, 2006.

[226] J. Gallardo, R. Rodríguez, M. Caudillo, and J. M. Rico, "A family of spherical parallel manipulators with two legs," *Mechanism and Machine Theory*, vol. 43, no. 2, pp. 201–216, 2008.

[227] T. Zhang, B. Li, D. Wang, L. Ma, and X. Zhao, "Kinematic analysis and its applications of a novel spherical parallel manipulator," in *2016 IEEE International Conference on Robotics and Biomimetics (ROBIO)*, pp. 1309–1312, 2016.

[228] H. Jiang, C. Xiao, J. Li, Y. Zhong, T. Zhang, and Y. Guan, "Design and modeling of a 2-DOF cable-driven parallel wrist mechanism," in *2019 IEEE International Conference on Robotics and Biomimetics*, pp. 1047–1052, 2019.

[229] T. Nemoto, J. Walter, C. Bachmann, M. Gerlich, S. Reitelshöfer, and J. Franke, "Highly dynamic 2-DOF cable-driven robotic wrist based on a novel topology," *IEEE Robotics and Automation Letters*, vol. 7, no. 2, pp. 5727–5734, 2022.

[230] K. Abe, K. Tadakuma, and R. Tadakuma, "ABENICS: active ball joint mechanism with three-DoF based on spherical gear meshings," *IEEE Transactions on Robotics*, vol. 37, no. 5, pp. 1806–1825, 2021.

[231] S. Bai and M. R. Hansen, "Evaluation of workspace of a spherical robotic wrist," in *2007 IEEE/ASME International Conference on Advanced Intelligent Mechatronics*, pp. 1–6, 2007.

[232] S. Bai and M. R. Hansen, "Forward kinematics of spherical parallel manipulators with revolute joints," in *2008 IEEE/ASME International Conference on Advanced Intelligent Mechatronics*, pp. 522–527, 2008.

[233] S. Bai, M. R. Hansen, and J. Angeles, "A robust forward-displacement analysis of spherical parallel robots," *Mechanism and Machine Theory*, vol. 44, no. 12, pp. 2204–2216, 2009.

[234] S. Bai, M. R. Hansen, and T. O. Andersen, "Modelling of a special class of spherical parallel manipulators with Euler parameters," *Robotica*, vol. 27, no. 2, pp. 161–170, 2009.

[235] S. Bai, "Optimum design of spherical parallel manipulators for a prescribed workspace," *Mechanism and Machine Theory*, vol. 45, no. 2, pp. 200–211, 2010.

[236] D. Marrugo, A. Vitola, J. L. Villa, and M. Rodelo, "Kinematic and workspace analysis of spherical 3RRR coaxial parallel robot based on screw theory," in *2020 IX International Congress of Mechatronics Engineering and Automation (CIIMA)*, pp. 1–6, 2020.

[237] A. T. Cruz-Reyes, M. Arias-Montiel, and R. Tapia-Herrera, "Kinematic analysis of a coaxial 3-RRR spherical parallel manipulator based on screw theory," in *IFToMM Symposium on Mechanism Design for Robotics*, pp. 28–37, 2021.

[238] G. Wu, "Multiobjective optimum design of a 3-RRR spherical parallel manipulator with kinematic and dynamic dexterities," *Modeling, Identification and Control*, vol. 33, no. 3, pp. 111–122, 2012.

[239] G. Wu, S. Caro, S. Bai, and J. Kepler, "Dynamic modeling and design optimization of a 3-DOF spherical parallel manipulator," *Robotics and Autonomous Systems*, vol. 62, no. 10, pp. 1377–1386, 2014.

[240] G. Wu, "Stiffness analysis and optimization of a co-axial spherical parallel manipulator," *Modeling, Identification and Control*, vol. 35, no. 1, pp. 21–30, 2014.

[241] G. Wu, S. Bai, and J. Kepler, "Mobile platform center shift in spherical parallel manipulators with flexible limbs," *Mechanism and Machine Theory*, vol. 75, pp. 12–26, 2014.

[242] G. Wu and S. Bai, "Design and kinematic analysis of a 3-RRR spherical parallel manipulator reconfigured with four-bar linkages," *Robotics and Computer Integrated Manufacturing*, vol. 56, pp. 55–65, 2019.

[243] G. Wu, N. Zhang, C. Cui, H. Shen, and X. Zhang, "Kinematics and orientation workspace of a 3-DOF parallel robotic wrist actuated by spherical four-bar linkages," in *International Symposium on Advances in Robot Kinematics*, pp. 268–276, Springer, 2020.

[244] X. Li, J. Liu, W. Chen, and S. Bai, "Integrated design, modeling and analysis of a novel spherical motion generator driven by electromagnetic principle," *Robotics and Autonomous Systems*, vol. 106, pp. 69–81, 2018.

[245] X. Li, S. Bai, and O. Madsen, "Dynamic modeling and trajectory tracking control of an electromagnetic direct driven spherical motion generator," *Robotics and Computer-Integrated Manufacturing*, vol. 59, pp. 201–212, 2019.

[246] X. Li, J. Liu, W. Chen, and S. Bai, "Analytical magnetics and torque modeling of a multi-layer electromagnetic driven spherical motion generator," *Journal of Magnetism and Magnetic Materials*, vol. 493, p. 165707, 2020.

[247] Q. Li, Q. Chen, C. Wu, and X. Hu, "Two novel spherical 3-DOF parallel manipulators with circular prismatic pairs," in *ASME 2006 International Design Engineering Technical Conferences and Computers and Information in Engineering Conference*, pp. 325–328, 2006.

[248] J. Lee, B.-W. Song, and W. Yang, "Design of exoskeleton-type wrist human-machine interface based on over-actuated coaxial spherical parallel mechanism," *Advances in Mechanical Engineering*, vol. 10, no. 2, p. 1687814017753896, 2018.

[249] J. Lee, H. Kim, and W. Yang, "Development of wrist interface based on fully actuated coaxial spherical parallel mechanism for force interaction," *Sensors*, vol. 21, no. 23, p. 8073, 2021.

[250] P. Laryushkin, M. Zakharov, K. Erastova, and V. Glazunov, "Spherical manipulator with parallel structure," *Russian Engineering Research*, vol. 37, no. 7, pp. 585–588, 2017.

[251] P. Laryushkin, A. Antonov, A. Fomin, and V. Glazunov, "Novel reconfigurable spherical parallel mechanisms with a circular rail," *Robotics*, vol. 11, no. 2, 2022.

[252] P. Laryushkin, A. Antonov, A. Fomin, and V. Glazunov, "Inverse and forward kinematics of a reconfigurable spherical parallel mechanism with a circular rail," in *ROMANSY 24 - Symposium on Robot Design, Dynamics and Control*, pp. 246–254, 2022.

[253] H. Khoshnoodi, A. Rahmani Hanzaki, and H. A. Talebi, "Kinematics, singularity study and optimization of an innovative spherical parallel manipulator with large workspace," *Journal of Intelligent & Robotic Systems*, vol. 92, no. 2, pp. 309–321, 2018.

[254] S. V. Kiselev, A. V. Antonov, and A. S. Fomin, "Parallel robots with a circular guide: systematic review of kinematic schemes and methods of synthesis and analysis," *Journal of Machinery Manufacture and Reliability*, vol. 51, no. 1, pp. 20–29, 2022.

[255] E. Cavallo, R. C. Michelini, and V. F. Filaretov, "Conceptual design of an AUV equipped with a three degrees of freedom vectored thruster," *Journal of Intelligent and Robotic Systems*, vol. 39, no. 4, pp. 365–391, 2004.

[256] B. Sudki, M. Lauria, and F. Noca, "Robotic penguin-like propulsor with novel spherical joint," in *APS Division of Fluid Dynamics Meeting Abstracts*, pp. R26–008, 2013.

[257] Ö. Selvi and S. Yavuz, "Dimensional optimisation of a 3-DoF spherical parallel manipulator for rehabilitation by using firefly algorithm," *International Journal of Mechanisms and Robotic Systems*, vol. 4, no. 2, pp. 107–119, 2018.

[258] J. Lee, J. Noh, J. Yang, and W. Yang, "A novel design of extended coaxial spherical joint module for a new modular type-multiple DOFs robotic platform," in *2018 IEEE/RSJ International Conference on Intelligent Robots and Systems (IROS)*, pp. 955–960, 2018.

[259] J. Noh, J. Lee, W. Yang, and S. Lee, "Design of a concentrically stacked modular actuator with forced air cooling for multi-DOF robotic systems," *Energies*, vol. 11, no. 11, 2018.

[260] J. Lee, J. Noh, S. Lee, and W. Yang, "A novel 4-DoF robotic link mechanism with E-CoSMo: kinematics based torque analysis," in *2019 IEEE/RSJ International Conference on Intelligent Robots and Systems (IROS)*, pp. 3577–3582, 2019.

[261] S. Leguay-Durand and C. Reboulet, "Optimal design of a redundant spherical parallel manipulator," *Robotica*, vol. 15, no. 4, pp. 399–405, 1997.

[262] J. Enferadi and A. Shahi, "On the position analysis of a new spherical parallel robot with orientation applications," *Robotics and Computer-Integrated Manufacturing*, vol. 37, pp. 151–161, 2016.

[263] S.-H. Lee, W.-K. Kim, S.-M. Oh, and B.-J. Yi, "Kinematic analysis and implementation of a spherical 3-degree-of-freedom parallel mechanism," in *2005 IEEE/RSJ International Conference on Intelligent Robots and Systems*, pp. 972–977, 2005.

[264] E. Gezgin, S. Özbek, D. Güzin, O. E. Ağbaş, and E. B. Gezer, "Structural design of a positioning spherical parallel manipulator to be utilized in brain biopsy," *The International Journal of Medical Robotics and Computer Assisted Surgery*, vol. 15, no. 5, p. e2011, 2019.

[265] G. Wu, "Kinematics and dynamics of an asymmetrical parallel robotic wrist," *Journal of Robotics*, vol. 2014, 2014.

[266] G. Wu and P. Zou, "Comparison of 3-DOF asymmetrical spherical parallel manipulators with respect to motion/force transmission and stiffness," *Mechanism and Machine Theory*, vol. 105, pp. 369–387, 2016.

[267] G. Wu and H. Shen, "Comparison of 3-DOF partially decoupled spherical parallel manipulators with respect to lateral stabilities," in *IFToMM World Congress on Mechanism and Machine Science*, pp. 2099–2108, 2019.

[268] G. Wu, "Parameter-excited instabilities of a 2UPU-RUR-RPS spherical parallel manipulator with a driven universal joint," *Journal of Mechanical Design*, vol. 140, no. 9, p. 092303, 2018.

[269] G. Wu, S. Caro, and J. Wang, "Design and transmission analysis of an asymmetrical spherical parallel manipulator," *Mechanism and Machine Theory*, vol. 94, pp. 119–131, 2015.

[270] G. Wu and H. Shen, "Lateral stability of a 3-DOF asymmetrical spherical parallel manipulator with a universal joint featuring infinite torsional

movement," in *International Symposium on Advances in Robot Kinematics*, pp. 233–241, Springer, 2018.

[271] G. Wu and S. Caro, "Torsional stability of a U-joint based parallel wrist mechanism featuring infinite torsion," in *ROMANSY 22 Robot Design, Dynamics and Control*, pp. 147–154, Springer, 2019.

[272] J.-A. Leal-Naranjo, J.-A. Soria-Alcaraz, C.-R. Torres-San Miguel, J.-C. Paredes-Rojas, A. Espinal, and H. Rostro-González, "Comparison of metaheuristic optimization algorithms for dimensional synthesis of a spherical parallel manipulator," *Mechanism and Machine Theory*, vol. 140, pp. 586–600, 2019.

[273] Y. Wu and M. Carricato, "Design of a novel 3-DoF serial-parallel robotic wrist: a symmetric space approach," in *Robotics Research*, pp. 389–404, Springer, 2018.

[274] K. E. A. Dumlu, "Trajectory tracking control for a 3-DOF parallel manipulator using fractional-order $PI^{\lambda}D^{\mu}$ control," *IEEE Transactions on Industrial Electronics*, vol. 61, no. 7, pp. 3417–3426, 2014.

[275] I. Yahyapour, M. Yazdani, M. T. Masouleh, and M. Tabrizi, "Dynamic modeling and computed torque control of a 3-DOF spherical parallel manipulator," in *2014 Second RSI/ISM International Conference on Robotics and Mechatronics*, pp. 280–285, 2014.

[276] J. Rodriguez and M. Ruggiu, "A novel method for the solution of the forward displacement problem of spherical parallel manipulators," *ZAMM-Journal of Applied Mathematics and Mechanics/Zeitschrift für Angewandte Mathematik und Mechanik*, vol. 93, no. 1, pp. 73–82, 2013.

[277] T. Li, Q. Li, and S. Payendeh, "NN-based solution of forward kinematics of 3DOF parallel spherical manipulator," in *2005 IEEE/RSJ International Conference on Intelligent Robots and Systems*, pp. 1344–1349, 2005.

[278] J.-P. Merlet, "Closed-form resolution of the direct kinematics of parallel manipulators using extra sensors data," in *1993 Proceedings IEEE International Conference on Robotics and Automation*, pp. 200–204, 1993.

[279] I. A. Bonev, J. Ryu, S.-G. Kim, and S.-K. Lee, "A closed-form solution to the direct kinematics of nearly general parallel manipulators with optimally located three linear extra sensors," *IEEE Transactions on Robotics and Automation*, vol. 17, no. 2, pp. 148–156, 2001.

[280] V. Parenti-Castelli and R. Di Gregorio, "Real-time actual pose determination of the general fully parallel spherical wrist, using only one extra sensor," *Journal of Robotic Systems*, vol. 18, no. 12, pp. 723–729, 2001.

[281] R. Vertechy and V. Parenti-Castelli, "Robust, fast and accurate solution of the direct position analysis of parallel manipulators by using extra-sensors," in *Parallel Manipulators, towards new applications*, IntechOpen, 2008.

[282] H. Saafi, M. A. Laribi, and S. Zeghloul, "Forward kinematic model improvement of a spherical parallel manipulator using an extra sensor," *Mechanism and Machine Theory*, vol. 91, pp. 102–119, 2015.

[283] H. Saafi, M. Vulliez, S. Zeghloul, and M. A. Laribi, "A new serial approach of the forward kinematic model of spherical parallel manipulators for real-time applications," *Proceedings of the Institution of Mechanical Engineers, Part C: Journal of Mechanical Engineering Science*, vol. 232, no. 4, pp. 677–684, 2018.

[284] M. Vulliez, H. Saafi, and S. Zeghloul, "A real-time serial approach for solving the forward kinematic model of spherical parallel manipulators," in *International Conference on Robotics in Alpe-Adria Danube Region*, pp. 128–135, 2016.

[285] I. Tursynbek, A. Niyetkaliyev, and A. Shintemirov, "Computation of unique kinematic solutions of a spherical parallel manipulator with coaxial input shafts," in *2019 IEEE 15th International Conference on Automation Science and Engineering*, pp. 1524–1531, 2019.

[286] I. Tursynbek and A. Shintemirov, "Infinite torsional motion generation of a spherical parallel manipulator with coaxial input axes," in *2020 IEEE/ASME International Conference on Advanced Intelligent Mechatronics*, pp. 1780–1785, 2020.

[287] B. Siciliano and O. Khatib, *Springer Handbook of Robotics*. Berlin, Heidelberg: Springer-Verlag, 2007.

[288] D. Sorensen, "Newton's method with a model trust region modification," *SIAM Journal on Numerical Analysis*, vol. 19, no. 2, pp. 409–426, 1982.

[289] M. F. E. Rohmer, S.P.N. Singh, "V-REP: A versatile and scalable robot simulation framework," in *2013 IEEE/RSJ International Conference on Intelligent Robots and Systems (IROS 2013)*, pp. 1321–1326, 2013.

[290] I. Tursynbek and A. Shintemirov, "Modeling and simulation of spherical parallel manipulators in CoppeliaSim (V-REP) robot simulator software," in *2020 International Conference Nonlinearity, Information and Robotics (NIR)*, pp. 1–6, 2020.

[291] R. Mobley, "Gears and gearboxes," in *Plant Engineer's Handbook*, pp. 629–637, Elsevier, 2001.

[292] R. Diankov, *Automated Construction of Robotic Manipulation Programs*. PhD thesis, Carnegie Mellon University, Robotics Institute, 2010.

[293] V. Petuya, E. Macho, O. Altuzarra, C. Pinto, and A. Hernandez, "Educational software tools for the kinematic analysis of mechanisms," *Computer Applications in Engineering Education*, vol. 22, no. 1, pp. 72–86, 2011.

[294] C. Pinciroli, V. Trianni, R. O'Grady, G. Pini, A. Brutschy, M. Brambilla, N. Mathews, E. Ferrante, G. Di Caro, F. Ducatelle, M. Birattari,

L. M. Gambardella, and M. Dorigo, "ARGoS: A modular, parallel, multi-engine simulator for multi-robot systems," *Swarm Intelligence*, vol. 6, no. 4, pp. 271–295, 2012.

[295] J. M. Porta, L. Ros, O. Bohigas, M. Manubens, C. Rosales, and L. Jaillet, "The CUIK suite: analyzing the motion closed-chain multibody systems," *IEEE Robotics & Automation Magazine*, vol. 21, no. 3, pp. 105–114, 2014.

[296] T. Habra, H. Dallali, A. Cardellino, L. Natale, N. Tsagarakis, P. Fisette, and R. Ronsse, "Robotran-YARP interface: A framework for real-time controller developments based on multibody dynamics simulations," in *Computational Methods in Applied Sciences*, pp. 147–164, Springer International Publishing, 2016.

[297] S. S. V. Gupta, R.G. Chittawadigi, "RoboAnalyzer," in *Proceedings of the Advances in Robotics on - AIR '17*, 2017.

[298] A. H. N. Koenig, "Design and use paradigms for Gazebo, an open-source multi-robot simulator," in *2004 IEEE/RSJ International Conference on Intelligent Robots and Systems (IROS 2004)*, pp. 2149–2154, 2004.

[299] M. Quigley, B. Gerkey, K. Conley, J. Faust, T. Foote, J. Leibs, E. Berger, R. Wheeler, and A. Ng, "ROS: An open-source robot operating system," in *Proc. of the IEEE Intl. Conf. on Robotics and Automation (ICRA) Workshop on Open Source Robotics*, 2009.

[300] O. Michel, "Webots: Professional mobile robot simulation," *Journal of Advanced Robotics Systems*, vol. 1, no. 1, pp. 39–42, 2004.

[301] A. Montaqim, "Offline programming software for industrial robots from RoboDK offers hundreds of virtual industrial robots from top robotics companies," *Robotic and Automation News*, 2015.

[302] S. Gottschalk, M. C. Lin, and D. Manocha, "OBBTree: A Hierarchical Structure for Rapid Interference Detection," in *Proceedings of the 23rd annual conference on Computer graphics and interactive techniques - ACM SIGGRAPH*, pp. 171–180, 1996.

[303] B. Dasgupta and T. S. Mruthyunjaya, "Singularity-free path planning for the Stewart platform manipulator," *Mechanism and Machine Theory*, vol. 33, no. 6, pp. 711–725, 1998.

[304] K. M. Lynch, N. Shiroma, H. Arai, and K. Tanie, "Collision-free trajectory planning for a 3-DOF robot with a passive joint," *The International Journal of Robotics Research*, vol. 19, no. 12, pp. 1171–1184, 2000.

[305] Y. Chen, X. Liu, S. Wei, Y. Zhang, and Q. Huang, "Trajectory planning simulation of 3-DoF parallel wrist mechanisms based on SimMechanics," in *2019 IEEE 9th Annual International Conference on CYBER Technology in Automation, Control, and Intelligent Systems (CYBER)*, pp. 877–882, 2019.

[306] I. Tursynbek and A. Shintemirov, "Infinite rotational motion generation and analysis of a spherical parallel manipulator with coaxial input axes," *Mechatronics*, vol. 78, p. 102625, 2021.

[307] C. M. Gosselin and J. Angeles, "Singularity analysis of closed-loop kinematic chains," *IEEE Transactions on Robotics and Automation*, vol. 6, no. 3, pp. 281–290, 1990.

[308] D. Chablat and P. Wenger, "Working modes and aspects in fully parallel manipulators," in *Proceedings. 1998 IEEE International Conference on Robotics and Automation*, vol. 3, pp. 1964–1969, 1998.

[309] C. M. Gosselin and J. Angeles, "A global performance index for the kinematic optimization of robotic manipulators," *Journal of Mechanical Design*, vol. 113, no. 3, pp. 220–226, 1991.

[310] R. Ranganath, P. S. Nair, T. S. Mruthyunjaya, and A. Ghosal, "A force-torque sensor based on a Stewart Platform in a near-singular configuration," *Mechanism and Machine Theory*, vol. 39, no. 9, pp. 971–998, 2004.

[311] H. Shah, M. S. Narayanan, and V. N. Krovi, "CAD-enhanced workspace optimization for parallel manipulators: A case study," in *2010 IEEE International Conference on Automation Science and Engineering*, pp. 816–821, 2010.

[312] A. Johnson, X. Kong, and J. Ritchie, "Determination of the workspace of a three-degrees-of-freedom parallel manipulator using a three-dimensional computer-aided-design software package and the concept of virtual chains," *Journal of Mechanisms and Robotics*, vol. 8, no. 2, p. 024501, 2016.

[313] E. Rohmer, S. P. N. Singh, and M. Freese, "CoppeliaSim (formerly V-REP): a versatile and scalable robot simulation framework," in *Proceedings of The International Conference on Intelligent Robots and Systems (IROS)"*, pp. 1321–1326, 2013.

[314] M. Satoh, "Icosahedral grids," in *Atmospheric Circulation Dynamics and General Circulation Models*, pp. 636–660, Springer Berlin Heidelberg, 2013.

[315] S. Zhang, Z. Lin, and G. Wu, "Motion planning of a 5-DOF anthropomorphic robotic arm under ROS environment," in *IFToMM International Conference on Mechanisms, Transmissions and Applications*, pp. 409–418, Springer, 2019.

[316] S. Boyd, S. P. Boyd, and L. Vandenberghe, *Convex optimization*. Cambridge University Press, 2004.

[317] Q. T. Dinh, W. Michiels, S. Gros, and M. Diehl, "An inner convex approximation algorithm for BMI optimization and applications in control," in *2012 IEEE 51st IEEE Conference on Decision and Control (CDC)*, pp. 3576–3581, 2012.

[318] D. Henrion and C. Louembet, "Convex inner approximations of nonconvex semialgebraic sets applied to fixed-order controller design," *International Journal of Control*, vol. 85, no. 8, pp. 1083–1092, 2012.

[319] D. Simon, J. Löfberg, and T. Glad, "Nonlinear model predictive control using feedback linearization and local inner convex constraint approximations," in *2013 European Control Conference (ECC)*, pp. 2056–2061, 2013.

[320] B. Omarali, T. Taunyazov, A. Bukeyev, and A. Shintemirov, "Real-time predictive control of an UR5 robotic arm through human upper limb motion tracking," in *Proceedings of the Companion of the 2017 ACM/IEEE International Conference on Human-Robot Interaction*, pp. 237–238, 2017.

[321] J. Mattingley and S. Boyd, "CVXGEN: A code generator for embedded convex optimization," *Optimization and Engineering*, vol. 13, no. 1, pp. 1–27, 2012.

[322] J. B. Kuipers, *Quaternions and rotation sequences: a primer with applications to orbits, aerospace, and virtual reality*. Princeton University Press, 1999.